Internal Reinforcement of Backfill behind Integral Bridge Abutments to Mitigate Approach Slab Distresses

Jie Han, Ph.D., P.E., F.ASCE
Hao Liu
Robert L. Parsons, Ph.D., P.E.
Saif Jawad, Ph.D.

The University of Kansas

Kansas
Department of Transportation

1	Report No. K-TRAN: KU-19-1	2	Government Accession No.	3	Recipient Catalog No.	

4	Title and Subtitle Internal Reinforcement of Backfill behind Integral Bridge Abutments to Mitigate Approach Slab Distresses	5	Report Date July 2022
		6	Performing Organization Code

7	Author(s) Jie Han, Ph.D., P.E., F.ASCE, Hao Liu, Robert L. Parsons, Ph.D., P.E., Saif Jawad, Ph.D.	8	Performing Organization Report No.

9	Performing Organization Name and Address The University of Kansas Department of Civil, Environmental & Architectural Engineering 1530 West 15th St Lawrence, Kansas 66045-7609	10	Work Unit No. (TRAIS)
		11	Contract or Grant No. C2130

12	Sponsoring Agency Name and Address Kansas Department of Transportation Bureau of Research 2300 SW Van Buren Topeka, Kansas 66611-1195	13	Type of Report and Period Covered Final Report July 2018–June 2021
		14	Sponsoring Agency Code RE-0752-01

15	Supplementary Notes For more information write to address in block 9.

16 Abstract

Integral abutment bridges have become popular worldwide by eliminating movable shoes which are expensive to purchase, install, and maintain in conventional bridges. However, the behavior of bridge abutments subjected to air temperature changes for integral bridges is different from that of conventional bridges. Expansion and contraction of bridge girders due to temperature variations are accommodated by joints between bridge girders and abutments for conventional bridges. Expansion of bridge girders at high temperatures moves the integral bridge abutment toward its backfill, causing high lateral earth pressures behind the abutment, while contraction of bridge girders at low temperatures moves the integral bridge abutment away from its backfill, causing backfill surface settlements. The backfill behind the abutment cannot maintain its stability after the integral abutment moves away so that the backfill material within the upper portion slumps and moves downward and toward the abutment. Cyclic movements of the integral abutment due to temperature changes disturb the backfill and further reduce its self-stability when the integral abutment moves away from the backfill in the next cycle. In addition, soil erosion and compression of backfill and foundation soil can aggravate the backfill surface settlements for both integral bridges and conventional bridges. An approach slab is commonly used to provide a smooth transition between the backfill and the bridge abutment. The approach slab may lose some support from the backfill as the backfill surface settles. Consequently, more traffic loads on the approach slab are transferred to the end of the approach slab near the adjacent pavement, resulting in a differential settlement at the joint between the approach slab and the adjacent pavement. A sleeper slab has been proposed for placement underneath the joint between the approach slab and the adjacent pavement, thus minimizing this differential settlement. However, an excessive gradient may still develop for the approach slab due to the differential settlement between two ends of the approach slab. This situation may be aggravated by the concave deformation of the approach slab due to traffic loading. Therefore, backfill surface settlements and traffic loading are the two main causes for the distresses of the approach slab. These distresses may be mitigated by the use of geosynthetic reinforcement because it is expected to increase the stability of the backfill and reduce the settlement of the sleeper slab. However, the benefits of the geosynthetic reinforcement for this application are not well investigated and confirmed.

Six physical model tests were conducted in this study to investigate the benefits of geogrid reinforcement in reducing the settlements of the backfill surface and the sleeper slab. In the physical models, a manual jack was used to push and pull the integral abutment to simulate the expansion and contraction of bridge girders due to temperature increase and decrease, respectively. In addition, a hydraulic cylinder was adopted to simulate traffic loading on the approach slab at four positions (Position I to Position IV) of the model abutment top related to the four seasons (spring to winter) in a year. Test results show that both the simulated seasonal temperature change and traffic loading induced backfill surface settlements. Geogrid reinforcement increased the stiffness of the soil under the sleeper slab and enhanced the sleeper slab to carry more traffic load transferred, thus reducing the traffic load transferred to the backfill behind the abutment. Consequently, the geogrids under the sleeper slab reduced the backfill surface settlements due to traffic loading. Horizontal geogrids in the backfill increased the backfill surface settlements near the abutment but reduced the settlements of the backfill away from the abutment. Geogrids with wrap-around facing significantly reduced the backfill surface settlements due to the seasonal temperature changes and traffic loading. An increase of the top geogrid length with wrap-around facing further reduced the backfill surface settlement.

17	Key Words Jointless bridges, Bridge abutments, Geogrids, Backfilling, Differential settlement	18	Distribution Statement No restrictions. This document is available to the public through the National Technical Information Service www.ntis.gov.

19	Security Classification (of this report) Unclassified	20	Security Classification (of this page) Unclassified	21	No. of pages 109	22	Price

Form DOT F 1700.7 (8-72)

This page intentionally left blank.

Internal Reinforcement of Backfill behind Integral Bridge Abutments to Mitigate Approach Slab Distresses

Final Report

Prepared by

Jie Han, Ph.D., P.E., F.ASCE
Hao Liu
Robert L. Parsons, Ph.D., P.E.
Saif Jawad, Ph.D.

The University of Kansas

A Report on Research Sponsored by

THE KANSAS DEPARTMENT OF TRANSPORTATION
TOPEKA, KANSAS

and

THE UNIVERSITY OF KANSAS
LAWRENCE, KANSAS

July 2022

PREFACE

The Kansas Department of Transportation's (KDOT) Kansas Transportation Research and New-Developments (K-TRAN) Research Program funded this research project. It is an ongoing, cooperative and comprehensive research program addressing transportation needs of the state of Kansas utilizing academic and research resources from KDOT, Kansas State University and the University of Kansas. Transportation professionals in KDOT and the universities jointly develop the projects included in the research program.

NOTICE

The authors and the state of Kansas do not endorse products or manufacturers. Trade and manufacturers names appear herein solely because they are considered essential to the object of this report.

This information is available in alternative accessible formats. To obtain an alternative format, contact the Office of Public Affairs, Kansas Department of Transportation, 700 SW Harrison, 2nd Floor – West Wing, Topeka, Kansas 66603-3745 or phone (785) 296-3585 (Voice) (TDD).

DISCLAIMER

The contents of this report reflect the views of the authors who are responsible for the facts and accuracy of the data presented herein. The contents do not necessarily reflect the views or the policies of the state of Kansas. This report does not constitute a standard, specification or regulation.

Abstract

Integral abutment bridges have become popular worldwide by eliminating movable shoes which are expensive to purchase, install, and maintain in conventional bridges. However, the behavior of bridge abutments subjected to air temperature changes for integral bridges is different from that of conventional bridges. Expansion and contraction of bridge girders due to temperature variations are accommodated by joints between bridge girders and abutments for conventional bridges. Expansion of bridge girders at high temperatures moves the integral bridge abutment toward its backfill, causing high lateral earth pressures behind the abutment, while contraction of bridge girders at low temperatures moves the integral bridge abutment away from its backfill, causing backfill surface settlements. The backfill behind the abutment cannot maintain its stability after the integral abutment moves away so that the backfill material within the upper portion slumps and moves downward and toward the abutment. Cyclic movements of the integral abutment due to temperature changes disturb the backfill and further reduce its self-stability when the integral abutment moves away from the backfill in the next cycle. In addition, soil erosion and compression of backfill and foundation soil can aggravate the backfill surface settlements for both integral bridges and conventional bridges. An approach slab is commonly used to provide a smooth transition between the backfill and the bridge abutment. The approach slab may lose some support from the backfill as the backfill surface settles. Consequently, more traffic loads on the approach slab are transferred to the end of the approach slab near the adjacent pavement, resulting in a differential settlement at the joint between the approach slab and the adjacent pavement. A sleeper slab has been proposed for placement underneath the joint between the approach slab and the adjacent pavement, thus minimizing this differential settlement. However, an excessive gradient may still develop for the approach slab due to the differential settlement between two ends of the approach slab. This situation may be aggravated by the concave deformation of the approach slab due to traffic loading. Therefore, backfill surface settlements and traffic loading are the two main causes for the distresses of the approach slab. These distresses may be mitigated by the use of geosynthetic reinforcement because it is expected to increase the stability of the backfill and reduce

the settlement of the sleeper slab. However, the benefits of the geosynthetic reinforcement for this application are not well investigated and confirmed.

Six physical model tests were conducted in this study to investigate the benefits of geogrid reinforcement in reducing the settlements of the backfill surface and the sleeper slab. In the physical models, a manual jack was used to push and pull the integral abutment to simulate the expansion and contraction of bridge girders due to temperature increase and decrease, respectively. In addition, a hydraulic cylinder was adopted to simulate traffic loading on the approach slab at four positions (Position I to Position IV) of the model abutment top related to the four seasons (spring to winter) in a year. Test results show that both the simulated seasonal temperature change and traffic loading induced backfill surface settlements. Geogrid reinforcement increased the stiffness of the soil under the sleeper slab and enhanced the sleeper slab to carry more traffic load transferred, thus reducing the traffic load transferred to the backfill behind the abutment. Consequently, the geogrids under the sleeper slab reduced the backfill surface settlements due to traffic loading. Horizontal geogrids in the backfill increased the backfill surface settlements near the abutment but reduced the settlements of the backfill away from the abutment. Geogrids with wrap-around facing significantly reduced the backfill surface settlements due to the seasonal temperature changes and traffic loading. An increase of the top geogrid length with wrap-around facing further reduced the backfill surface settlement.

Acknowledgements

Table of Contents

List of Tables

Lists of Figures

This page intentionally left blank.

Chapter 1: Introduction

This chapter provides a brief introduction about the justification for this research and the structure of this report. Integral abutment bridges have become popular around the world because it requires less cost to construct and maintain than conventional bridges with movable shoes and joints between bridge girders and bridge abutments. However, movements of integral bridge abutments due to expansion and contraction of bridge girders cause backfill surface settlements, resulting in differential settlement between the abutment and the backfill. The backfill settlements may cause an abrupt change of the gradient from the pavement to the bridge even if an approach slab and a sleeper slab are included in design to provide a smooth transition between the backfill and the abutment. To mitigate the backfill surface settlements and the abrupt change of the road gradient, geosynthetic reinforcement is proposed to improve the self-stability of the backfill and increase the stiffness of the soil under the sleeper slab. For easy presentation, the backfill behind the abutment is referred to as "backfill" while the backfill below the sleeper slab is referred to as "soil" in this report.

1.1 Background

For a conventional bridge, bridge girders are supported by bridge abutments or piers using hinged or moveable shoes. The joints between the bridge girders and the bridge abutment at both ends of the bridge girders accommodate relative movements between the abutment and the girders due to temperature changes, bridge girder creep, and shrinkage of concrete. However, the moveable shoes and joints can pose some problems for the conventional bridge. First, product and installation of the moveable shoes are expensive. Second, water infiltration through the joints, especially when water is contaminated by deicing salt in winter, corrodes the moveable shoes, resulting in costly maintenance. Finally, soil particles falling into the joints during contraction at colder temperatures may damage the bridge girders or the abutment when the bridge girders expand at high temperature.

To mitigate these problems associated with the conventional bridges, the bridge girders are integrated structurally with the bridge abutment in the so-called "integral abutment bridge" (IAB). The IABs have several advantages over the conventional bridges. First, elimination of moveable

1

shoes reduces a bridge's cost because the product, installation, and maintenance of the moveable shoes are expensive and not required for IABs. Second, seismic stability of the IABs is higher than that of the conventional bridges because the bridge girders, the bridge abutment, and the backfill integrated as an entire structure better resist the forces induced by an earthquake. Third, the effect of the wind load is less significant for the IABs than that for the conventional bridges because thinner bridge decks are required for the IABs than for the conventional bridges. Consequently, the IABs have been increasingly used worldwide.

1.2 Problem Statement

Bridge abutments are typically supported by pile or drilled shaft foundations to rock, and the settlements of bridge abutments are insignificant as a result. However, the backfill and foundation soil are prone to settle due to several factors, such as temperature changes, soil erosion, and traffic loading, resulting in differential settlement at the interface between the abutment and the backfill (Liu, Han, Jawad, & Parsons, 2020). The bridge girders expand or contract at high or low temperature, but the response of the bridge abutment to expansion and contraction of the bridge girders is different between the IABs and the conventional bridges. For the conventional bridges, expansion and contraction of the bridge girders are accommodated by the joints between the bridge girders and the bridge abutment. However, expansion and contraction of the bridge girders due to daily and seasonal temperature changes cause cyclic movements of integral bridge abutments. Expansion and contraction of the bridge girder in IABs move the bridge abutment toward and away from the backfill, respectively. Movements of the integral bridge abutment (IBA) toward the backfill due to expansion of the bridge girders increase the lateral earth pressures behind the abutment. However, the backfill slumps downward and toward the abutment when the abutment moves away from the backfill due to contraction of the bridge girders, thus resulting in backfill surface settlements. The reason for the backfill surface settlements induced by the abutment top movement cycles is that the backfill (commonly cohesionless soil) cannot maintain its stability as the abutment top moves away from the backfill. The backfill material moving downward from the upper portion increased the resistance at the abutment bottom. Consequently, each cycle of bridge girder expansion and contraction (i.e., abutment top movement cycle) results

in a net outward movement of the abutment toe away from the backfill. In addition, the backfill surface settlements increase with the number of abutment top movement cycles due to temperature changes.

To ensure a smooth transition between the backfill and the bridge abutment, an approach slab with one end supported on the integral abutment, and the other end supported on the backfill, is commonly used. The cyclic movements of the abutment cause backfill surface settlements. As the backfill near the abutment settles, the approach slab loses some support from the backfill and may create voids between the approach slab and the backfill as a result. More traffic load is transferred to the end of the approach slab near the pavement so that the end of the approach slab near the adjacent pavement settles more than the adjacent pavement, resulting in a differential settlement at the joint between the approach slab and the adjacent pavement. The differential settlement between the two ends of the approach slab results in an abrupt change of the road gradient from the pavement to the bridge. The approach slab under traffic loads with no or limited support from the backfill deforms concavely and increases the degree of the gradient change.

To mitigate the above problems, internal geosynthetic reinforcements (e.g., geogrid and woven geotextile) may be used to reinforce the backfill for its self-stability when the abutment moves away from the backfill due to contraction of girders. A sleeper slab may be placed under the joint to mitigate the differential settlement between the approach slab and the pavement. To increase the bearing capacity and reduce the settlement of the sleeper slab, geosynthetic reinforcement may be used to reinforce the soil below the sleeper slab. However, the benefits of the geosynthetic reinforcement for improving the self-stability of the backfill, increasing the bearing capacity, and reducing the settlement of the soil under the sleeper slab are not well investigated and confirmed.

1.3 Research Objective

The objective of this research was to evaluate the benefits of internal reinforcement using geogrids to mitigate approach slab distresses through physical model testing in the laboratory. In this research, the backfill surface settlements induced by seasonal temperature changes were investigated by a physical model test. Then another physical model test considering the seasonal

temperature changes and traffic loading was conducted to investigate the effects of traffic loading on the backfill surface settlements. Finally, this research evaluated the benefits of placing geogrid reinforcements in the backfill and in the soil under the sleeper slab to mitigate the distresses of the approach slab (i.e., settlements of the backfill surface and the sleeper slab).

1.4 Research Methodology

This research investigated the benefits of geogrid reinforcement to mitigate the distresses of approach slabs through literature review and laboratory tests. The literature review first describes the reasons for the backfill surface settlements, and the research findings about the influence factors including the air temperature changes and traffic loading, and then discusses the past research using geogrid reinforcements to reduce the backfill surface settlements and the settlements of sleeper slabs. The laboratory tests included the property tests and the physical model tests. Direct shear tests and triaxial compression tests were conducted to determine the peak and residual friction angles of the Kansas River sand as the backfill material in this research. Pullout tests were performed to evaluate the interface properties between the geogrid and the Kansas River sand. Physical model tests were conducted to simulate bridge abutments subjected to seasonal temperature changes and traffic loading. The movements of the abutment and the lateral earth pressures behind the abutment during backfill placement and compaction were measured and analyzed. The effects of seasonal temperature changes and traffic loading on the backfill surface settlements, and the mitigation benefits of geogrid reinforcements in the backfill and the soil under the approach slab were investigated using the physical model tests.

1.5 Report Organization

This report consists of six chapters. Chapter 1 introduces the background, problem statement, research objective, research methodology, and report organization. Chapter 2 presents the literature review about the reasons for backfill surface settlements, including temperature changes and traffic loading, and the measures (i.e., geogrid reinforcements) used to mitigate settlements of backfill and sleeper slabs. Chapter 3 introduces the test setup designed for this research and the results of property tests, including direct shear tests and triaxial compression tests of the Kansas River sand, and pullout tests of geogrids in the Kansas River sand. Chapter 4 presents

the test results and analysis of the abutment movements, and the lateral earth pressures behind the abutment induced by backfill placement and compaction. Chapter 5 presents the test results and analysis focused on the effects of seasonal temperature changes and traffic loading on backfill surface settlements, and the benefits of geogrid reinforcements in the backfill and in the soil under the sleeper slab to mitigate the distresses of the approach slabs.

Chapter 2: Literature Review

This chapter provides a review of the reasons for the backfill surface settlements, discusses previous research about problems induced by air temperature changes for integral bridges, and reviews previous research about the effects of traffic loading on backfill surface settlements and the benefits of using geosynthetics to reinforce the backfill and the soil under the sleeper slab. To the authors' best knowledge, no published results of physical model tests have been found with regard to the investigation of the combined effect of seasonal temperature changes and traffic loading. In addition, no published results have been found on physical model tests used to investigate the benefits of geosynthetic reinforcements in backfill and soil under sleeper slabs at the same time.

2.1 Reasons for Backfill Settlement

Bridge abutments are typically supported by pile or drilled shaft foundations to rock; therefore, the abutment is often not susceptible to significant settlement. However, pavements on top of the backfill near the abutment can settle due to seasonal temperature changes and compression of the backfill and the foundation soil. As a result, differential settlement at the interface between the abutment and the adjacent pavement can develop, and this differential settlement is referred to as "the bump at the end of the bridge" problem. A number of researchers have investigated the causes for the bump problem (Hoppe, 1999; Schaefer & Koch, 1992; Briaud, James, & Hoffman, 1997; Abu-Hejleh, Hanneman, White, Wang, & Ksouri, 2006) and identified the main contributing factors for the bump problem including (1) compression of foundation and backfill soils; (2) poor compaction of backfill soil; and (3) poor drainage and soil erosion. Liu, Han, Jawad, and Parsons (2020) classified the causes into three groups: (1) internal factors; (2) external factors; and (3) other factors related to construction, design, and inspection. Based on typical components of bridges, internal factors include embankment and foundation, drainage system, approach and sleeper slabs, connection/joint, abutment, and superstructure, while the external factors mainly include traffic volume and climate condition (e.g., rainfall, seasonal and daily temperature changes).

2.1.1 Internal Factors

2.1.1.1 Embankment and foundation

At bridges, approach embankments are commonly constructed behind abutments over foundation soils. Foundation soils are subjected to the weight of the embankment and traffic loads. The embankment can settle due to its own weight and the traffic loads. The settlements of the embankment and the foundation soil consist of three parts. First, immediate compression of soils happens during construction. This induced settlement is typically immediate and small as compared with that due to consolidation; therefore, it has almost no contribution to the bump problem (Hopkins & Deen, 1970). Puppala, Saride, Archeewa, Hoyos, and Nazarian (2009) pointed out that unsaturated soils have less contribution to the initial compression than saturated soils. The immediate settlement is followed by primary consolidation that is induced by drainage of water out of soil voids. Primary consolidation involves dissipation of excess pore water pressure and the rate of water pressure dissipation depends on soil properties (e.g., compressibility, permeability, stress history, and void ratio). Primary consolidation can last from a few months for granular soils to a few years for clays. Secondary consolidation takes place after primary consolidation due to the adjustment of soil fabrics under applied stresses. For some soft, plastic and organic clays, the magnitude of settlement induced by secondary consolidation can be as large as that induced by primary consolidation.

2.1.1.2 Drainage system

A drainage system for pavements/bridge structures consists of surface and subsurface drainage. The surface drainage component is used to divert surface water away from the structure as soon as possible and prevent formation of ponding water or delayed runoff of water. The subsurface drainage component is used to collect and remove infiltrated water into embankments through cracks or joints so that water-induced softening and deterioration of backfill soils can be avoided. A properly designed and installed subsurface/surface drainage system can prevent or minimize the problems associated with increased soil water content (e.g., reduction of soil strength and modulus and increase of deformation) and water flow through in backfill soils (e.g., soil erosion).

2.1.1.3 Approach/sleeper slab

Approach slabs are often used to create a smooth transition between bridge abutments and adjoining pavements. Wong and Small (1994) indicated that constructing the approach slab at an angle to the horizontal and sloping down into the pavement could reduce surface gradient and provide smooth riding. Smooth rides, reduced impacts on back walls, and enhanced drainage control are three key advantages of approach/sleeper slabs, while increased initial cost and construction time are their disadvantages (Briaud et al., 1997; Hoppe, 1999).

2.1.1.4 Connection and joint

The connection between an approach slab and an abutment can affect the performance of the approach slab. Two typical types of connections are used (White, Sritharan, Suleiman, Mekkawy, & Chetlur, 2005). The first type is to extend longitudinal steel reinforcements from the bridge deck to the approach slab or use steel bars connecting the approach slab to the corbels of the bridge. The second type is to place the approach slab on the abutment as a joint opening of 2 to 3 in. (50 to 75 mm). The approach slab can rotate around the abutment if there is a gap between the approach slab and the backfill. Rupturing and cracking of concrete near the connection between the approach slab and the bridge abutment may occur if they are connected mechanically. To accommodate expansion and contraction of bridge girders, expansion joints are necessary between bridge girders/abutment, abutment/approach slab, and approach slab/adjoining pavement. Soil particles may fall into the joints during contraction cycles caused by cold temperature and cause damage to concrete during expansion cycles caused by hot temperature if the joints are not sealed correctly. Additionally, water infiltration through the joints may corrode bearings, or soften and carry away soil particles from the backfill if water is not handled properly. Therefore, joints should meet the requirements for durability, movement, maintenance, and resistance to damage from snow-removal operations with moderate cost (Kunin & Alampalli, 2000).

2.1.1.5 Abutment

Four types of abutments are commonly used in practice (Puppala et al., 2009): (a) close and high abutment, (b) stub or perched abutment, (c) pedestal or spill-through abutment, and (d) integral abutment. The close and high abutment (U-type) has two side walls and a front wall, which

rest on spread footings embedded in natural ground. For the areas near the walls where it is difficult for a large compactor to reach, the uniformity of compaction cannot be guaranteed. For this type of abutment, the walls are subjected to large lateral earth pressures. The stub or perched abutment includes a cap back wall and wing walls on the top of piles driven through compacted fill. Aside from the quality of compaction, the differential settlement between this type of abutment and its backfill is often significant. The pedestal or spill-through abutment is supported on columns; therefore, compaction of the backfill material between columns and near the abutment is limited. Integral abutments are connected to bridge girders mechanically; therefore, the piles supporting the abutment are subjected to lateral loads induced by expansion and contraction of bridge girders. This type of abutment is more sensitive to temperature variations.

2.1.1.6 Skewness of superstructure

Skewness of bridges to the centerline of the road makes uniform compaction of backfill much more difficult, thus aggravating the bump problem in skewed bridges.

2.1.2 External Factors

2.1.2.1 Climate

Seasonal temperature changes can result in contraction and expansion of bridge girders. For Integral Abutment Bridges (IABs), during summer, temperature increases lead to expansion of the bridge girders, and movement of the bridge abutment toward the backfill of the approach embankment. Therefore, lateral earth pressures behind the abutment increase. During winter, contraction of bridge girders causes the bridge abutment to move away from the backfill of the embankment. As a result, a wedge-shaped portion of the embankment moves toward the bridge abutment. This wedge cannot be pushed back to the original position, mainly due to the non-linear behavior of soils (Horvath, 2005). The net movement between the bridge abutment and the wedge-shaped portion of the retained soil in winter increases after each cycle of temperature change, thus creating voids under the pavement. Precipitation (rainfalls and snowfalls) can produce water infiltrating through joints and cracks that induces soil erosion and/or increases water content of soils if the drainage system is not effective.

2.1.2.2 Traffic volume

Traffic volume, including velocities of vehicles and magnitudes and repetitions of traffic loads, can all influence the settlement of the approach pavement. Laguros, Zaman, and Mahmood (1990) concluded that the traffic volume has an impact on the bridge approach settlement. Briaud et al. (1997) concluded that high traffic load is one of the factors causing the bump. Based on a model test, Seo (2003) found that the number of vehicular loading cycles is one of the predominant factors contributing to the development of bumps, and that the velocity and weight of the travelling wheel have an impact on the total settlement under approach slabs.

2.1.3 Other Factors Related to Construction, Design, and Inspection

Hopkins (1985) and Briaud et al. (1997) indicated that poor compaction of the approach embankment (Wahls, 1990) and improper backfill material are two of the key factors contributing to the settlement of approach pavements. Kramer and Sajer (1991) pointed out that design problems (e.g., improper lift thickness of embankment fill and unsatisfied compaction requirements), construction problems (e.g., improper equipment, over-excavation of abutment construction, and survey errors), and inspection problems (e.g., lack of knowledge and improper training of inspectors) can all contribute to the bump problem. Additionally, construction sequence may influence the approach slab settlement.

2.2 Research about Temperature Change

As stated previously, expansion of bridge girders at high temperatures moves the integral bridge abutment toward the backfill, resulting in increased lateral earth pressures behind the abutment. Contraction of bridge girders at low temperatures moves the integral bridge abutment away from the backfill so that the backfill slumps downward to fill the gaps created, densifying the backfill right behind the abutment bottom. Consequently, the densified backfill behind the abutment bottom restrains the abutment bottom from moving back to its previous position. The net displacements of the abutment toe away from the backfill, the lateral earth pressures behind the abutment at high temperatures, and the backfill surface settlements accumulate over years. A number of researchers have investigated the effects of seasonal and/or daily temperature changes

on integral abutment bridges through physical model tests, numerical analysis, and field monitoring.

2.2.1 Physical model test and numerical analysis

Table 2.1 lists a few physical model tests and numerical analyses conducted by different researchers to investigate the effects of temperature changes on integral abutments available in the literature. These researchers focused on two main problems related to lateral earth pressures behind the abutment and backfill surface settlements (Liu, Han, Jawad, & Parsons, 2021). Some researchers (e.g., Wood & Nash, 2000) also investigated the bending moment in the abutment caused by air temperature changes. Past research investigated the effects of magnitude of temperature change, backfill density, wall stiffness, interface roughness between the abutment and the backfill, and initial direction of the abutment movement on the backfill surface settlements. The investigated abutments can be grouped into three types: abutments supported by spread footings, base-hinged abutments, and embedded abutments. The hinged-base abutment was the most popular abutment used in recent physical modeling (Tatsuoka et al., 2009; Lehane, 2011; Havinga, Tschuchnigg, Marte, & Schweiger, 2017).

2.2.2 Field monitoring

Behavior of integral abutment bridges due to air temperature changes has been investigated through field monitoring. Table 2.2 contains a summary of the information on 30 monitored bridges. Figure 2.1 shows the distribution of the number of field studies in terms of total length of the bridge, material of bridge girders, and type of footings supporting the abutment of the bridges listed in Table 2.2. The numbers of bridges with the total length of no longer than 200 ft, 200 to 333 ft, 333 to 667 ft, and not shorter than 667 ft were 15, nine, three, and two, respectively. The bridge girders in 18 bridges were made of concrete while those in eight bridges were made of steel. Of the 30 bridges, 18 bridges used steel H-piles to support the integral bridge abutments because the H-piles would supply little resistance to the abutment movement, and rotate in response to bridge expansion and contraction. In addition, the weak axis of the H-piles was orientated along the expansion and contraction direction of some bridges to further reduce the resistance to movement of the integral bridge abutment from the steel H-piles. It appears that some integral

11

bridge abutments were supported by spread footings before 2001, but integral bridge abutments supported by flexible deep foundations (e.g., steel H-piles) became more popular worldwide afterwards.

Table 2.1: Physical Model Tests and Numerical Analyses in the Literature

Reference	Key objectives	Method of study	Foundation type	Key variables
Springman, Norrish, and Ng (1996)	To evaluate influence of ΔT, backfill density and wall stiffness	Centrifuge test and FEA	Embedded and spread-base walls	ΔT, backfill density, interface roughness, initial direction and wall flexibility
Cheng (1999)	To analyze centrifuge test data and numerical simulation	Centrifuge test and FD	Spread-base walls	ΔT, backfill density, interface roughness and wall flexibility
England, Tsang, and Bush (2000)	To examine limits of K escalation and settlement	Small-scale model tests and numerical analysis	Simplified base-hinged rigid walls	ΔT, void ratio, initial direction, inclusion of daily cycles
Wood and Nash (2000)	To evaluate wall pressure and bending moment during monotonic deck expansion	FD using FLAC	Simplified base-hinged rigid walls	Soil strength and relative soil/wall stiffness
Carder and Hayes (2000)	To evaluate behavior of idealized soil element below spread-base integral abutments	Literature review and cyclic samples using a triaxial apparatus	Spread-base walls	Soil grading and soil type
Tan (2007)	To investigate mechanisms of shakedown and failure mechanism behind integral wall	Small scale model tests and FEA	Embedded and spread-base walls (rod model)	ΔT, wall embedment depth, initiation direction, vertical load, joint rotational stiffness, wall flexibility
Tatsuoka et al., (2009)	To verify a new type of integral bridge	Small scale model tests	Simplified base-hinged wall supported by piles and full height rigid wall not supported by pile	Initiation direction
Lehane (2011)	To estimate lateral stresses on deep integral bridge abutments.	Centrifuge test	Simplified base-hinged rigid walls	ΔT, backfill density, backfill particle shape, abutment height, depth of abutment's effective rotation point
Havinga et al., (2017)	To determinate backfill settlement and investigate lateral earth pressure change	Small-scale, mid-scale model tests and DEM	Simplified base-hinged rigid walls	ΔT, backfill density, initiation direction,

Note: ΔT = temperature difference; K = lateral earth pressure coefficient; FEA = finite element analysis; FD = finite difference.

Table 2.2: Summary of Instrumented IABs in Field
(Continued to next page)

| References	Length (ft)	Skew angle (degrees)	Span length (ft)	Girder type	Pile type and bending orientation	Bridge width (ft)
Elgaaly, Sandford, and Colby (1992)	168	20	168	Five inverted U steel frames	Shallow foundation	37.7
Darley and Alderman (1995)	189	--	2@94.5	Reinforced concrete deck	shallow foundation	32.5
Darley and Alderman (1995)	160	--	2@80	Reinforced concrete deck	shallow foundation	41.3
Darley, Carder, and Barker (1998)	200	--	--	--	shallow foundation	--
Barker and Carder (2001)	167	--	87.7, 79.7	12 PPC beams	spread bases (abutment socketed in the bases)	60.3
Frosch, Chovichien, Durbin, and Fedroff (2006)	367	8	62, 3@81, 62	Five PPC girders	CFT	48
Muraleetharan, Miller, Kirupakaran, Krier, and Hanlon (2012)	167	0	51.7, 63.3, 51.7	Reinforced concrete deck	CFT	36.7
Ooi, Lin, and Hamada (2010)	81.3	0	81.3	12 PC voided planks	Drilled shafts	56.7
Huffaker (2013)	324.5	Curved	85.8, 152.8, 85.8	Eight PC girder	Driven piles	71
Kong, Cai, and Kong (2015)	4007	Curved	--	--	PPC piles	50
Abendroth, Greimann, and LaViolette (2007)	110	20	110	Five PC girders	PC piles	30.3
Jorgenson (1983)	450	0	6@75	Five PC box girders	HP 250 × 62 (weak axis)	32
Girton, Hawkinson, and Greimann (1991)	324.5	45	80, 2@82.3,80	PC girders (C80R)	--	40
Girton, Hawkinson, and Greimann (1991)	320	30	98, 124, 98	steel girder	HP (strong axis)	32
Lawver, French, and Shield (2000)	220	0	3@73.3	Four PPC bridge girders	HP 310 × 79 (weak axis)	40
Civjan, Breña, Butler, and Crovo (2004); DeJong et al. (2004); Breña, Bonczar, Civjan, Delong, and Crovo (2007)	274.3	0	81.3, 111.7, 81.3	Four steel plate girders	HP 250 × 85 (weak axis)	32.7
Khodair and Hassiotis (2005)	--	--	--	--	HP 360 × 152	--

Table 2.2: Summary of Instrumented IABs in Field (Continued)

References	Length (m)	Skew angle (degrees)	Span length (m)	Girder type	Pile type and bending orientation	Bridge width (m)
Frosch et al. (2006)	990	13	86.7, 3@98.3, 114.7, 4@101.7, 86.7	Four PC girders	HP 360 × 132 (strong axis)	35.7
Shoukry, William, and Riad (2006)	149.3	55	49.3, 50.8, 49.3	--	HP 310 ×79	44.7
Huntley (2009); Huntley and Valsangkar (2013); Huntley and Valsangkar (2014)	253.3	0	2@126.7	Eight PC girders	HP 310 ×132	58.7
Kalayci, Civjan, and Breña (2012)	225.3	Curved	2@112.7	Five steel plate girders	HP 360 ×174	37.7
Kim and Laman (2012)	426.7	0	89.3, 2@124, 89.3	Four PC girders	HP 310 ×110 (weak axis)	43
Kim and Laman (2012)	174.7	0	47.7, 89.3, 37.7	Four PC girders	HP 310 ×110 (weak axis)	45.3
Kim and Laman (2012)	115.7	0	115.7	Four PC girders	HP 310 ×110 (weak axis)	45.3
Kim and Laman (2012)	63	0	63	Four PC girders	HP 310 ×110 (weak axis)	45.3
Kirupakaran (2013)	210	10	60, 90, 60	Four PC girders	HP 250 × 62 (weak axis)	24
Kalayci et al. (2012); Civjan, Kalayci, Quinn, Brena, and Allen (2013)	123.3	15	123.3	Five steel plate girders	HP 310×125	47.3
Kalayci et al. (2012); Civjan et al. (2013)	143.3	0	143.3	Five steel plate girders	HP 310×125	34
Deng, Phares, Greimann, Shryack, and Hoffman (2015)	327.7	Curved	86.3, 151.3, 86.3	Four I-shaped plate girders	HP 250 × 85 (weak axis)	26.3

Note: PC = prestressed concrete; PPC = prestressed precast concrete; CFT = concrete-filled steel tube; HP = steel H-pile.
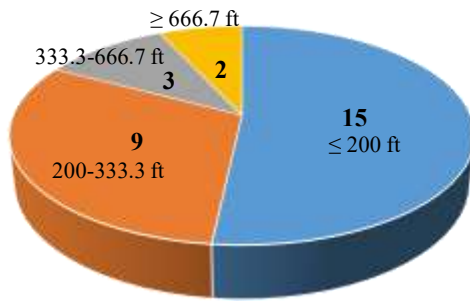
a. Total length of integral bridge
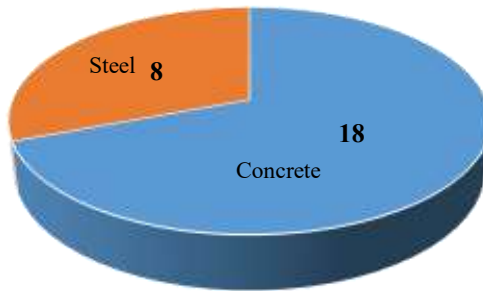
b. Material for bridge girders

c. Type of footing to support integral abutment
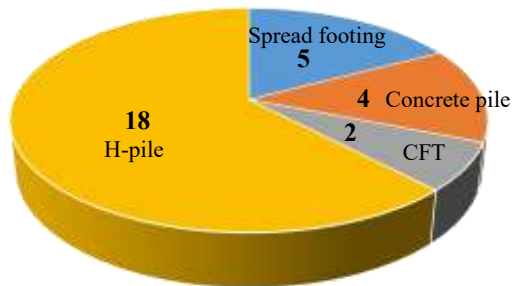
Figure 2.1: Integral Bridges Monitored in Field

Based on the field monitoring results of the integral bridges, the following conclusions can be made (Liu, Han, & Parsons, 2021b):

(a) Frame abutment bridges as an alternative for IABs should not exceed 200 ft in length. Over-lengthening and large restraint from backfill would over-stress bridge girders and decks at high temperatures.

(b) Measures have been used in the field to prevent failures of abutments and piles, such as a pressure relief system behind the abutment; non-rigid connections between the bridge girders and the abutment, or between the bridge abutment and the piles; and placement of compressible material (e.g., sand and aggregate) around H-piles.

(c) Effective bridge temperature (EBT) estimated based on air temperature can be used to predict the maximum bridge length change, but air temperature cannot represent the entire bridge temperature due to planar and vertical temperature gradients in the bridge.

(d) Abutment movement modes depend on several factors, such as abutment type, bridge length, and abutment height. For frame bridge abutments, expansion and contraction of the bridge have little effect on the bottom of the abutment. For tall H-pile-supported abutments, rotational movement of the abutment is likely the primary movement mode due to temperature changes.

(e) Pile axial load fluctuation with temperature change can be caused by redistribution of dead loads in the continuous frame structure due to temperature gradient and change of the vertical portion of the force from the backfill (i.e., larger uplift forces during bridge expansion, but smaller down-drag forces during bridge contraction). In addition, the bending moment perpendicular to the traffic moving direction on top of H-piles varies with bridge expansion and contraction.

(f) Mode and magnitude of abutment movement can affect the magnitude and distribution of lateral earth pressures behind the abutment. Earth pressure ratcheting was observed in some experimental studies but did not always occur in the field, due to the difference in the primary movement mode of the abutment.

(g) The skew effect on IAB behavior should be taken into account for design if the skew angle exceeds 10°. It is likely that the obtuse side of the abutment in a skewed bridge moves more into the backfill than the acute side when the bridge expands, and this skew effect diminishes with time.

2.3 Past Research about Traffic Loading

To mitigate the effects of the differential settlement at the interface between the abutment and the backfill on moving vehicles, an approach slab is commonly used to provide a smooth transition between the backfill and the bridge abutment. Figure 2.2 shows the approach slab distresses when an approach slab is adopted. As the backfill settles, the approach slab loses some support from the backfill, and more traffic load is transferred to the end of the approach slab near the adjacent pavement. Consequently, the end of the approach slab settles more than the adjacent pavement, generating a differential settlement (δ) at the joint between the approach slab and the adjacent pavement. A sleeper slab may be placed underneath the joint to mitigate the differential settlement between the approach slab and the adjacent pavement. In addition, the differential settlement between the two ends of the approach slab forms an abrupt change of the road gradient from the pavement to the bridge. Furthermore, the concave deformation of the approach slab due to traffic loading can aggravate this abrupt change of the road gradient. Reinforcing the soil under the sleeper slab with geosynthetics can increase the stiffness of the soil under the sleeper slab, thus reducing the differential settlement between the two ends of the approach slab. This technique will be discussed further in the following section.
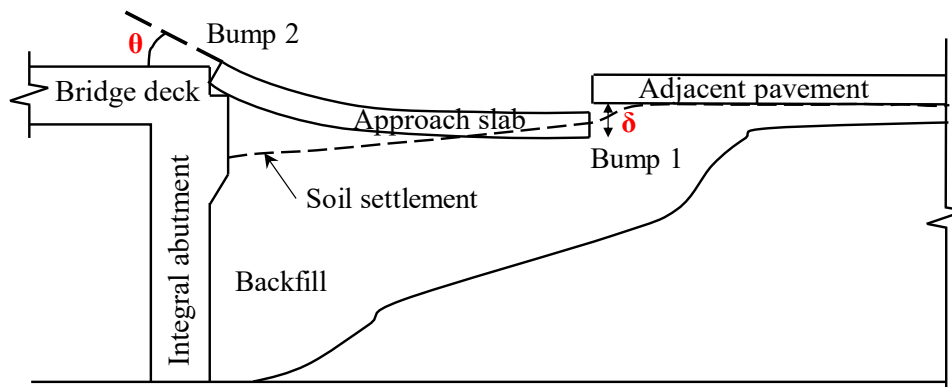
Figure 2.2: Approach Slab Distress

The research about the effects of traffic loading on the backfill settlements is limited. Seo (2003) developed a device with a circular track and conducted 16 small-scale physical model tests to evaluate the performance of approach slabs. The test wheel was driven around the circular track by a rotating arm powered by a motor. The physical model tests investigated the effects of several

17

parameters, including the type of approach slab (one-span or two-span), length of approach slab, soil type, velocity, and weight of the vehicle on the bump developed. From the test results, the following conclusions can be made: (a) good compaction of soil during construction could minimize the bump significantly and (b) the velocity as well as the weight of a vehicle could contribute to bump development.

2.4 Geosynthetic Reinforcement

Daily and seasonal temperature changes are a natural phenomenon, and therefore problems for integral abutment bridges due to expansion and contraction of bridge girders are inevitable and unavoidable (Horvath, 2000, 2004, 2005). Horvath (2000, 2005) suggested that effective mitigation measures for the temperature-induced problems for integral bridge abutments include (a) increasing the self-stability of the backfill when the abutment moves away from the backfill due to bridge girder contraction, thus reducing the backfill surface settlement and (b) placing a vertical layer of compressible inclusion between the back of the abutment and the backfill, thus reducing the relative movement between the abutment and the backfill when the abutment moves toward the backfill due to bridge girder expansion. Horvath (2000) conducted numerical analyses to study the mitigation measures for IBAs under four conditions: (a) unreinforced backfill; (b) Expanded Polystyrene (EPS) geofoam inclusion with unreinforced backfill; (c) EPS geofoam inclusion with reinforced backfill; and (d) EPS geofoam inclusion and EPS lightweight fill. Tatsuoka et al. (2009) conducted physical model tests and found that the backfill with horizontal geogrids not connected to the abutment reduced the backfill settlement, but increased the lateral earth pressures behind the abutment when no compressible inclusion was placed between the abutment and the backfill. Liu, Han, and Parsons (2021a) conducted six physical model tests to investigate the mitigation effects of EPS foam and geogrid reinforcements in the backfill to reduce the backfill surface settlements. EPS foam and geogrids with wrap-around facing could mitigate the lateral earth pressures behind the abutment and the backfill surface settlements. In addition, geogrid reinforcements under the sleeper slab could reduce the settlement of the sleeper slab and reduce the differential settlements between the two ends of the approach slab as a result. Chen and Abu-Farsakh (2016) investigated the effects of geogrid reinforcement on the backfill settlements

and contact stresses under the approach slab and the sleeper slab caused by a static 20-ton large cone truck in a field case study.

However, these numerical analyses, physical model tests, and the field case study had some limitations. First, the constitutive models used for the numerical analyses might not have accurately simulated the real behavior of materials including backfill and geosynthetics. Second, the pile-supported abutment was assumed to rotate only about its base, which might be different in the field (Darley, Carder, & Barker, 1998; Huntley & Valsangkar, 2013, 2014; Lawver, French, & Shield, 2000). Third, to the authors' best knowledge, no physical model tests were done to investigate the combined effects of temperature changes and traffic loading, and the mitigation benefits of geosynthetics to reduce backfill surface settlement.

Chapter 3: Physical Model Tests

This chapter first introduces a dimensional analysis of physical model tests and then describes the physical model tests including the test setup, plan, construction and testing procedure, and monitoring system. This chapter also describes the property tests for the materials (Kansas River sand and geogrid) used in this study.

3.1 Dimensional Analysis

Before the selection of dimensions of the model and magnitude of traffic load, a dimensional analysis was performed in this study. The scale factor for the model dimensions was selected as 1/5 to the dimensions of a typical bridge abutment in field as a prototype model (i.e., 18.3 ft high). The model dimensions were selected according to this scale factor. Details about these dimensions will be presented in the next section. A similar scale factor was used by other researchers at the University of Kansas for other geosynthetic-reinforced retaining wall studies using the same test box (e.g., Jawad, Han, Al-Naddaf, & Abdulrasool, 2020; Kakrasul, Han, & Rahmaninezhad, 2020). The same type of geogrid as that used in Jawad et al. (2020) and Kakrasul et al. (2020) was used in this study as well.

To determine the magnitude of the traffic load needed for this study, the first step of dimensional analysis was to define the variables affecting the settlements of the backfill and the sleeper slab. Since displacement of abutment top (δ), abutment bending stiffness (E_1I_1, E_1 is concrete elastic modulus and I_1 is abutment moment of inertia), abutment thickness (D_1), abutment height (H), approach slab stiffness (E_2I_2, E_2 is concrete elastic modulus and I_2 is approach slab moment of inertia), approach slab thickness (D_2), backfill Young's modulus (E_3), backfill depth (D_3) and traffic load (f) all affect the backfill surface settlements and the settlements of the sleeper slab, they were considered as parameters as listed in Table 3.1.

After defining these parameters, they were grouped into three groups including the force group (i.e., F Group), the time group (T Group), and the length group (L group) as did by Seo (2003). Then a variable was selected from each group as the repeating variable, and the rest of the variables were termed as nonrepeating variables. In this study, the traffic load (f), the approach slab thickness (D_1), and the gravity (g) were chosen to be repeating variables. Dimensional analysis

requires that the product of power of repeating variables and each nonrepeating variable becomes one (i.e., the product should be dimensionless). Table 3.2 lists the group and its corresponding variables and repeating variables.

Table 3.1: Parameters and Dimensions

Quantity	Parameters	Dimension
Abutment top displacement	Δ	L
Abutment bending stiffness	$E_1 I_1$	FL^2
Abutment thickness	D_1	L
Abutment height	H	L
Approach slab bending stiffness	$E_2 I_2$	FL^2
Approach slab thickness	D_2	L
Backfill Young's modulus	E_3	F/L^2
Backfill height	D_3	L
Traffic load	f	FT^2/L
Gravity	G	L/T^2

Table 3.2: Group and Variables

Group	Variables	Repeating Variable
F Group	$E_1 I_1$, $E_2 I_2$, E_3, f	f
L Group	δ, D_1, H, D_2, D_3	D_1
T Group	G	g

Equation 3.1 through Equation 3.6 show the calculation procedure and the result of the Young's modulus of the backfill as an example:

$$\pi_1 = E_3{}^a f^b D_1^c g^d \rightarrow \left(\frac{F}{L^2}\right)^a \left(\frac{FT^2}{L}\right)^b (L)^c \left(\frac{L}{T^2}\right)^d = 1$$

Equation 3.1

$$F^a \cdot F^b \rightarrow a + b = 0$$

Equation 3.2

$$L^{-2a} \cdot L^{-b} \cdot L^c \cdot L^d \rightarrow c + d - 2a - b = 0$$

Equation 3.3

$$T^{2b} \cdot L^{-2d} \rightarrow 2b - 2d = 0$$

Equation 3.4

If $a = 1$, then $b = -1, d = -1$, and $c = 2$

$$\pi_1 = \frac{E_3 D_1^2}{fg}$$

The dimensions for the model could be determined from the following equation:

$$(\pi_1)_{prototype} = \left[\frac{E_3 D_1^2}{fg}\right]_{prototype} = (\pi_1)_{model} = \left[\frac{E_3 D_1^2}{fg}\right]_{model}$$

In the same manner, Equation 3.7 through Equation 3.12 were obtained and used for the dimensional analysis:

$$\pi_2 = \delta^a f^b D_1^c g^d \rightarrow \pi_2 = \frac{\delta}{D_1}$$

$$\pi_3 = (E_1 I_1)^a f^b D_1^c g^d \rightarrow \pi_3 = \frac{E_1 I_1}{f D_1^2 g}$$

$$\pi_4 = H^a f^b D_1^c g^d \rightarrow \pi_4 = \frac{H}{D_1}$$

$$\pi_5 = (E_2 I_2)^a f^b D_1^c g^d \rightarrow \pi_5 = \frac{E_2 I_2}{f D_1^2 g}$$

$$\pi_6 = D_2^a f^b D_1^c g^d \rightarrow \pi_6 = \frac{D_2}{D_1}$$

$$\pi_7 = D_3{}^a f^b D_1^c g^d \rightarrow \pi_7 = \frac{D_3}{D_1}$$

Because the 28-day compressive strength of concrete (fc) used in this study was 5.9 ksi, its elastic modulus was 4351 ksi according to $E_a = 57000\sqrt{f_c}$ (ACI Committee 318, 2008). The integral abutment, the approach slab, and the sleeper slab in the prototype were assumed to be made of the same concrete material as the one in this study. In addition, the typical Young's modulus of the backfill material in the prototype was assumed to be approximately 5.8 ksi (Caristo,

Barnes, & Mitoulis, 2018). According to AASHTO (2012), the maximum axle load of the H-20 design truck is 32 kips and the typical lane width is approximately 10 to 12 ft; therefore, the wheel load of 16 kips is applicable to one half of a lane (5 ft). According to the dimensional analysis results, a traffic load of 0.7 kips was needed, but a load of 674 lb was selected in this study for convenience in the physical model tests to represent a 32-kip axle load of the H-20 design truck on a lane in real projects. Table 3.3 shows the dimensional analysis results and the parameters adopted in this study.

Table 3.3: Dimensional Analysis Results

Quantity	Symbol	Prototype	Model (Target)	Model (actual)
Abutment top displacement (in)	δ	6	1.2	1.2
Abutment bending stiffness (lb·ft^2)	E_1I_1	1.96×10^9	3.15×10^6	3.15×10^6
Abutment thickness (in)	D_1	24	4.8	4.8
Abutment height (ft)	H	18.3	3.66	3.66
Approach slab bending stiffness (lb·ft^2)	E_2I_2	1.42×10^8	2.27×10^5	2.27×10^5
Approach slab thickness (in)	D_2	10	2	2
Backfill Young's modulus (ksi)	E_3	5.80	5.80	1.45
Backfill height (ft)	D_3	17.5	3.5	3.5
Traffic load (lb)	f	1.6×10^4	639	661
Gravity (ft/sec^2)	g	32.14	32.14	32.14

3.2 Test Setup

Figure 3.1 shows the main components of the test setup for a physical model used in this study including the abutment, the manual jack, the vertical cylinder, the backfill, the approach slab, the sleeper slab, and the adjacent pavement. Wooden plates with a thickness of 2 inches were bolted to the test box frame which was built by welding steel tube beams together to form the rear, bottom, and right sides of the test box. For ease of construction, the front side of the test box was built by placing three Plexiglas plates with steel angles from the bottom to the top during backfill placement. To ensure the rigidity of the front side, one tube beam was placed beside the steel angle of each Plexiglas plate and was bolted to the test box frame. In addition, the test box frame was fixed to a reaction frame to prevent movement of the test box. A manual jack was utilized to push the abutment toward the backfill and pull the abutment away from the backfill to simulate

expansion and contraction of bridge girders, respectively. One end of the manual jack was connected with the reaction frame and the other end was connected to the abutment top (at the height of 39 inches) by a hinge and a load cell. The hinge eliminated any moment to be applied to the abutment top, while the load cell measured the force required to push and pull the abutment top. After the abutment top was displaced to simulate seasonal temperature changes, the manual jack was used to simulate the bridge girder to investigate the performance of the abutment under traffic loading. The hydraulic cylinder was used to apply loads on the approach slab 2 ft away from the back facing of the abutment to simulate traffic loading. The top end of the cylinder was fixed to the test box frame, while the bottom end was connected with a strip footing by a hinge and a small load cell. The steel strip footing was 12 in. long, 4 in. wide, and 0.4 in. thick. Because the top surface of the pre-cast approach slab was not finished perfectly smooth during its casting, a rubber plate with dimensions of 12 in. long, 6 in. wide, and 0.2 in. thick was attached to the bottom of the steel strip footing to improve the contact between the strip footing and the approach slab during traffic loading.
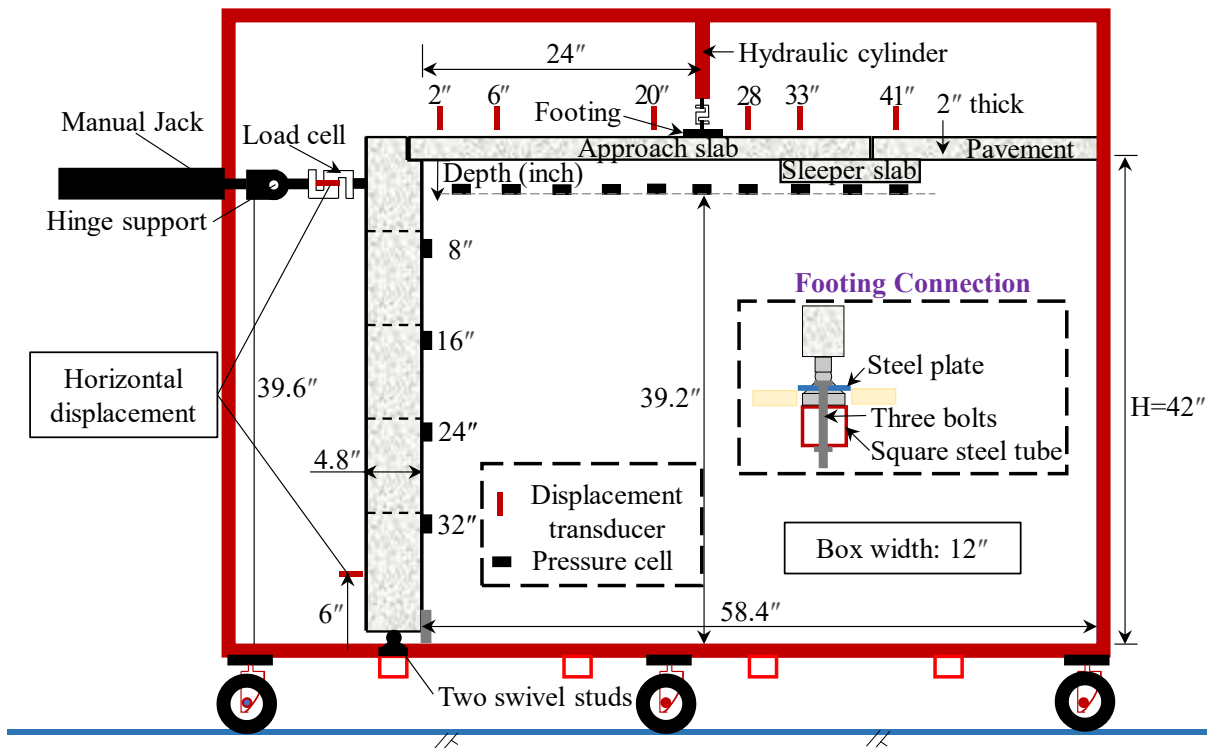

Figure 3.1: Test Setup of the Physical Model Test (modified from Liu et al., 2021a)

The height of an integral bridge abutment could be as high as 20 ft (Horvath, 2000; Kim & Laman, 2012), and the thickness of a 20 ft high integral abutment could be 2 ft (Horvath, 2000). Different state Departments of Transportation (DOTs) used different specifications for dimensions of the approach slabs and the sleeper slabs. The shortest and longest lengths of approach slabs were 10 ft and 40 ft, respectively, while the thickness of approach slabs ranged from 8 in. for a 15 ft long slab to 17 in. for a 30 ft long slab (Hoppe, 1999; Thiagarajan et al., 2010). A sleeper slab is commonly placed underneath the joint between the approach slab and the adjacent pavement to reduce the differential settlement between them. According to Chen and Abu-Farsakh (2016), two thirds of the sleeper slab was placed underneath the approach slab, while the rest was placed underneath the adjacent pavement.

For this study the physical model was designed at a ratio of 1/5 to the prototype model. The prototype integral abutment adopted in this study was 18.3 ft high and 2 ft thick (3.7 ft high and 4.8 in. thick for the model integral abutment). The approach slab, the sleeper slab, and the concrete pavement in the prototype were 10 in. thick (2 in. thick for the model slabs and pavement), and the approach slab and the sleeper slab were 16.7 ft and 5.0 ft long (3.3 ft long for the model approach slab and 1 ft long for the model sleeper slab), respectively. The left end of the approach slab with a length of approximately 1 in. was supported by the bridge abutment, while the right end of the approach slab with a length of approximately 8 in. was placed on top of the sleeper slab. The bottom of the sleeper slab was 3.3 ft above the bottom of the backfill. Joints with a width of approximately 0.2 in. between the approach slab and the bridge abutment, between the approach slab and the adjacent pavement, and between adjacent pavement and the right side of the text box were included for the abutment top cyclic movements and traffic loading.

The five abutment blocks of the abutment, the approach slab, the adjacent pavement, and the sleeper slab were pre-cast using a quick concrete mix and its compressive strengths measured at 7 and 28 days were 4.7 and 5.9 ksi, respectively. A short-threaded rod with two nuts was pre-cast into the top block to serve as a connector with the hinge, while two coupling nuts were pre-cast into the bottom block to serve as the connectors between the abutment and the two swivel studs. In addition, three holes were blocked out in the bottom block for tightening the three nuts on the threaded rods. Furthermore, three holes were blocked out in all the five concrete blocks for

the three thread rods to go through during abutment construction. To reinforce the top and bottom blocks, a layer of steel rebar mesh was placed in the middle of each concrete block. The assembled abutment was 3.7 ft high, 4.8 in. wide, and 12 in. thick.

Double plastic sheets with grease between were placed between the backfill material and the front, rear, and bottom sides of the test box to reduce the boundary effects. Since the right side of the test box was 39 inches away from the potential Rankine active failure plane, no measures were taken to mitigate the boundary effects between the backfill material and the right side of the test box. For the approach slab supported by the integral bridge abutment, the backfill material, and the sleeper slab, the traffic load transferred to the abutment was expected to decrease but the traffic load transferred to the sleeper slab was expected to increase as the traffic load moved away from the back facing of the abutment. The distance between the center of the strip footing (i.e., traffic load) and the back facing of the abutment (2 ft) was chosen as 2 ft (i.e., two times the length of the sleeper slab (1 ft)); therefore, most of the traffic load was expected to transfer to the backfill and the sleeper slab. Considering a combined behavior of translation and rotation for integral bridge abutments in response to seasonal temperature changes (Darley et al., 1998; Lawyer et al., 2000), a special footing connection, as shown in Figure 3.1, was adopted to allow limited translation of the abutment toe without preventing the abutment from free rotation.

According to Younan and Veletsos (2000), relative flexibility (d_w) of a wall was the primary parameter affecting the response of a wall-soil system. Since an integral abutment functions as a retaining structure to retain the backfill, the relative flexibility of the abutment can be defined as follows:

$$d_w = 12(1 - v_a^2)\frac{G_b}{E_a}\left(\frac{H}{t_a}\right)^3 = \frac{6E_b(1 - v_a^2)}{E_a(1 + v_b)}\left(\frac{H_b}{t_a}\right)^3$$

Equation 3.13

Where:

E_a & E_b = Young's moduli of the abutment and the backfill, respectively,

t_a = the thickness of the abutment (4.8 in. in this study),

H_b = the backfill height (42 in. in this study),

v_a & v_b = Poisson's ratios of concrete (0.20) and the backfill, respectively, and

G_b = the shear modulus of the backfill.

The 28-day compressive strength (f_c) of the concrete was 5.9 ksi; therefore, Young's modulus of the abutment was 4351 ksi based on the equation $E_a = 57000\sqrt{f_c}$ (ACI Committee 318, 2008). According to Al-Naddaf (2019), the Young's modulus and Poisson's ratio of the backfill (dense sand) were estimated as 3.6 ksi and 0.3, respectively. Therefore, the relative flexibility of the abutment was 2.47, indicating the abutment was rigid (Ertugrul & Trandafir, 2013, 2014).

3.3 Test Plan

Table 3.4 lists the plan of the six model tests conducted in this study and Figure 3.3 shows their cross sections. Test T1 investigated the effects of seasonal temperature changes on backfill surface settlements and lateral earth pressures behind the abutment, while Test T2 investigated the combined effects of seasonal temperature changes and traffic loading on backfill surface settlements and lateral earth pressures behind the abutment. Test 3 used geogrids to reinforce the soil under the sleeper slab to reduce traffic loading-induced settlements of the sleeper slab and the backfill surface settlement, while Test T4 and Test T5 used horizontal geogrids and geogrids with wrap-around facing to reduce the backfill surface settlement induced by seasonal temperature changes and traffic loading, respectively. However, since the geogrids in Test T4 and the horizontal portion of the geogrids in Test T5 were 2.5 ft long (i.e., the rear end of the geogrids in Test T4 and Test T5 was 31 in. away from the back facing of the abutment) and the left end of the sleeper slab was 31 in. away from the back facing of the abutment. The geogrids in Test T4 and Test T5 only provided lateral restraint to the soil under the left side of the sleeper slab. In Test T6, the length of the horizontal portion of the top two geogrid layers with wrap-around facing was increased to 54 in. so that the top two geogrid layers could also reinforce the soil under the right side of the sleeper slab.

Table 3.4: Test Plan

Test No.	Reinforcement of backfill	Reinforcement under sleeper slab	Traffic loading
T1	NO	NO	NO
T2	NO	NO	YES
T3	NO	YES	YES
T4	Horizontal geogrids	NO	YES
T5	Wrap-around geogrids	NO	YES
T6	Wrap-around geogrids	YES	YES
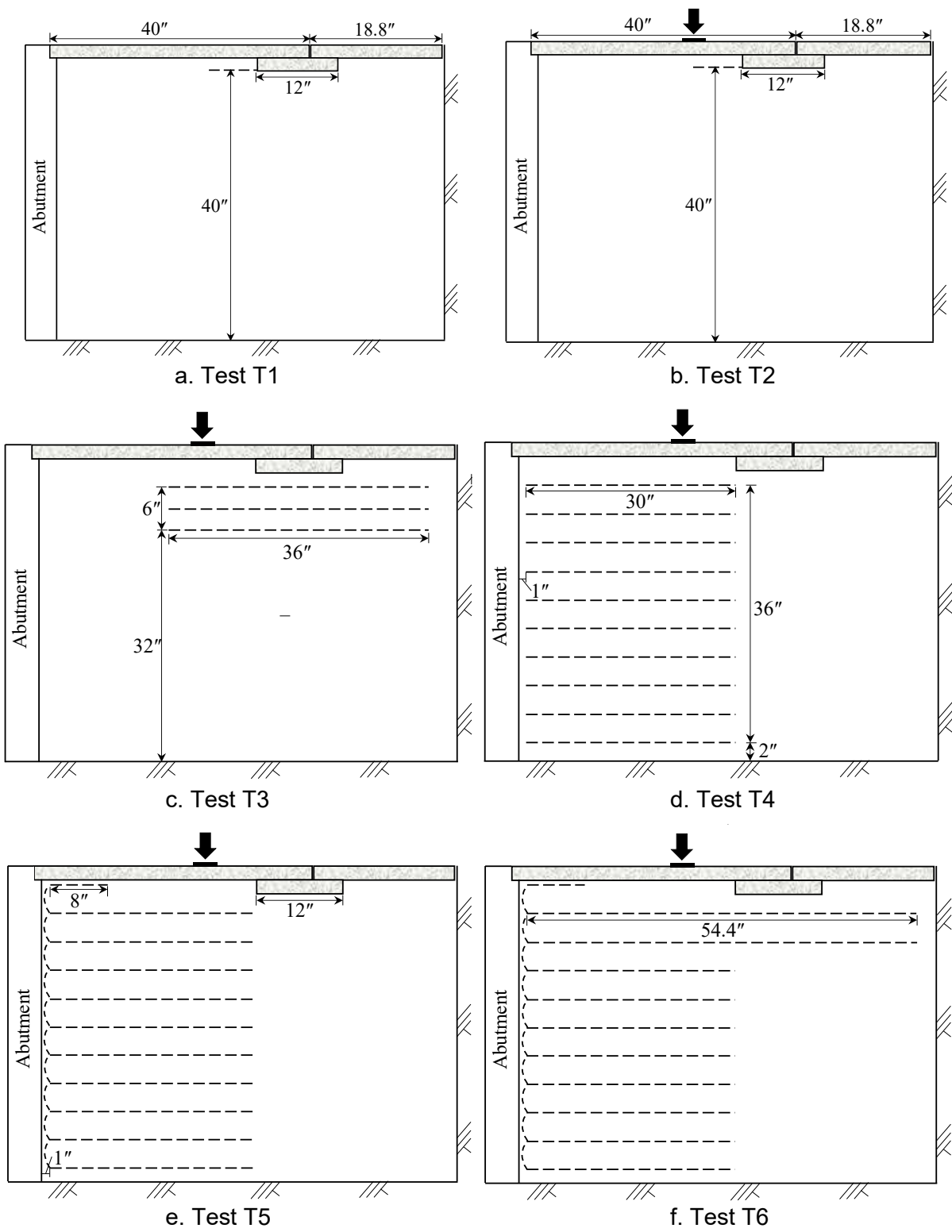
Figure 3.2: Cross Sections of Model Tests

3.4 Backfill and Geogrid

### 3.4.1 Kansas River sand

Kansas River sand was chosen as the backfill material and its properties are provided in Table 3.5. Han, Wang, Al-Naddaf, and Xu (2017) reported that the coefficients of uniformity (C_u) and curvature (C_c) of this sand were 3.18 and 0.99, respectively, and its minimum and maximum dry unit weights were 102 and 120 pcf, respectively. The backfill was compacted by a hand tamper to a relative density (D_r) of 75% (dry unit weight of 115 pcf) using the mass-volume control method in the model tests.

Table 3.5: Parameters of Kansas River Sand

Parameter	Value
Coefficient of uniformity, C_u	3.18
Coefficient of curvature, C_c	0.93
Mean particle size, D_{50}	0.236 in
Classification (USCS)	Poorly graded sand (SP)
Maximum dry weight, γ_{dmax}	120 pcf
Minimum dry weight, γ_{dmin}	102 pcf
Relative density, D_r	75%
Unit weight at D_r=75%, γ	115 pcf

Figure 3.3 shows the results of four direct shear tests conducted for the Kansas River sand at D_r=75% under the normal stresses of 7.3, 14.5, 21.8, and 29.0 psi. Figure 3.4 shows the results of triaxial compressive tests of this sand under the confining stresses of 8.3, 15.4, and 22.6 psi. The direct shear tests showed that the peak and residual friction angles of this sand were 42.1° and 33.6°, respectively, while the triaxial compression tests indicated that the peak and residual friction angles of this sand were 40.7° and 36.3°, respectively.
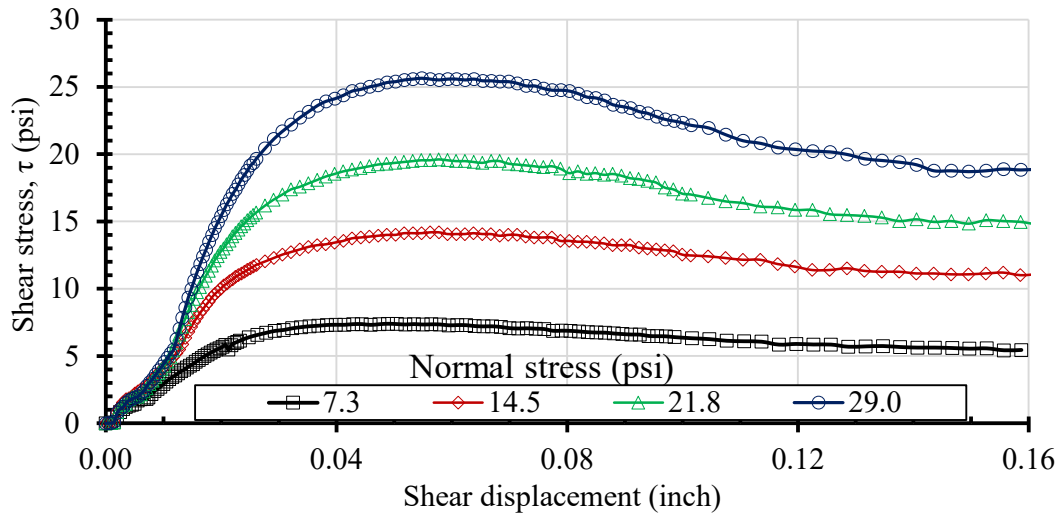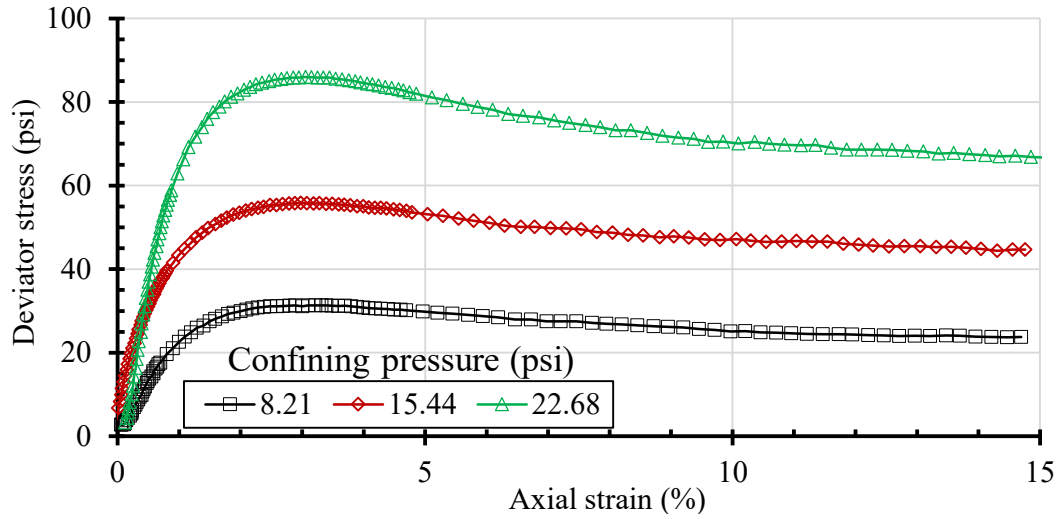
a. Shear stress versus shear displacement
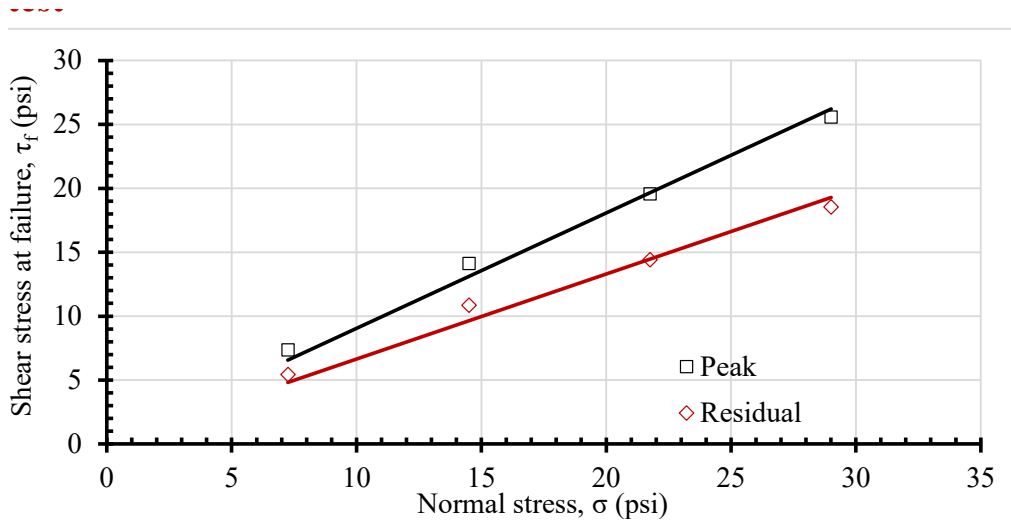
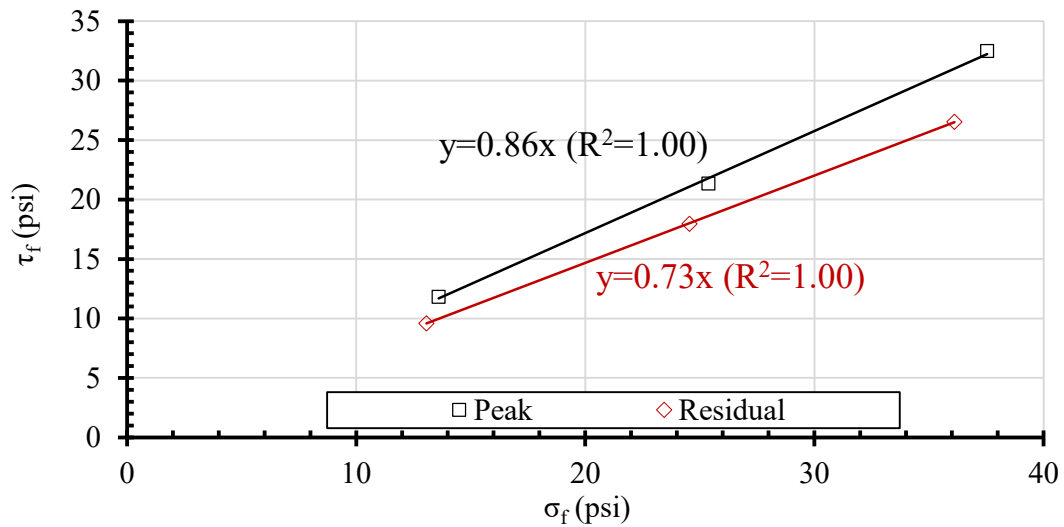

b. Peak and residual strength envelops

Figure 3.3: Direct Shear Test Results

a. Deviator stress versus axial strain

b. Peak and residual strength envelops

Figure 3.4: Triaxial Compressions Test Results

3.4.2 Geogrid reinforcement

Uniaxial geogrids have been commonly used to reinforce backfill in mechanically stabilized earth (MSE) walls (Abu-Hejleh, Wang, & Zornberg, 2000; Abu-Hejleh, Zornberg, Wang, McMullen, & Outcalt, 2001; Pierson, Parsons, Han, & Brennan, 2011; Jiang, Han, Parsons, & Brennan, 2016). Punched-drawn uniaxial geogrids typically have aperture sizes of 10 to 20 inches in the longitudinal direction in practice. Xiao, Han, and Zhang (2016) conducted a scale analysis for model MSE walls with similar dimensions and selected a weak punched-drawn biaxial

geogrid made of polypropylene that was modified by cutting of two out of every four ribs to simulate the uniaxial geogrid. The modified geogrid is referred to as the model uniaxial geogrid in this report. Table 3.6 shows that the ultimate tensile strength of the biaxial geogrid in the cross-machine direction was 1.3 kip/ft while Figure 3.5 shows that the ultimate tensile strength of the geogrid in the cross-machine direction after ribs were removed was 1.2 kip/ft (i.e., slightly reduced).

Table 3.6: Properties of Biaxial Geogrid

Index properties	MD	XMD
Aperture dimensions (in)	1.0	1.3
Minimum rib thickness (in)	0.03	0.03
Tensile strength at 2% strain (lb/ft)	281	452
Tensile strength at 5% strain (lb/ft)	582	918
Ultimate tensile strength (lb/ft)	850	1302

Note: MD = machine direction and XMD = cross-machine direction
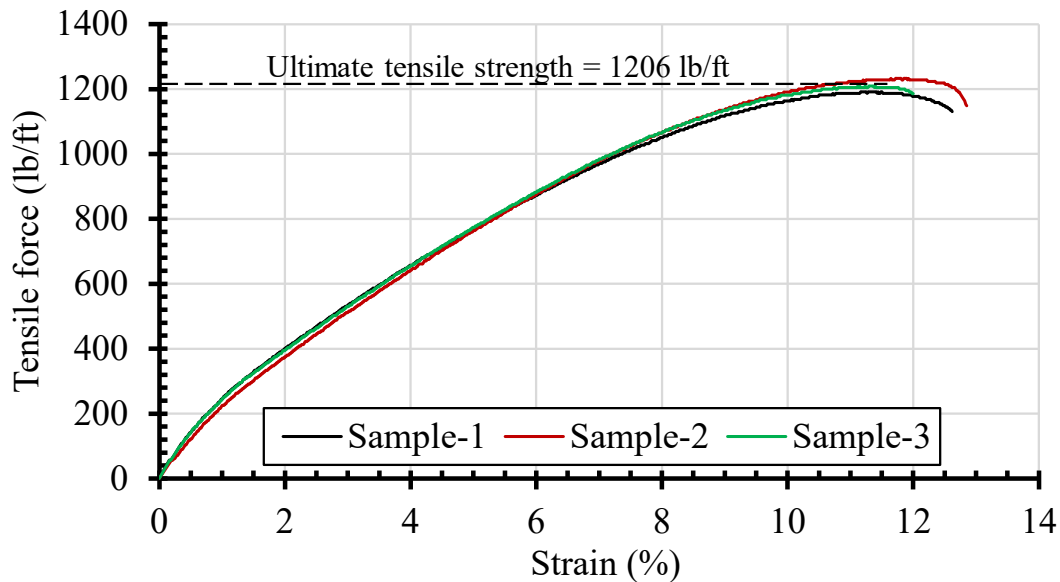
**Figure 3.5: Tensile Force versus Strain of the Model Uniaxial Geogrid**

Figure 3.6 shows the pullout test results of the geogrid after removal of ribs under normal stresses of 0.5, 1.1, and 1.6 psi, showing that the interface friction angle between the geogrid and the Kansas River sand at D_r=75% was 31.7°. Given that the peak friction angle of the sand was

42.1° from the direct shear tests, the interaction coefficient or reduction factor (R_{int} = $tan31.7°/tan42.1°$) between the geogrid and the sand was 0.68.
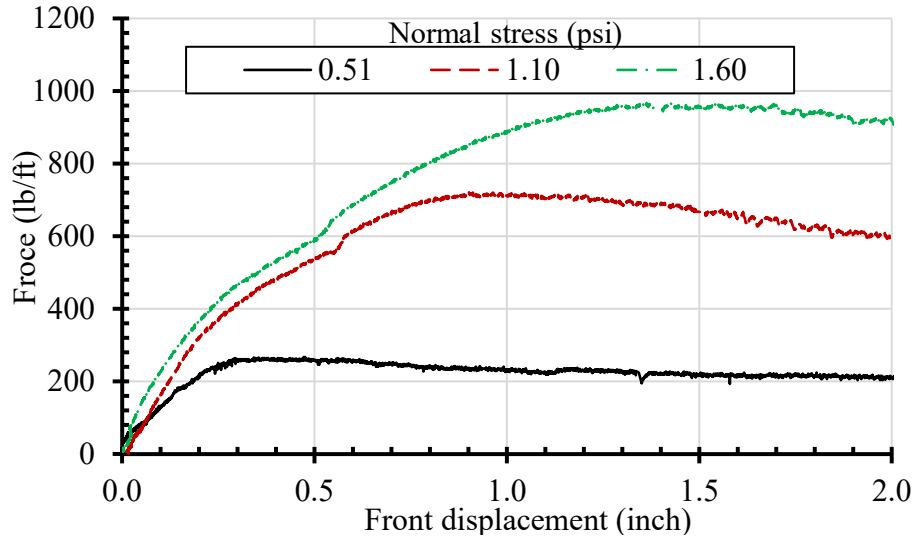
a. Force versus front displacement
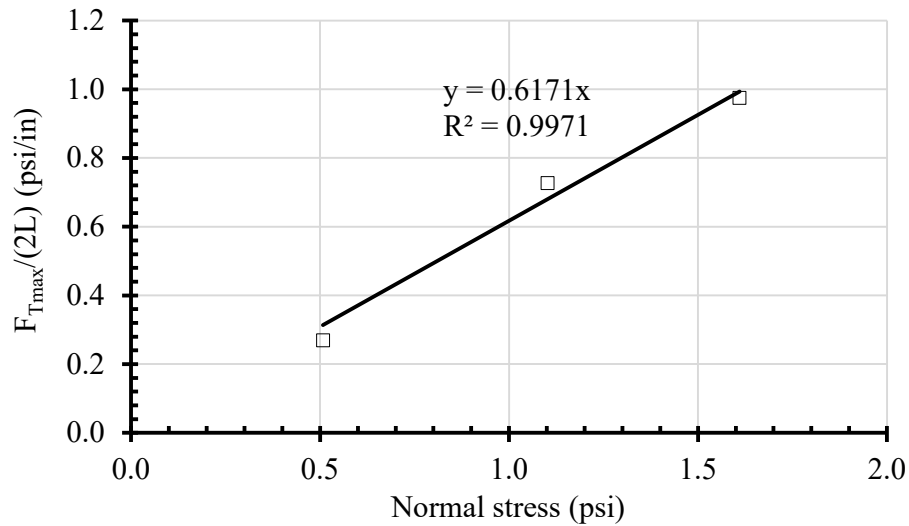
b. Peak shear stress versus normal stress

Figure 3.6: Pullout Test Results of the Model Uniaxial Geogrid in the Sand

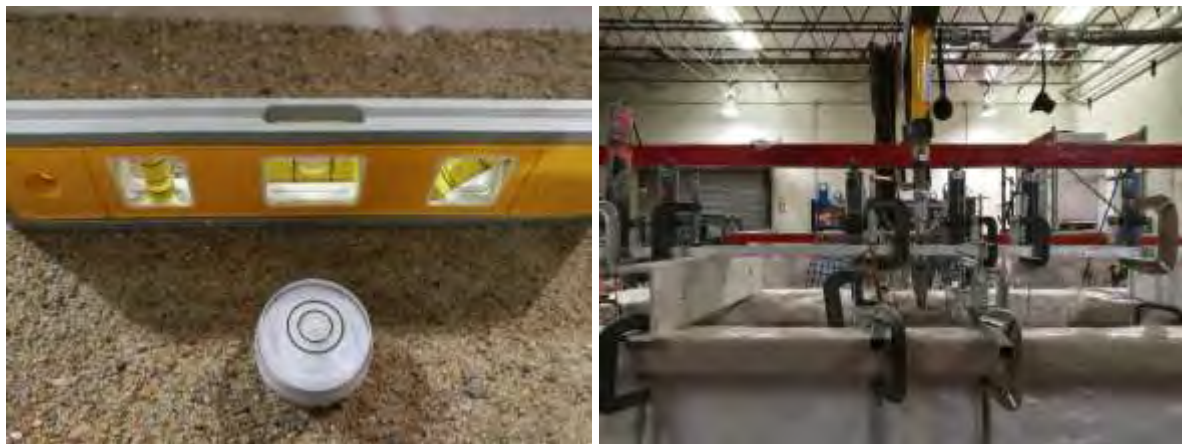## 3.5 Construction and Instrumentation

Before placement of the backfill, the abutment was supported by the footing connection and the manual jack. Two displacement transducers (DT) (i.e., the top DT at the height of 39 in.

and the bottom DT at the height of 6 in.) were fixed onto the test box frame to measure the abutment movements. Four earth pressure cells were attached onto the back face of the abutment, after which the double plastic sheet was placed around the rear, bottom, and front sides of the test box. In Test T5, the front portion of a first geogrid layer was placed vertically and leaned against the back face of the abutment after the first lift (2 in. thick) of sand was placed and compacted. After the second lift (4 in. thick) of the backfill was placed and compacted, the front geogrid portion was wrapped around the second lift of the backfill and then pulled back a little to create a gap between the wrap-around face and the back face of the abutment to be filled with sand later. A small piece (10 in. wide and 14 in. long) of nonwoven geotextile was placed between the wrap-around facing of the geogrid layer and the backfill to prevent the sand from flowing through the geogrid apertures. The same process was repeated until the last layer of geogrid was installed. The earth pressure cells in the backfill and under the sleeper slab were installed during the placement of the last lift of the backfill. After placement and compaction of the backfill, the approach slab and the adjacent pavement were placed on top of the backfill surface and the sleeper slab, and then six DTs were installed on the text box frame to measure the settlements of the backfill surface and the sleeper slab using tell-tales. All other test models were constructed in a similar way with some exceptions for Test T1, Test T2, and Test T3. The thickness of the uppermost lift of the backfill in Test T1 to Test T3 and the bottom (first) lift in Test T4 to Test T6 was 2 in., and no wrap-around facing was used in Test T4. Before starting the test, all readings of the load cells, the earth pressure cells, and the displacement transducers were zeroed out to focus on the effects of temperature changes and traffic loading. Figure 3.7 shows the construction and instrumentation of the model for Test T4.

Figure 3.7: Model Construction and Instrumentation in Test T4
(a) Placement of horizontal geogrid, (b) Placement of earth pressure cells, (c) Leveling of backfill surface, (d) Installation of DTs to measure backfill surface settlement

3.6 Testing Procedure

In each test, the abutment had four positions as shown in Figure 3.8 to simulate the abutment at four different seasons in one year. The abutment was assumed to construct in the spring as Position I. Position II, Position III, and Position IV represented the abutment at the positions in the summer, fall, and winter.
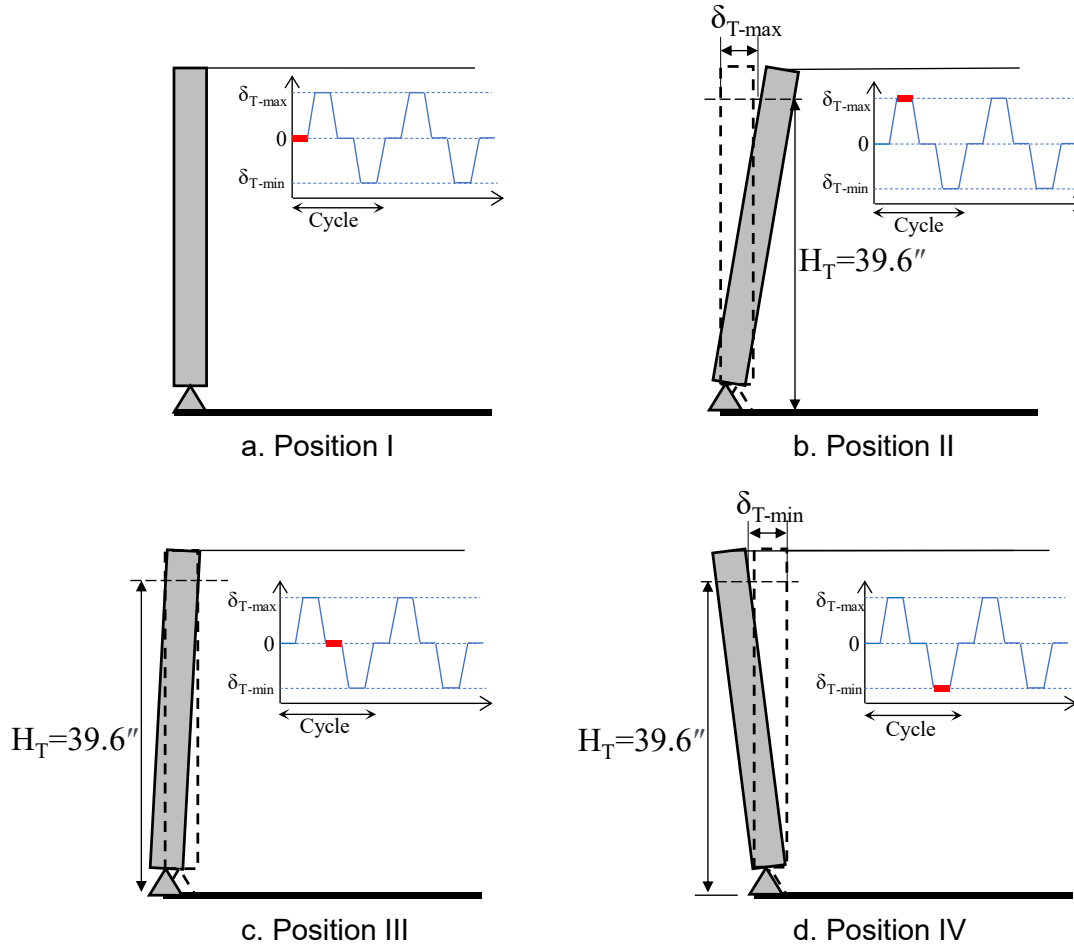
Figure 3.8: Positions of the abutment during each seasonal temperature change: (a) Position I; (b) Position II; (c) Position III; and (d) Position IV

Figure 3.9 shows the abutment top cyclic movements and traffic loading. After construction of each physical model, the manual jack pushed the abutment top at the height of 39 in. toward the backfill from Position I (δ_T=0.00 in.) to Position II (δ_T=0.12 in.) to simulate the temperature increase from the spring to the summer, after which the manual jack pulled the abutment top from Position II to Position III (δ_T=0.00 in.) and then to Position IV (δ_T=-0.12 in.) for simulations of the temperature decrease from the summer to the fall and then to the winter. Finally, the manual jack pushed the abutment top back to Position I to complete a seasonal temperature change cycle. In total, 10 abutment top movement cycles were applied to investigate the behavior of the backfill due to seasonal temperature changes. For each abutment top movement cycle, there were four positions (from Position I to Position IV) to simulate the four seasons (from the spring to the winter). In Test T2 through Test T6, 100 cycles of traffic loading were applied on

the approach slab at each position of every abutment top movement cycle; therefore, each position of abutment top in the Test T2 through Test T6 could be divided into three phases: before traffic loading, during traffic loading, and after traffic loading.

a. Abutment top cyclic movement

b. Traffic loading (if any) at each position of abutment top
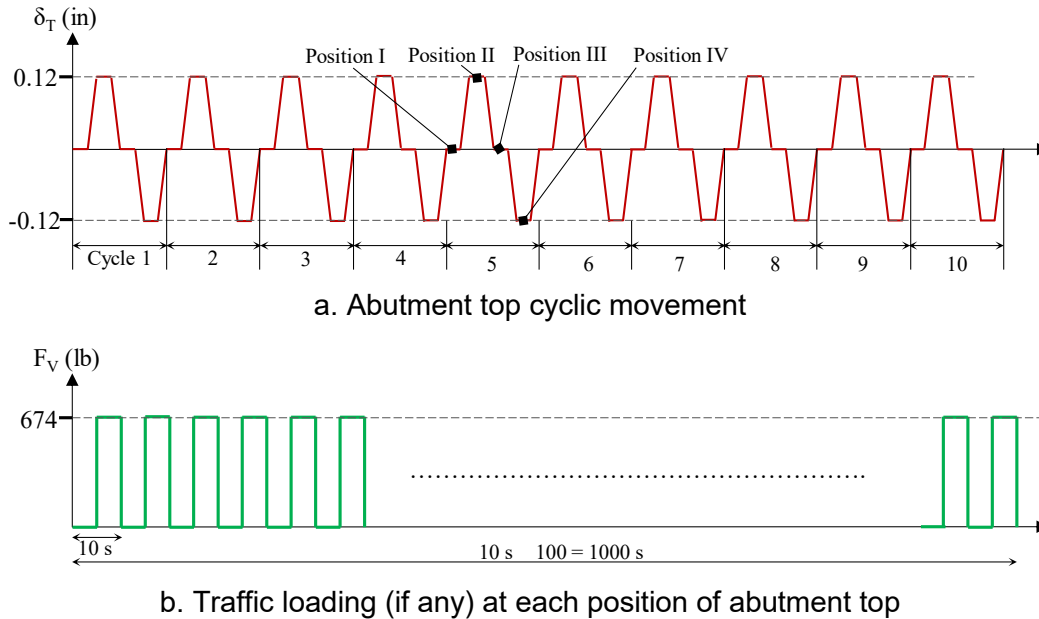
Figure 3.9: Test Procedure

3.7 Monitoring

In addition to the two load cells (LCs) used to measure the horizontal force to hold the abutment in place and the vertical (traffic) load, 14 earth pressure cells (EPCs) and eight displacement transducers (DTs) were used in each test. Four EPCs were attached to the back face of the abutment to measure lateral earth pressures behind the abutment at depths of 8, 16, 24 and 32 in. from the top, respectively; while another 10 EPCs were placed horizontally under the approach slab to monitor contact stresses caused by traffic loading at different distances from the back face of the abutment. Two DTs (top DT at the height of 39 in. and bottom DT at the height of 6 in.) were used to control and record the abutment movements, while the other six DTs were used to monitor the backfill surface settlements at distances of 2, 6, 20, 28, 33 and 41 in. from the back face of the abutment, respectively, through tell-tales. The readings of the two DTs at distances of 33 and 41 in. away from the back face of the abutment were the settlements at the left and right sides of the sleeper slab.

Chapter 4: Test Results and Analysis of Physical Models during Construction

This chapter presents the analysis of the data obtained from the earth pressure cells, the load cell, and the displacement transducers during placement and compaction of the backfill in all the physical model tests. The effects of horizontal geogrid reinforcements and geogrid wrap-around facing on the measured lateral earth pressures and displacements are examined.

4.1 Lateral Earth Pressure

Before examining the measured lateral earth pressures in each model in this study, it is important to understand the effect of compaction on the distribution of lateral earth pressures behind a wall. Duncan, Williams, Sehn, and Seed (1991) found that when a backfill was compacted against a non-yielding structure, the residual lateral earth pressure in the compacted soil could be higher than that in the uncompacted soil, and it even approached the passive earth pressure of the backfill near the surface. The higher lateral earth pressure and coefficient are credited to the higher over-consolidation ratio (OCR) of the backfill after compaction. Mayne and Kulhawy (1982) developed a relationship between the at-rest earth pressure coefficient K_0 and the OCR of a soil as shown in Equation 4.1 and K_0 can be calculated using the internal friction angle (φ) and OCR of the soil:

$$K_0 = (1 - sin\varphi) \cdot OCR^{sin\varphi}$$

Equation 4.1

Based on the friction angle of the Kansas River sand (i.e., $\varphi = 42.1°$ from the direct shear tests), K_0 was calculated as 0.33.

For some numerical analyses (e.g., Hatami & Bathurst, 2006; Guler, Hamderi, & Demirkan, 2007; Huang, Han, Parsons, & Pierson, 2013), a uniform surcharge pressure was applied on the top of each backfill lift to simulate compaction. The magnitude of the surcharge pressure depends on compaction equipment. A surcharge pressure of 8 kPa has been commonly used to simulate typical compaction equipment in field (e.g., Hatami & Bathurst, 2006; Guler et al., 2007). Considering lower compaction energy was used in the laboratory tests in this study, a surcharge

pressure of 0.29, 0.58, or 1.16 psi was evaluated. It is assumed that this surcharge pressure results in an over-consolidated condition at a depth from the backfill surface with an OCR value as follows:

$$OCR = (\gamma z + p)/(\gamma z)$$

<div align="right">**Equation 4.2**</div>

Where:

γ = the unit weight of the backfill,

z = the depth from the backfill surface, and

p = the surcharge pressure due to compaction.

Figure 4.1 shows the calculated coefficient of lateral earth pressure behind the abutment during the backfill placement using Equation 4.1 and Equation 4.2. The coefficient of lateral earth pressure decreased as the depth from the backfill surface increased and then approached the normally-consolidated at-rest coefficient (OCR=1). The depth at which the coefficient of lateral earth pressure decreased close to the normally-consolidated at-rest coefficient is referred to as the influence depth due to compaction. Figure 4.1 indicates that the influence depth and the lateral earth pressure coefficient within this influence depth increased as the surcharge pressure increased. In addition, the lateral earth pressure coefficient below the influence depth converged to the normally-consolidated at-rest coefficient, which was also found by Chen and Fang (2008).
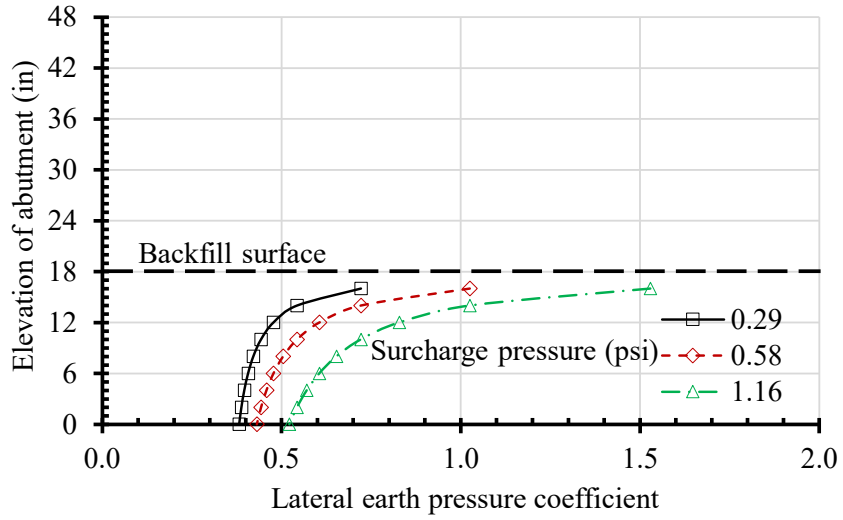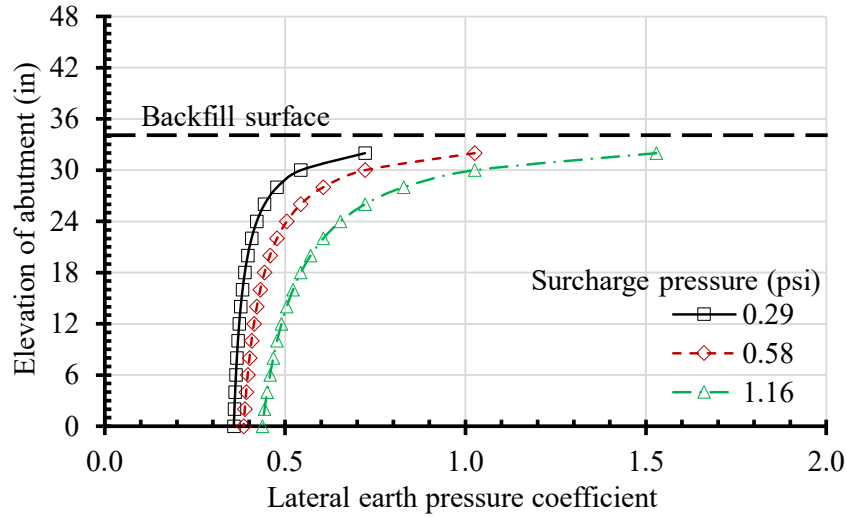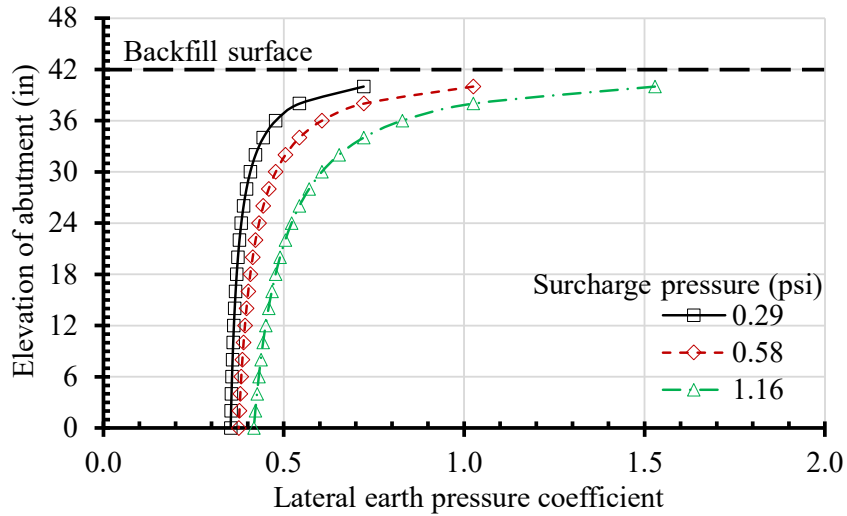
a. 18-in. high backfill
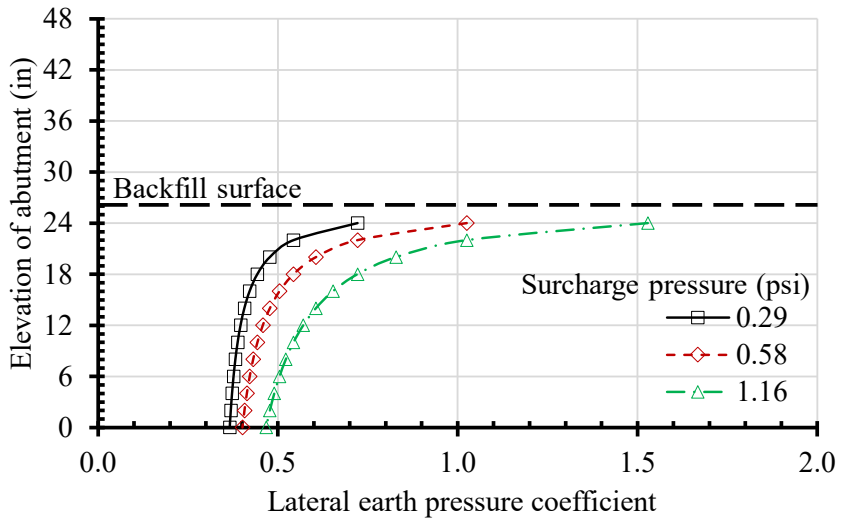
b. 26-in. high backfill

Figure 4.1: Calculated Lateral Earth Pressure Coefficients Considering Surcharge Pressure

(Continued to next page)

c. 34-in. high backfill

d. 42-in. high backfill

Figure 4.1: Calculated Lateral Earth Pressure Coefficients Considering Surcharge Pressure (Continued)

In practice, the effect of compaction on the distribution and magnitude of lateral earth pressures behind a retaining wall is often neglected, and the lateral earth pressure coefficient is assumed to be constant along the height of a non-yielding wall. In this case, the lateral earth pressures increase linearly with the depth of the backfill. The measured or theoretically calculated non-linear lateral earth distribution may be equivalent to the linear distribution by determining an equivalent constant lateral earth pressure coefficient, K_e. The equivalency can be achieved by equalizing the moment induced by the actual lateral earth pressures behind the abutment with

regard to the abutment toe to the moment induced by the linearly distributed lateral earth pressures using a constant lateral earth pressure coefficient with regard to the abutment toe. Figure 4.2 shows the variation of the calculated equivalent constant lateral earth pressure coefficient, K_e, behind the abutment as the height of the backfill surface increased when a surcharge pressure of 0.29, 0.58 or 1.16 psi was used to simulate compaction. Figure 4.2 shows that the equivalent constant lateral earth pressure coefficient decreased as the height of the backfill surface increased and/or the magnitude of the surcharge pressure decreased.
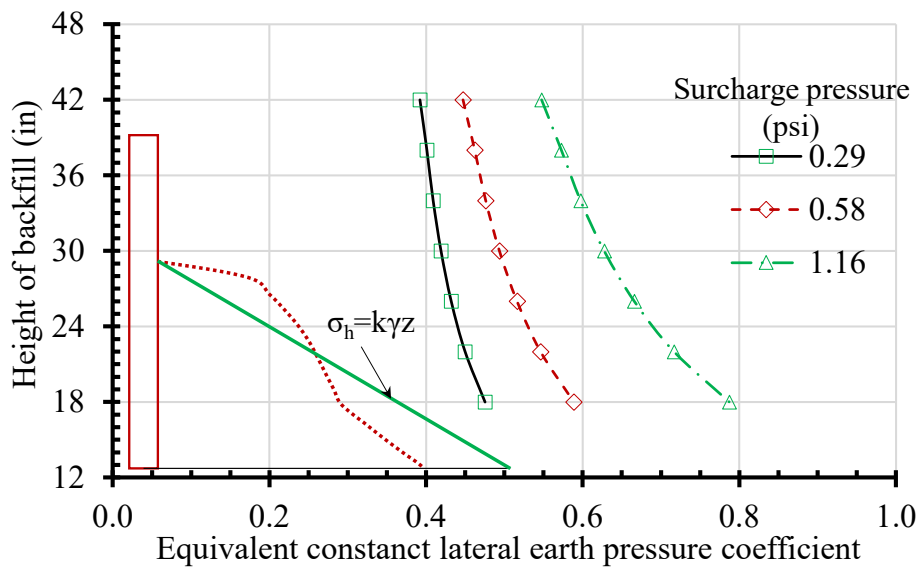
Figure 4.2: Equivalent Constant Lateral Earth Pressure Coefficient after Backfill Placement and Compaction

If the backfill was assumed to be normally consolidated and the movement of the abutment was not allowed, the lateral earth pressure coefficients at rest and the active state were 0.33 and 0.20, respectively, based on the measured friction angle (42.1°) by direct shear tests in this study. The lateral earth pressure coefficient (K) after backfill placement and compaction in each test could be calculated using the readings from the earth pressure cells behind the abutment by Equation 4.3:

$$K = \frac{\sigma_h}{\gamma z}$$

<div align="right">**Equation 4.3**</div>

Where:

γ = the unit weight of the backfill (115 pcf),

z = the depth of an earth pressure cell from the backfill surface, and

σ_h = the lateral earth pressure measured by the earth pressure cell.

Unlike the non-yielding wall, the abutment in this study was supported by the manual jack and the footing connection that allowed the abutment to have limited movement during backfill placement and compaction. Since Test T1 to Test T3 did not have any geogrid reinforcement in the backfill near the abutment, Test T2 was chosen to represent the tests without any geogrid reinforcement. Figure 4.3 shows the lateral earth pressure coefficients calculated using the readings from the earth pressure cells while Figure 4.4 shows the displacements of the abutment calculated using the readings of the top and the bottom DTs in Test T2, Test T4, Test T5, and Test T6. In general, the lateral earth pressure coefficient decreased as the backfill surface approached the final height of the abutment (42 in.) in Test T2, and this finding is consistent with that shown in Figure 4.1. After the backfill placement and compaction, the lateral earth pressure coefficient at the elevation of 10 in. even decreased to below the normal-consolidated at-rest earth pressure coefficient (0.33) in Test T2. The lateral earth pressure coefficient lower than 0.33 at the elevation of 10 in. in Test T2 might be attributed to the outward movement of the abutment from the backfill. This outward movement (i.e., negative displacement) increased as the backfill surface approached the height of 42 in. in Figure 4.4(a).

Horizontal geogrids were adopted to reinforce the backfill in Test T4. Since the geogrids could restrain lateral spreading of the backfill due to compaction, compaction had less effect on the abutment in Test T4 than that in Test T2. Therefore, the abutment in Test T4 had smaller outward movements than Test T2, as shown in the comparison between Figure 4.4(b) and Figure 4.4(a). The coefficient of lateral earth pressure behind the abutment at a given height was affected by two mechanisms. First, compaction of backfill could increase this coefficient due to the induced over-consolidation, which decreased as the height of the backfill surface increased. Second, this coefficient decreased as the abutment moved away from the backfill because of creating an active state. The magnitude of the outward movement of the abutment was also affected by backfill

placement and compaction. Geogrids with wrap-around facing were utilized in Test T5 and Test T6. A comparison between Test T4 and Test T5 indicates that horizontal geogrid reinforcements in the backfill reduced the outward movements of the abutment from the backfill but increased the lateral earth pressures behind the abutment as compared with the geogrid reinforcements with wrap-around facing. The top two geogrid layers in Test T6 were longer than those in Test T5. Figure 4.3(c) and Figure 4.3(d) show that the lateral earth pressure coefficient at an elevation of 34 in. was lower in Test T6 than that in Test T5 after the backfill placement and compaction, while Figure 4.4(c) and Figure 4.4(d) show that the abutment movements in Test T5 and Test T6 were almost the same after backfill placement and compaction. This comparison indicates that the longer length of the top geogrids might reduce the compaction energy applied to the backfill below the reinforcement so that the lateral earth pressure coefficient decreased.
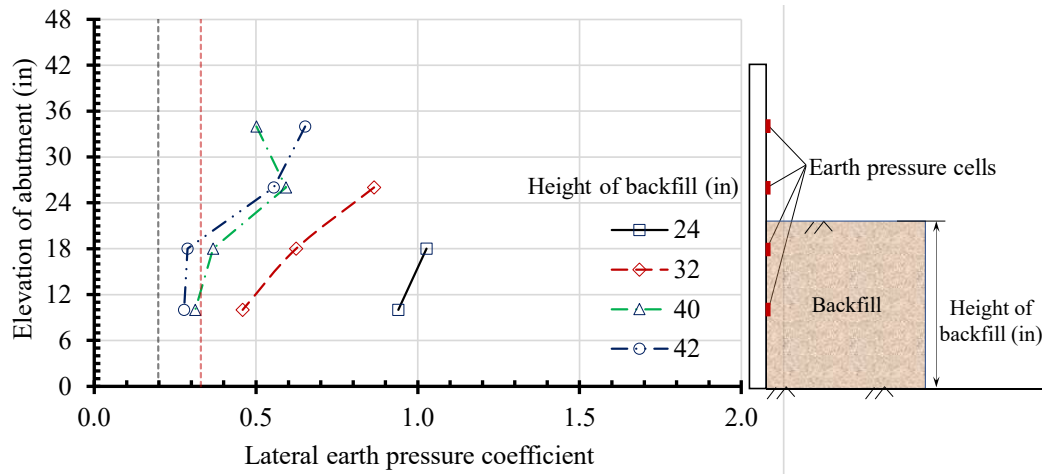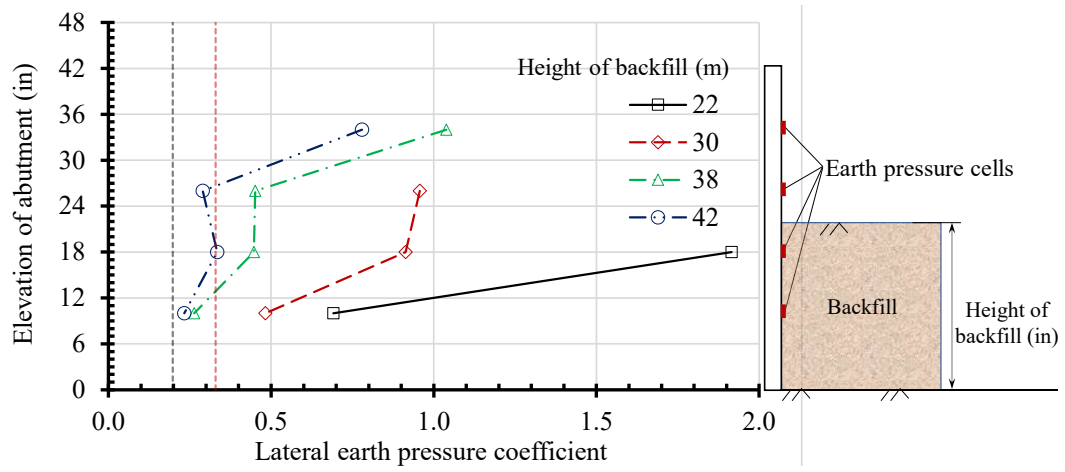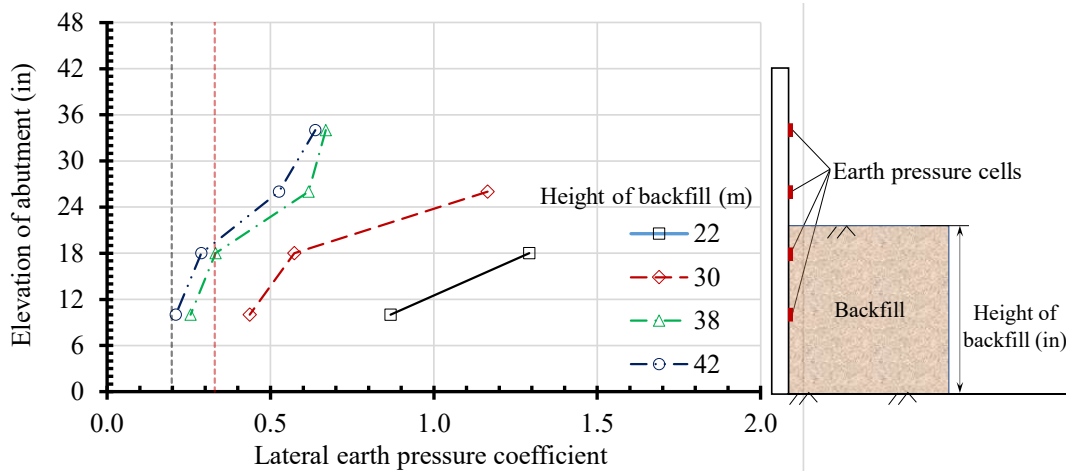
a. Test T2
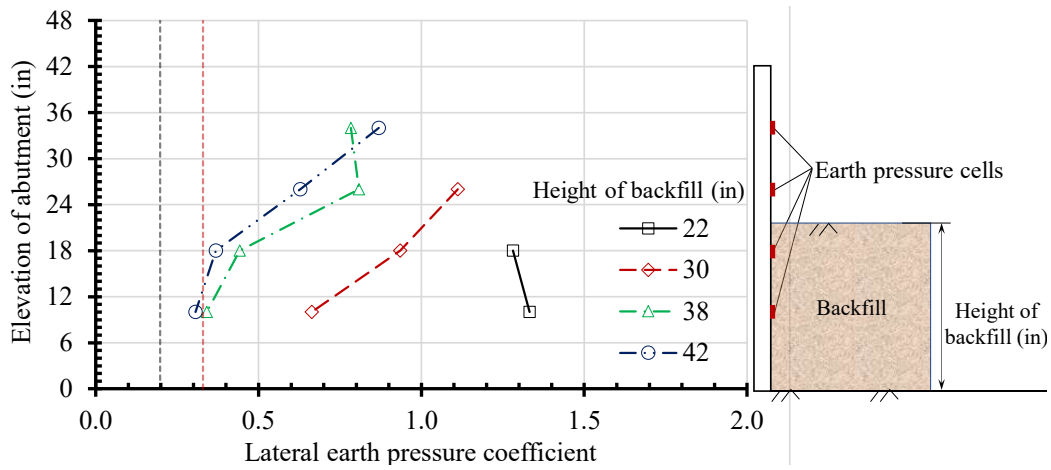
b. Test T4

Figure 4.3: Coefficient of Lateral Earth Pressure behind the Abutment
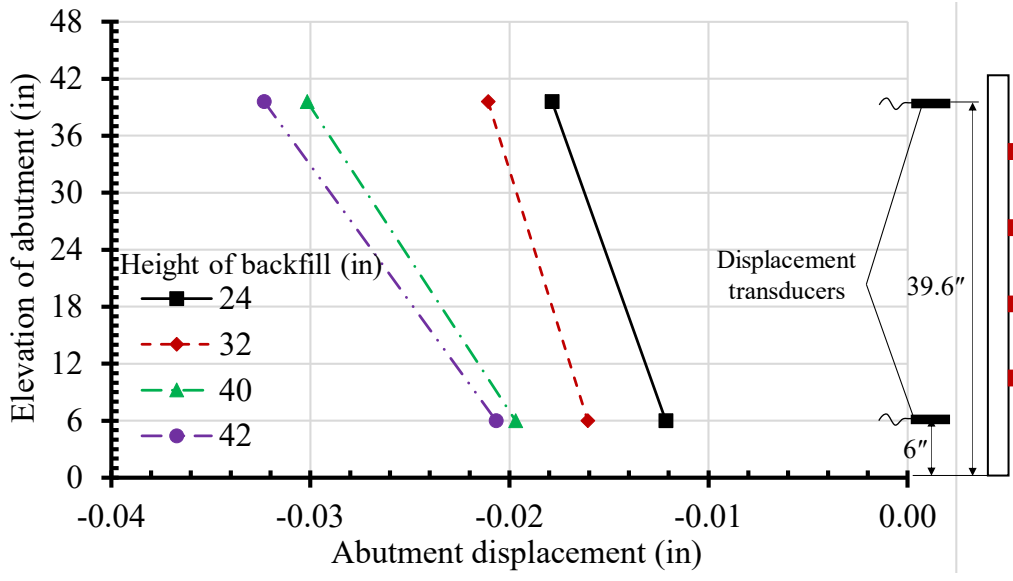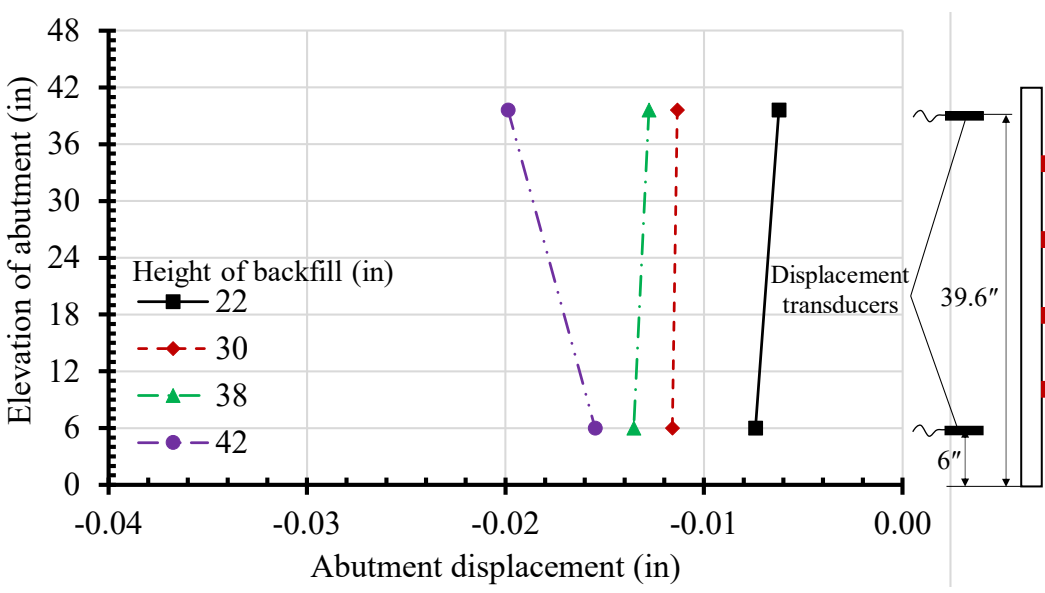(Continued to next page)

c. Test T5

d. Test T6

Figure 4.3: Coefficient of Lateral Earth Pressure behind the Abutment (Continued)

a. Test T2

b. Test T4

Figure 4.4: Abutment Movement in Physical Model Tests
(Continued to next page)
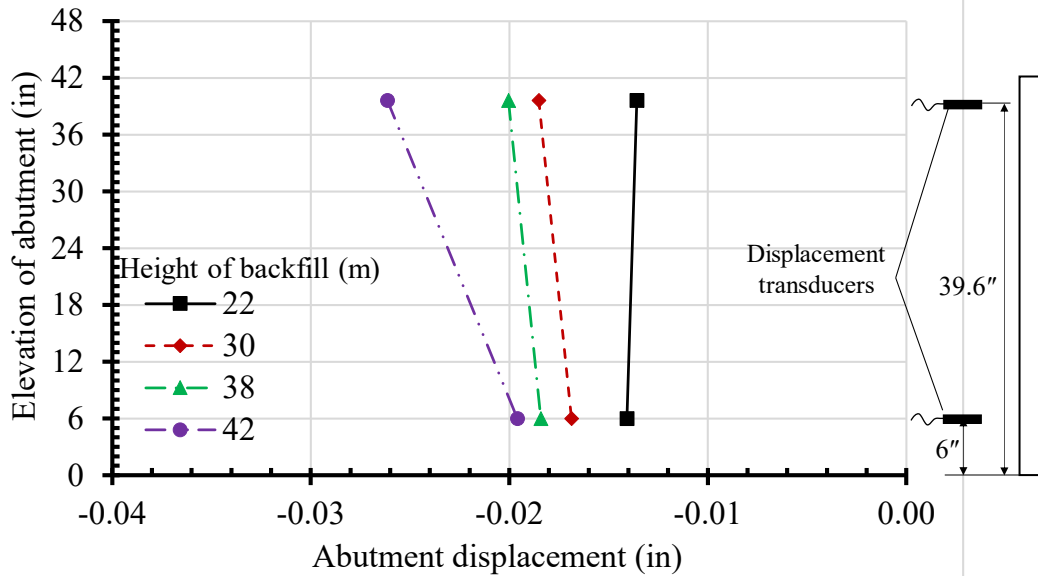
c. Test T5
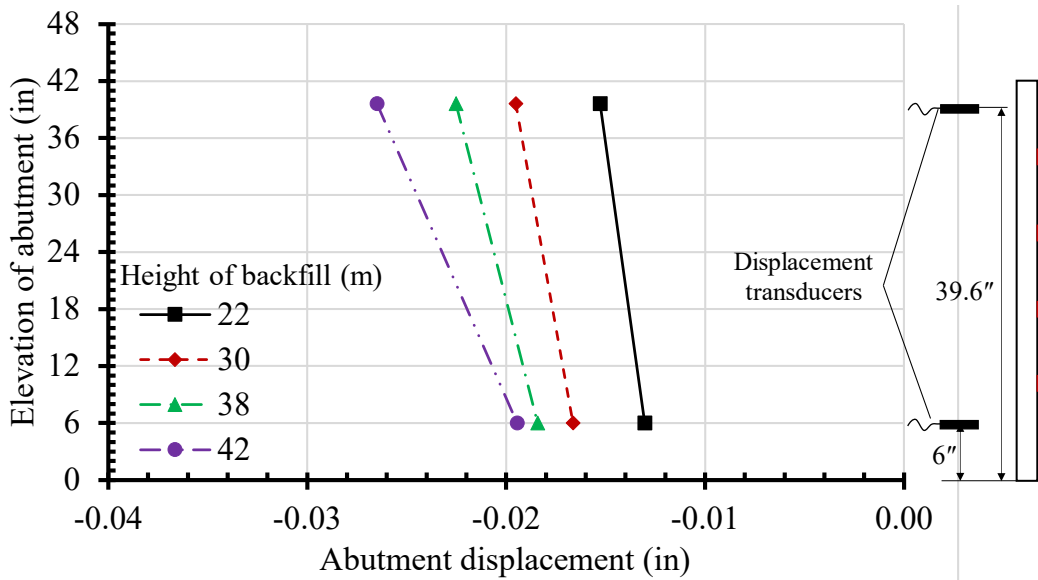
d. Test T6

Figure 4.4: Abutment Movements in Physical Model Tests (Continued)

4.2 Force to Hold the Abutment

Figure 4.3 shows that the lateral earth pressure coefficient changed with the elevation of the abutment. However, the lateral earth pressure coefficient is often assumed to be constant along the abutment for design convenience in practice so that the lateral earth pressures behind the abutment increase linearly from 0 at the backfill surface to $K_e \gamma h$ at the bottom of the backfill, as

shown in Figure 4.5. During the backfill placement and compaction, the force (F) to hold the abutment was monitored. The equivalent constant lateral earth pressure coefficient, K_e, could be calculated based on the moment, MP, induced by the linearly increasing lateral earth pressures on the abutment with regard to the abutment toe equal to the moment, MF, provided by the force to hold the abutment in place with regard to the abutment toe during the backfill placement and compaction as shown in Equation 4.4. When the height of the backfill is h, a resultant force from the lateral earth pressures behind the abutment is applied at the height of $h/3$ and the moment induced by this resultant force can be calculated using Equation 4.5. The moment provided by the force to hold the abutment in place can be calculated using Equation 4.6. By replacing MP and MF in Equation 4.3 with Equation 4.4 and Equation 4.5, the equivalent constant lateral earth pressure coefficient (K_e) can be calculated.

$$M_P - M_F = 0$$

Equation 4.4

$$M_P = P \times \frac{h}{3} = K_e \gamma h \cdot \frac{h}{2} \cdot B \cdot \frac{h}{3} = (K_e \gamma h^3 B)/6$$

Equation 4.5

$$M_F = F \cdot h_T$$

Equation 4.6

Where:

B = the width of the backfill (i.e., 12 in. in the model test),

F = the force to hold the abutment, and

h_T = the height of the manual jack (i.e., 39 in.).

When the height of the backfill was low, the equivalent constant lateral earth pressure coefficient, K_e, calculated using the readings from the load cell was not consistent because the measured values were small. Figure 4.5 shows the equivalent constant lateral earth pressure coefficient, K_e, calculated using the readings from the load cell when the height of the backfill reached above 20 in. The calculated K_e values depended on the reinforcement method of the backfill and the movement of the abutment in this study. Figure 4.5 indicates that the K_e value decreased as the height of the backfill increased, which is consistent with what is shown in Figure 4.2. As the height of the backfill increased, the lateral earth pressures at the greater depth, due to compaction, were equal or close to the normally-consolidated at-rest lateral earth pressures as

49

shown in Figure 4.1 and Figure 4.3. As a result, the compaction effect on the K_e value decreased as the height of the backfill increased. In addition, Test T4 to Test T6 had higher K_e values than Test T2 because of their smaller outward movements of the abutment thanks to the geogrid reinforcements.
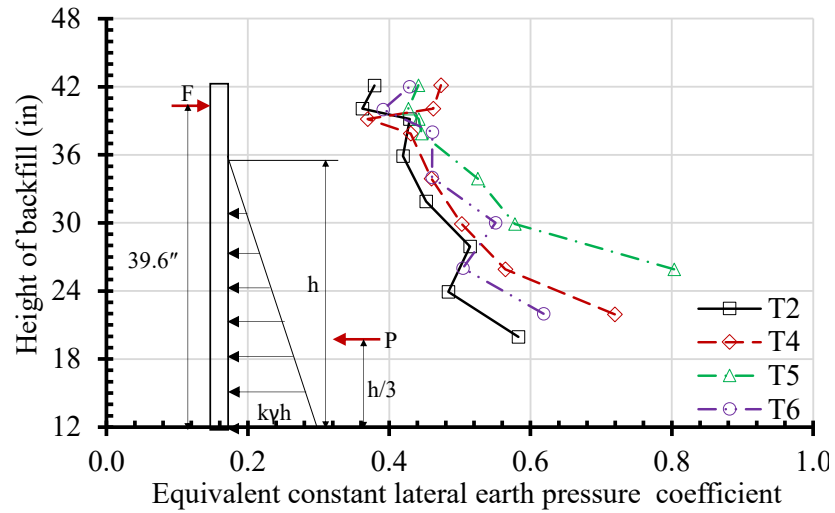
Figure 4.5: Equivalent Lateral Earth Pressure Coefficient Calculated Using the Readings of the Load Cell

Chapter 5: Test Results and Analysis of Physical Models Subjected to Seasonal Temperature Changes and Traffic Loading

This chapter presents the test results of six physical model tests and evaluates the performance of the abutment subjected to simulated seasonal temperature changes and traffic loading. The evaluations were performed based on the analysis of their effects on abutment movements, backfill surface settlements, and additional lateral earth pressures behind the abutment. This chapter also examines the benefits of geogrid reinforcements in the backfill behind the abutment and in the foundation soil under the sleeper slab.

5.1 Effects of Seasonal Temperature Change

5.1.1 Abutment movement

Movement of the abutment at any elevation can be estimated based on the following derived formula when the movements of the abutment at two specific heights are measured:

$$\delta_h = \frac{\delta_T(h - h_B) + \delta_B(h_T - h)}{h_T - h_B}$$

Equation 5.1

Where:

δ_T, δ_B = the measured movements of the abutment at the two heights (h_T is 39 in. at the top and h_B is 6 in. at the bottom in this study), respectively, and

δ_h = the movement of the abutment at a height of h.

The movement of the abutment at the toe was calculated as h was set to zero. All these abutment movements were assumed to be positive when the abutment moved toward the backfill.

In this study, the abutment top was pushed and pulled by the manual jack to simulate seasonal temperature changes while the hydraulic cylinder was used to apply traffic loading. The DTs to measure abutment movements, the backfill surface settlements, and the settlements of the sleeper slab were zeroed out before the abutment top cyclic movement and traffic loading (if any).

Figure 5.1 shows the measured abutment top movements and the calculated abutment toe movements using Equation 5.1 in Test T1. The abutment toe moved toward the backfill when the abutment top moved away from the backfill (from 0.12 in. to -0.12 in.), and the abutment toe

moved away from the backfill when the abutment top moved toward the backfill (from -0.12 in. to 0.12 in.). In addition, the outward movement of the abutment toe away from the backfill increased at a decreasing rate with the number of the abutment top movement cycles. The abutment top movement toward the backfill disturbed the stress state within the upper portion of the backfill. At the same time, the abutment bottom moved away from the backfill when the abutment top moved toward the backfill. As a result, the backfill within the lower portion moved laterally toward the abutment due to less resistance from the abutment bottom. The upper portion of the backfill yielded progressively and slumped downward and toward the bottom of the abutment as the abutment top moved away from the backfill. Simultaneously, the abutment bottom compressed the lower portion of the backfill as the abutment bottom moved toward the backfill. The cyclic movements of the abutment allowed the backfill to slump from the upper portion to the lower portion and densified the backfill within the lower portion, thus increasing the resistance from the backfill when the abutment bottom moved back. Consequently, the abutment toe had an accumulated net movement away from the backfill after the abutment top movement cycles. As the number of the abutment top movement cycles increased, a lesser amount of sand slumped downward from the upper portion to the lower portion, thus reducing the rate of the outward movement of the abutment toe away from the backfill.
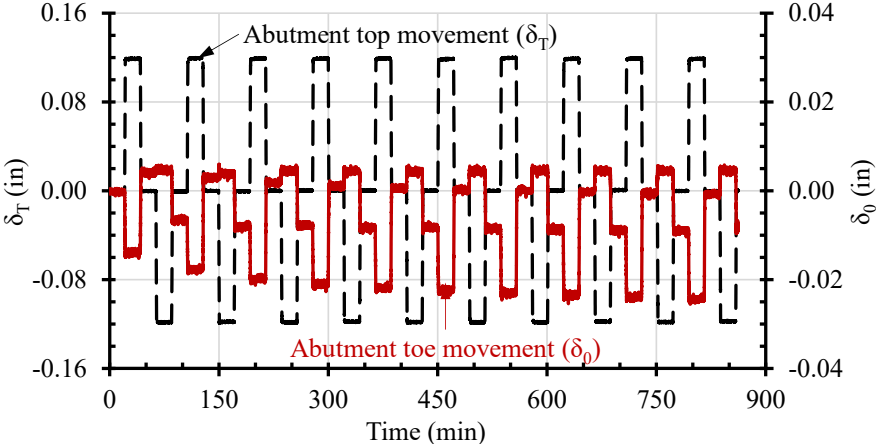
Figure 5.1: Abutment Top and Toe Movements in Test T1

5.1.2 Additional lateral earth pressure behind abutment

The readings of the load cell used to measure the force required to hold the abutment top in place and the four earth pressure cells behind the abutment changed during backfill placement and compaction. Their readings were zeroed out before the abutment top cyclic movements and traffic loading (if any) to examine the effects of temperature changes and traffic loading. In this report, their readings are referred to as the measured additional forces (i.e., the readings from the load cell) and the measured additional lateral earth pressures (i.e., the readings from the pressure cells). Figure 5.2 shows the measured additional lateral earth pressures behind the abutment in Test T1. Their values at four elevations were positive when the abutment top was at Position I or Position II. When the abutment top was at Position III, however, the measured additional lateral earth pressures were positive only at the elevation of 10 in. (i.e., the depth of 32 in. from the abutment top).
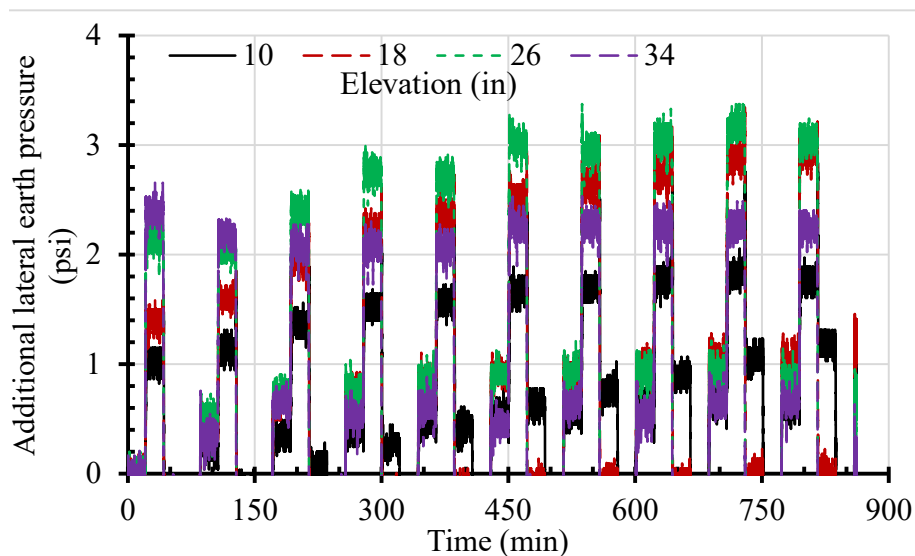
Figure 5.2: Measured Additional Lateral Earth Pressures at Different Elevations in Test T1

Figure 5.3 shows the variations of the measured additional lateral earth pressures behind the abutment at Position I and Position II of the abutment top with the cycles. When the abutment top was at Position I, the additional lateral earth pressures at elevations of 10, 18, and 26 in. increased with the number of abutment top movement cycles at a decreasing rate. However, the additional lateral earth pressures at the elevation of 33 in. increased first and then decreased to a

stable value. When the abutment top was at Position II, the additional lateral earth pressures at elevations of 10 and 18 in. increased with the number of the abutment top movement cycles. At the same position, the additional lateral earth pressure at the elevation of 26 in. decreased first and then increased from the second abutment top movement cycle, while the additional lateral earth pressure at the elevation of 33 in. decreased to a stable value with the number of the abutment top movement cycles. As discussed in Chapter 3, compaction by the hand tamper during backfill placement resulted in an over-consolidated state within the upper portion of the backfill. The abutment top movement cycles disturbed the over-consolidated stress state within the upper portion of the backfill, thus reducing the additional lateral earth pressures at elevations of 26 and 33 in. when the abutment top was at Position II. Slumping of the backfill material from the upper portion downward resulted in accumulation of the material and densified the backfill at elevations of 10, 18, and 26 in., thus increasing the additional lateral earth pressures at these elevations. With an increase of the number of the abutment top movement cycles, a lesser amount of material could enter these lower elevations; therefore, the rate of the additional lateral earth pressure increase decreased.

Figure 5.4 shows the measured additional forces required to push and pull the abutment top. The force required to hold the abutment top at Position II increased with the number of the abutment top movement cycles at a decreasing rate. The changes of the additional forces to hold the abutment top at Position II agreed well with the changes of additional lateral earth pressures behind the abutment at Position II with the number of the abutment top movement cycles as shown in Figure 5.3(b).
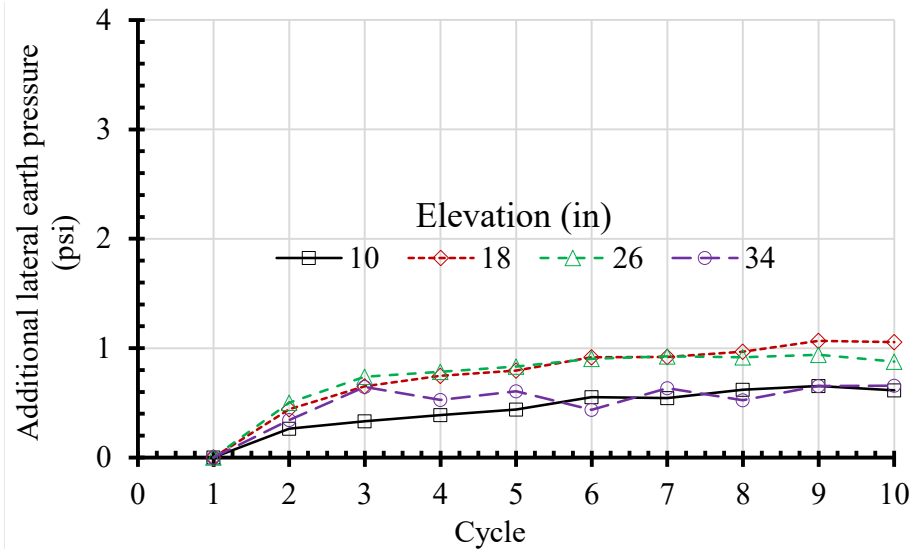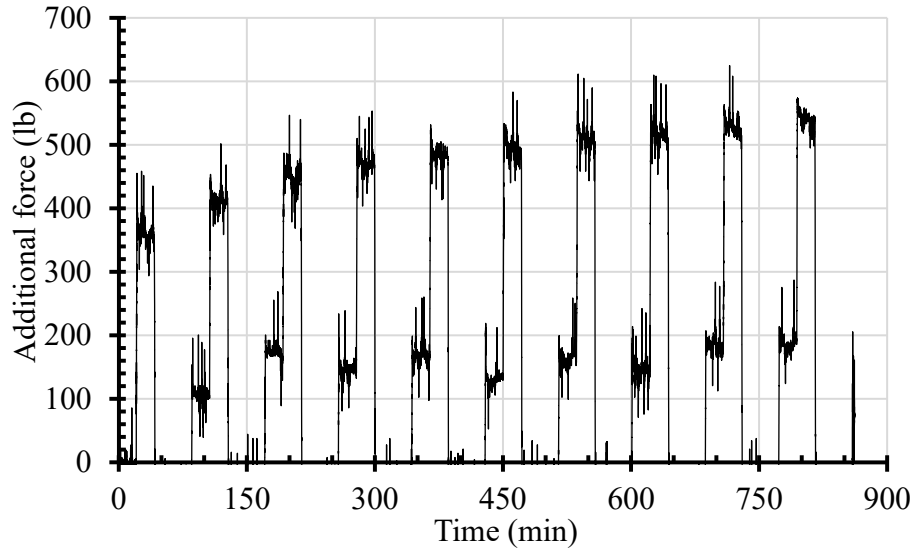
a. Position I
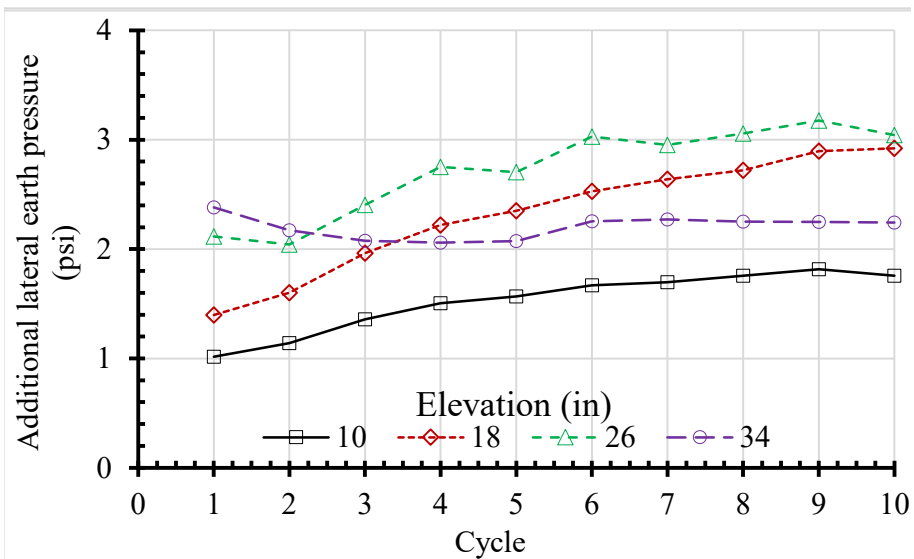
b. Position II

**Figure 5.3: Variations of Measured Additional Lateral Earth Pressures in Test T1**

Figure 5.4: Additional Forces to Push and Pull the Abutment Top in Test T1

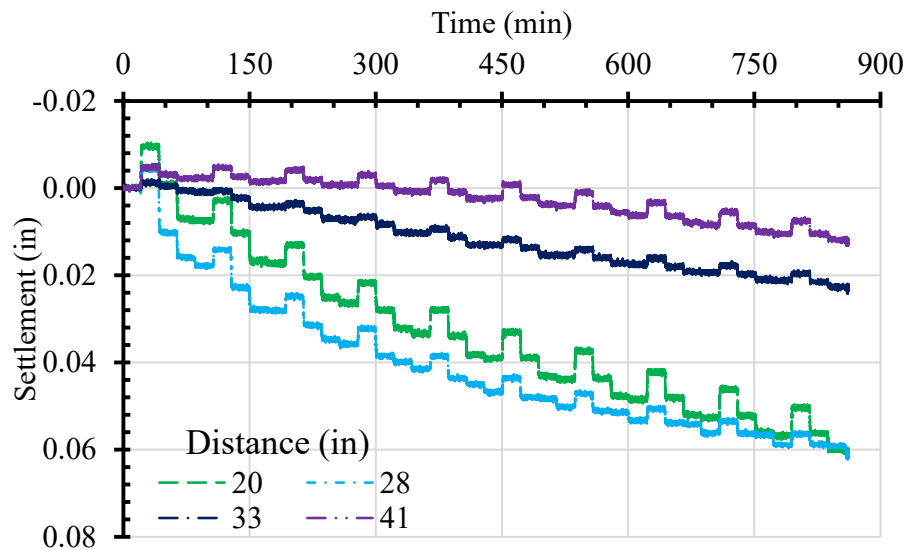### 5.1.3 Backfill surface settlement

Figure 5.5 shows the backfill surface settlements in Test T1 due to the simulated temperature changes. The pattern of the settlements represents a cycle of the abutment top movement from Position I, to Position II, Position III, and Position IV. The backfill surface moved upward when the abutment top moved toward the backfill (from Position IV to Position II), and the backfill surface moved downward when the abutment top moved away from the backfill (from Position II to Position IV). The downward movements of the backfill surface were larger than the upward movements of the backfill surface for each abutment top movement cycle because a passive movement had a larger influence area than an active movement. As a result, the backfill surface settlements increased with the number of the abutment top movement cycles. In addition, the effects of the abutment top movement cycles on the backfill surface settlements decreased as the distance of the backfill surface from the back facing of the abutment increased. The backfill surface settlements at distances of 2 and 6 in. from the back face of the abutment (within the active zone defined by the Rankine failure plane at the angle of 66.2°) were much larger than that at distances of 20 and 28 in. (between the Rankine failure plane and the repose failure plane at the angle of 42.2°) as shown in Figure 5.6. Please note different vertical scales used in Figures 5.5(a) and Figure 5.5(b) for better display.
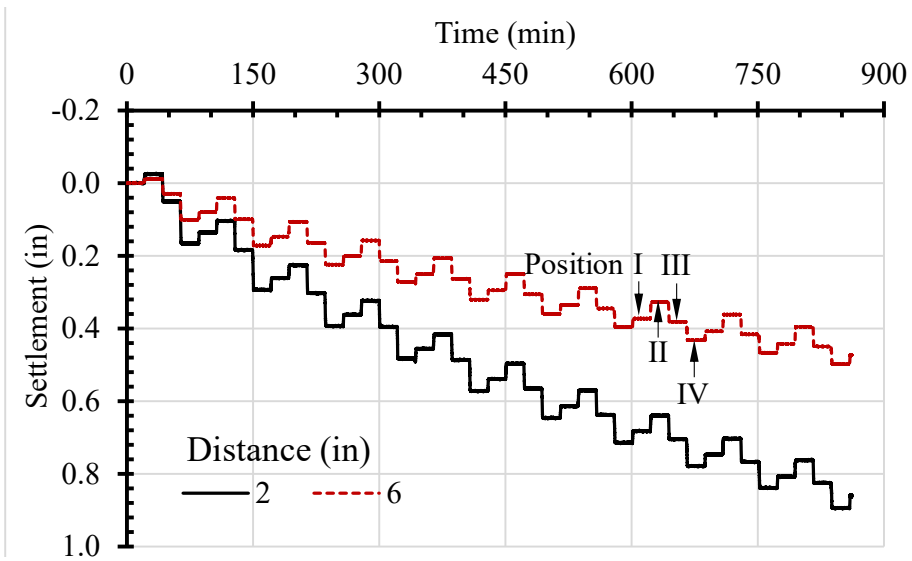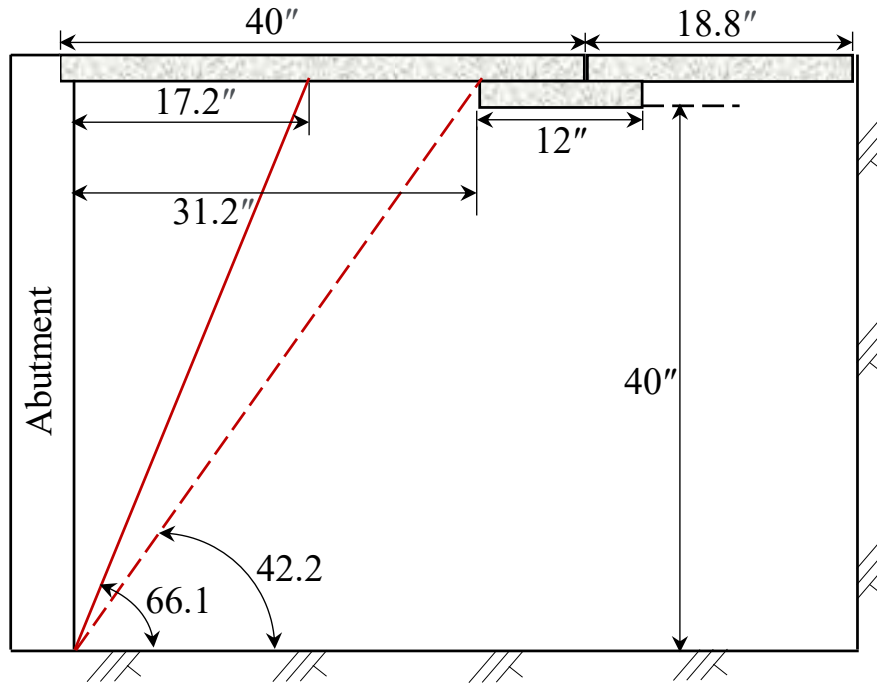
a. Backfill surface settlement near the abutment

b. Backfill surface settlement away from the abutment

Figure 5.5: Backfill Surface Settlements due to Abutment Top Cyclic Movements in Test T1

57

**Figure 5.6: Potential Influence Ranges under Active Movement**

Figure 5.5(b) shows that the backfill surface settlements at the distance of 28 in. were larger than that at the distance of 20 in. initially, however, the difference between their settlements decreased as the number of abutment top movement cycles increased. The backfill surface measured by the DT at the distance of 28 in. from the back face of the abutment was close to the left end of the sleeper slab, which was 31 in. away from the back face of the abutment. Since the approach slab was supported by the abutment, the backfill, and the sleeper slab, cyclic movements of the abutment top moved the approach slab relative to the sleeper slab. Their relative movements might have affected the backfill around the sleeper slab.

The DTs at distances of 33 and 41 in. measured smaller settlements because they were located beyond the repose failure plane defined by the friction angle of the sand. These two DTs were across the sleeper slab at its left and right sides. The settlement at the left side was more affected by the abutment top movement cycles because the left side was closer to the abutment than the right side. In addition, the relative movements between the approach slab and the sleeper slab had more effect on the left side of the sleeper slab that was under the approach slab.

5.2 Combined Effects of Seasonal Temperature Change and Traffic Loading

5.2.1 Abutment movement

In addition to the effects from the abutment top movements due to seasonal temperature changes in Test T1, the effect of traffic loading was considered in Test T2. As stated before, each abutment top movement cycle due to simulated temperature changes was divided into four positions (Position I to Position IV) that represent the four seasons in a year. At each position of the abutment top, traffic loading was applied and divided into three phases: before traffic loading, during traffic loading, and after traffic loading. Figure 5.7 shows the first abutment top movement cycle in Test T2. At each position of the abutment top, the test lasted for approximately 20.7 min, which included 2 min for before traffic loading, 16.7 min (100 × 10 s=1000 s) for during traffic loading, and 2 min for after traffic loading. Then the abutment top moved from the current position to the next position within 1 min. Therefore, each abutment top movement cycle totally lasted for approximately 86.8 min as shown in Figure 5.6. In addition, the large changes of the movements were induced by the simulated temperature changes while the small changes of the movements were caused by traffic loading. Figure 5.8 shows the measured abutment top movements and the calculated abutment toe movements in Test T2 due to simulated temperature changes and traffic loading. Although the abutment was supported by the footing connection and the manual jack, traffic loading still could induce small movements of the abutment for three reasons. First, the supports to the abutment by the manual jack and the footing connection were not perfectly rigid. Second, the traffic load was partially transferred to the abutment because one end of the approach slab was supported on the abutment. Finally, contact stresses between the approach slab and the backfill generated additional lateral earth pressures behind the abutment, which could move the abutment. The contact stress effect will be discussed further in a later section. Figure 5.8 shows that the traffic load applied on the approach slab moved the abutment top and the abutment toe, and then the abutment top and toe moved back as the traffic load on the approach slab was released. As a result, the abutment had permanent movements after 100 cycles of traffic loading.
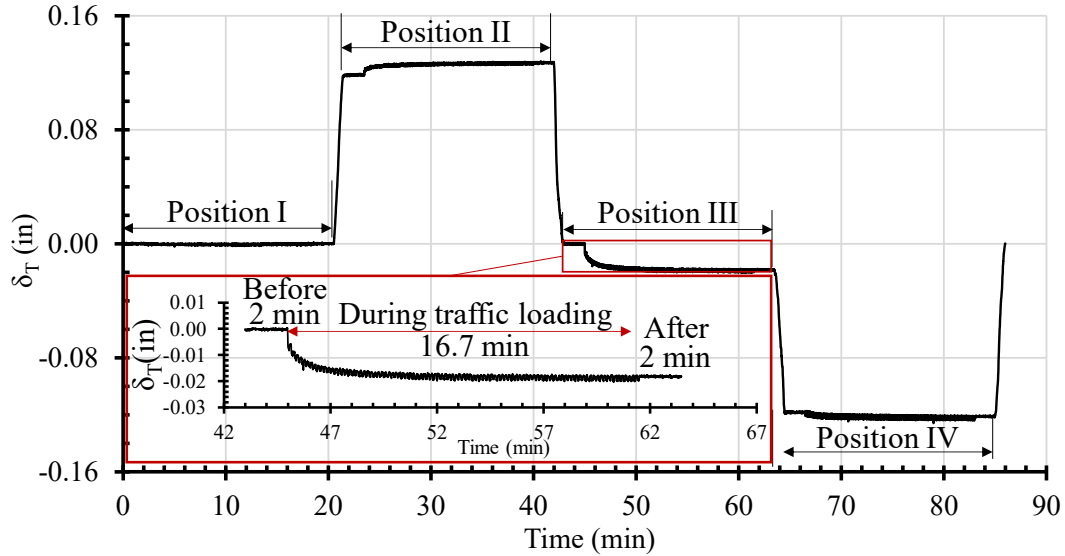
Figure 5.7: The First Abutment Top Movement Cycle including Traffic Loading
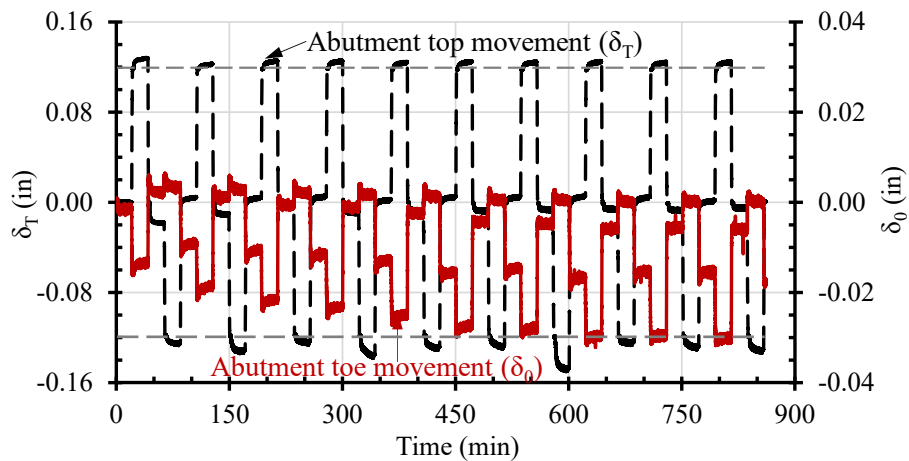
Figure 5.8: Movements of Abutment Top and Toe in Test T2 due to Simulated Temperature Changes and Traffic loading

Figure 5.9 shows the abutment toe movements at the four positions (Position I to Position IV) of the abutment top in Test T1 and Test T2 before traffic loading for that position. The abutment toe moved farther away from the backfill in Test T2 than that in Test T1. The backfill material moving downward from the upper portion of the backfill to the lower portion restrained the abutment toe from moving back to its previous position, thus increasing the abutment toe outward movements. Traffic loading-induced abutment movements in Test T2 increased the amount of sand moving downward and increased the resistance from the backfill for the abutment

bottom to move back. As a result, the outward movement of the abutment toe from the backfill in Test T2 was larger than that in Test T1.
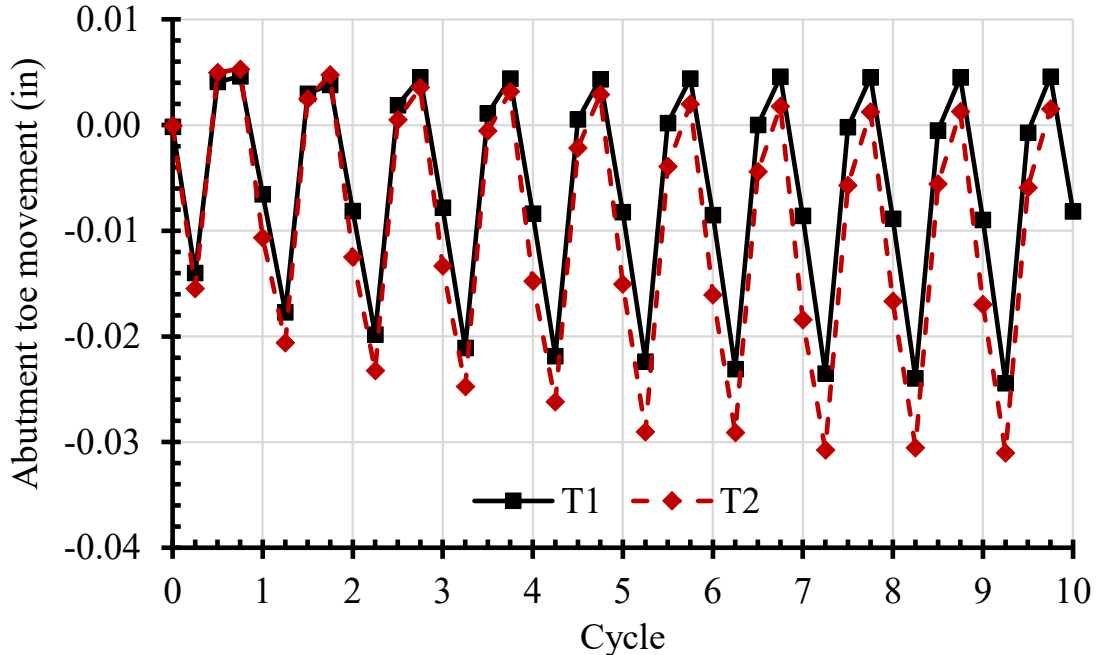
Figure 5.9: Movements of the Abutment Toe in Test T1 and Test T2 before Traffic Loading

5.2.2 Additional lateral earth pressure behind abutment

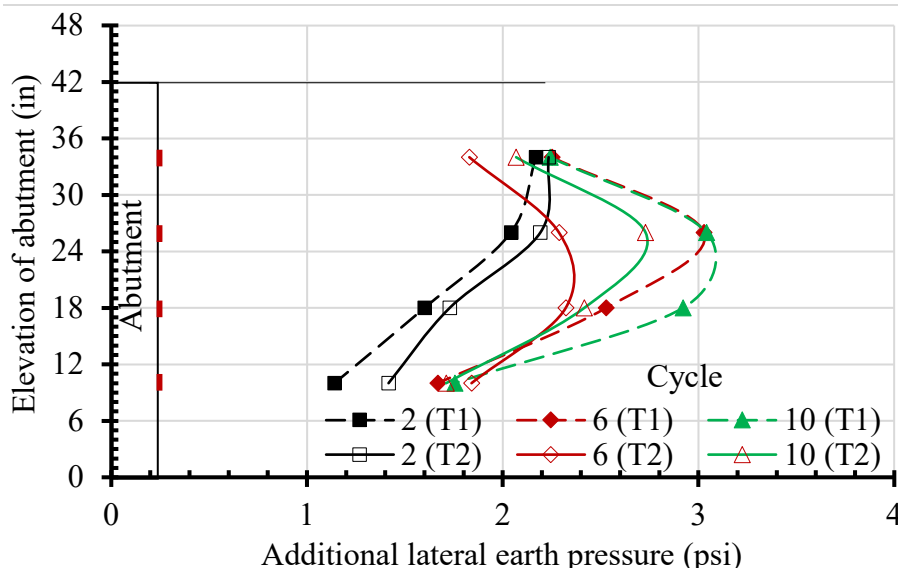Figure 5.10 shows the additional lateral earth pressures behind the abutment at Position II in Test T1 and Test T2 before traffic loading for that position. The additional lateral earth pressures behind the abutment at Position II in Test T2 were higher than those in Test T1 for the second abutment top movement cycle. During the second abutment top movement cycle, the accumulated backfill surface settlements due to simulated temperature changes and traffic loading were small and the over-consolidated stress state in the upper portion of the backfill was not affected too much by the simulated temperature changes and traffic loading. Therefore, traffic loads on the approach slab induced the contact stresses on the backfill surface under the approach slab. The contact stresses due to traffic loading between the approach slab and the backfill compressed and densified the backfill material underneath the approach slab. In addition, the small abutment movements due to traffic loading as shown in Figure 5.7 compressed and densified the backfill material right behind the abutment. As a result, the abutment top movement at Position II induced higher

61

additional lateral earth pressures behind the abutment in Test T2 than that in Test T1. However, the additional lateral earth pressures at elevations of 18, 26, and 33 in. at Position II were lower in Test T2 than those in Test T1 in the sixth and tenth abutment top movement cycles. After some abutment top movement cycles, the backfill surface settlements, especially near the abutment, became large due to accumulated effects of the simulated temperature changes and traffic loading. As a result, the approach slab near the abutment lost the support from the backfill near the abutment because a void developed between the approach slab and the backfill as indicated by zero or nearly zero contact stresses as shown in the later section. Therefore, traffic loading could no longer compact the backfill near the abutment. In addition, the over-consolidated stress state in the upper portion of the backfill was disturbed by the simulated temperature changes and traffic loading after some abutment movement cycles, and shear bands may occur in the upper portion of the backfill. Consequently, the additional lateral earth pressures at Position II within the upper portion of the backfill were lower in Test T2 than in Test T1 during the sixth and tenth abutment top movement cycles.

Figure 5.10: Additional Lateral Earth Pressures behind the Abutment at Position II in Test T1 and Test T2
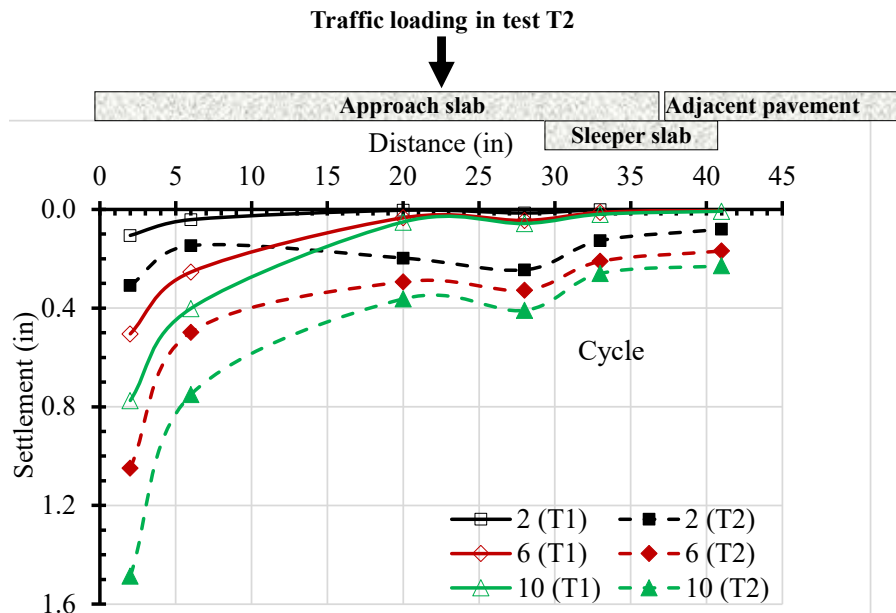
5.2.3 Backfill surface settlement

Figure 5.11 shows the backfill surface settlements at distances of 2 and 6 in. from the back face of the abutment. Traffic loading increased the backfill surface settlements near the abutment significantly. The backfill surface settlements at distances of 2 and 6 in. in Test T2 with traffic loading were almost twice those at the same distances in Test T1 without traffic loading. The contact stresses induced by traffic loading compressed the backfill material near the abutment until a void developed between the approach slab and the backfill as discussed later. Additionally, traffic loading-induced abutment movements resulted in additional backfill material slumping downward from the upper portion in Test T2. Consequently, traffic loading significantly increased the backfill surface settlements at distances of 2 and 6 in. in Test T2.
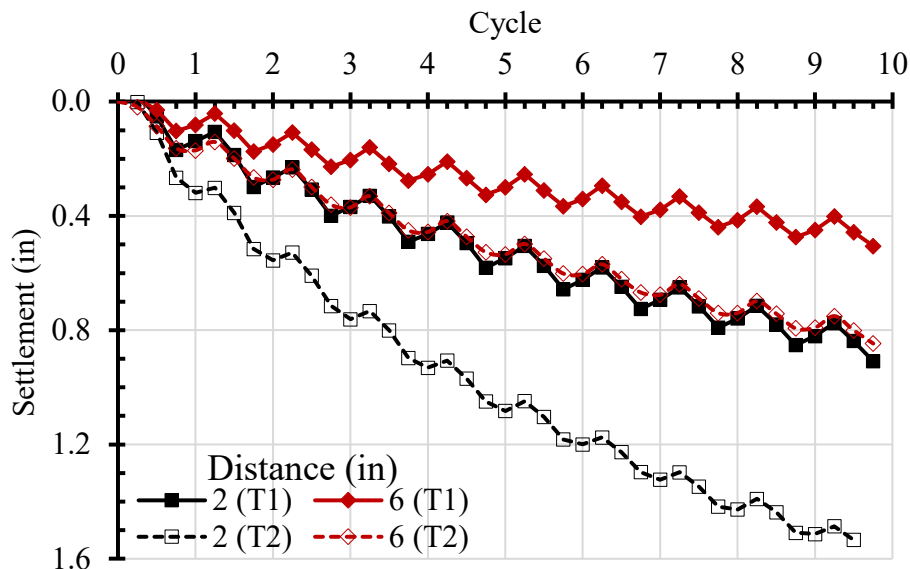
Figure 5.11: Backfill Surface Settlements near the Abutment in Test T1 and Test T2 before traffic loading

Figure 5.12 shows the backfill surface settlements at Position II in Test T1 and Test T2 before traffic loading for that position during the second, sixth, and tenth abutment top movement cycles. Traffic loading in Test T2 increased the backfill surface settlements at distances of 20 and 28 in., and the settlements of the sleeper slab. The traffic load was supported by the abutment, the backfill, and the sleeper slab. The contact stresses under the approach slab due to the concave deformations of the approach slab under the traffic load (at the distance of 24 in.) induced larger

settlements at distances of 20 and 28 in. than that at the distance of 6 in. in the second abutment top movement cycle. The abutment movements due to the simulated temperature changes and traffic loading had more effects on the backfill surface settlements at the distance of 6 in. than those at distances of 20 and 28 in. Consequently, the backfill surface settlements at the distance of 6 in. were larger than those at distances of 20 and 28 in. in the sixth and tenth abutment top movement cycles. In addition to the contact stresses between the approach slab and the backfill at the distance of 28 in., the traffic load transferred to the sleeper slab at the distance of 28 in. increased the settlement at that distance than that at the distance of 20 in. In addition, the traffic load transferred to the sleeper slab resulted in the settlement of the sleeper slab.

Figure 5.12: Backfill Surface Settlements at Position II in Test T1 and Test T2 during the Second, Sixth, and Tenth Abutment Movement Cycles

## 5.3 Effects of Reinforced Soil under Sleeper Slab

5.3.1 Abutment movement

Three geogrid layers with a length of 36 in. each were placed at elevations of 30, 33, and 37 in. under the sleeper slab in Test T3 to reduce the settlement of the sleeper slab due to traffic loading. Figure 5.13 shows the comparison of the abutment toe movements at the four abutment

positions (Position I to Position IV) before traffic loading at each position in Test T2 and Test T3. The abutment toe in Test T3 with the geogrid reinforcements under the sleeper slab had more outward movements from the backfill than that in Test T2 due to the increased resistance from the lower portion of the backfill reinforced by the geogrid layers.
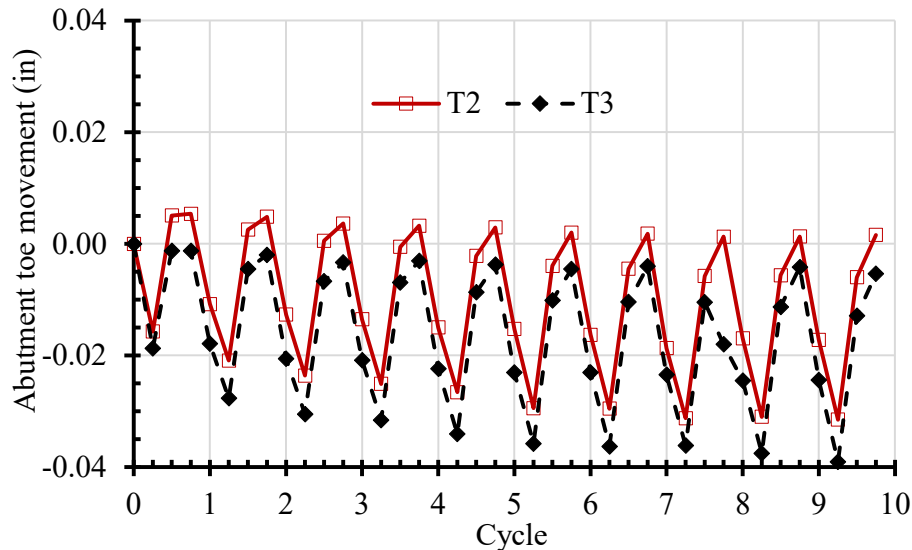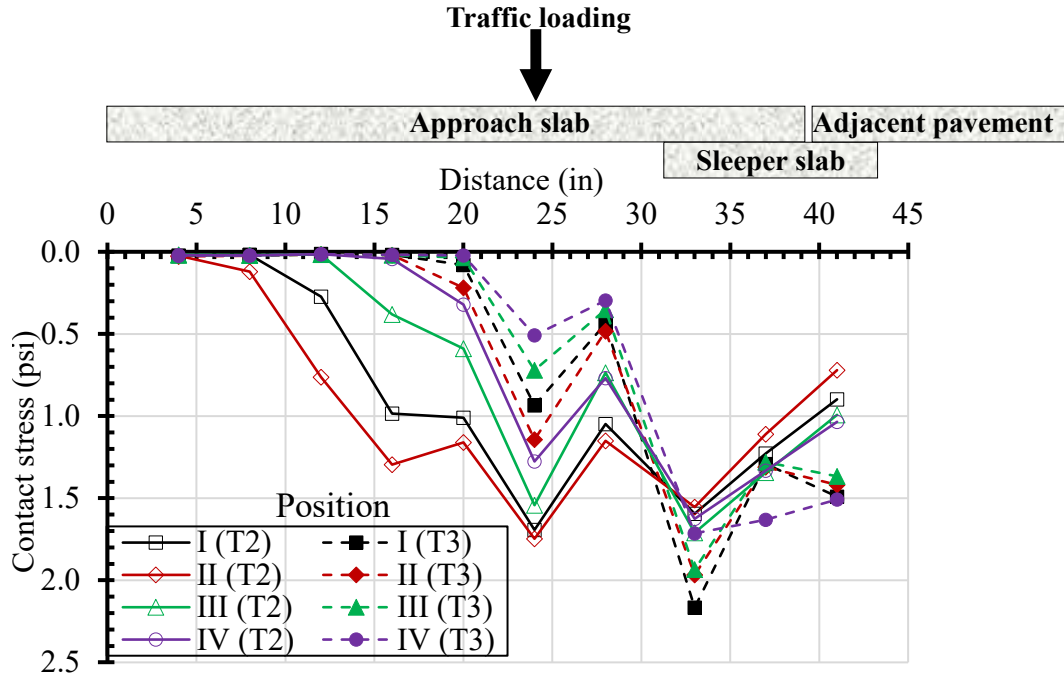

Figure 5.13: Movements of the Abutment Toe in Test T2 and Test T3

5.3.2 Contact stresses under sleeper slab and approach slab

Figure 5.14 shows the contact stresses under the approach slab and the sleeper slab induced by traffic loading in Test T2 and Test T3 during the second, sixth, and tenth abutment top movement cycles. The contact stresses under the approach slab were higher for Position II than those for Position I in Test T2. Because the abutment top movement toward the abutment from Position I to Position II pushed the backfill surface upward, more traffic load was transferred to the backfill at Position II than that at Position I. When the abutment top moved from Position II to Position IV, the approach slab lost some support from the backfill due to the downward movement of the backfill surface as evidenced with nearly zero stress measurement. In addition, the support to the approach slab from the backfill decreased with the number of the abutment top movement cycles due to the increased settlement of the backfill below the approach slab. As compared with Test T3, the approach slab in Test T2 had more support from the backfill but less support from the sleeper slab. Since the geogrid reinforcements increased the stiffness of the soil under the sleeper

slab in Test T3, more traffic load was transferred to the sleeper slab, but less traffic load was transferred to the backfill under the approach slab.

a. Second abutment top movement cycle

Figure 5.14: Contact Stresses under the Approach Slab and the Sleeper Slab in Test T2 and Test T3

(Continued to next page)
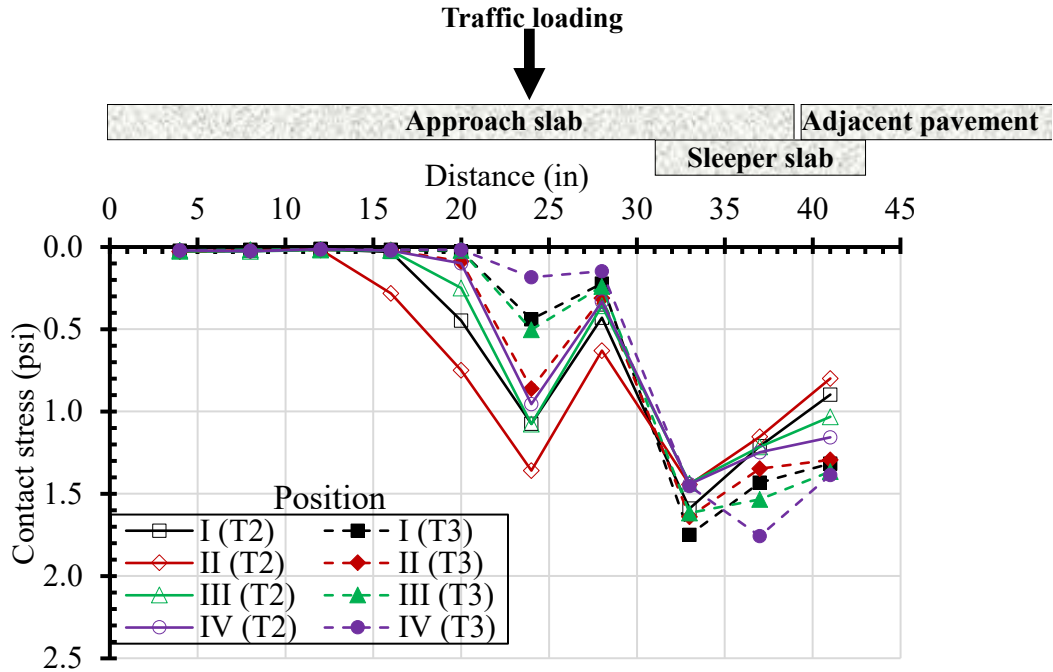
b. Sixth abutment top movement cycle
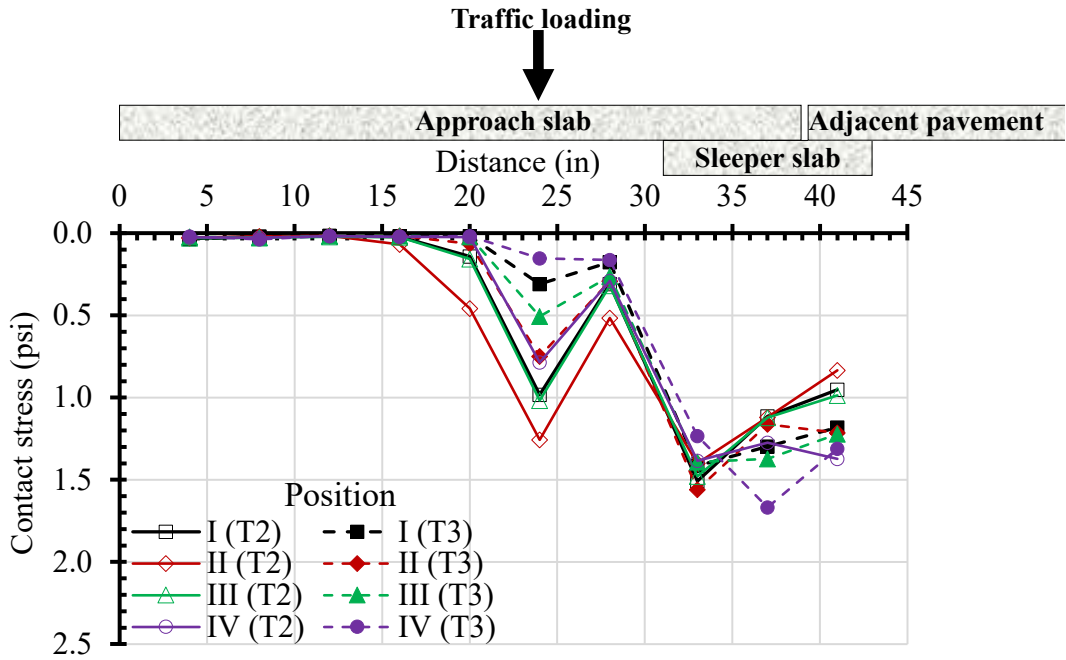
c. Tenth abutment top movement cycle

Figure 5.14: Contact Stresses under the Approach Slab and the Sleeper Slab in Test T2 and Test T3 (Continued)

The traffic load of 674 lb applied on the approach slab was supported by the abutment, the backfill under the approach slab, and the sleeper slab. Figure 5.13 shows that the traffic load transferred to the backfill under the approach slab was more in Test T2 than in Test T3. The sleeper slab in Test T3 carried slightly more load than that in Test T2. Since the approach slab in Test T3 received much less support from the backfill and slightly more support from the sleeper slab, more traffic load was transferred to the abutment in Test T3 than that in Test T2. The farther movements of the abutment toe away from the backfill in Test T3 than that in Test T2, as shown in Figure 5.13, might contribute to less support from the backfill, thus leading to more traffic load transferred to the abutment in Test T3 than in Test T2. The contact stresses within a distance of 12 to 20 in. away from the back face of the abutment were much higher in Test T2 than in Test T3, especially during the second and sixth abutment top movement cycles. These higher contact stresses in Test T2 aggravated the failure of the upper portion of the backfill near the abutment (within the distance of 12 in. away from the abutment).

5.3.3 Additional lateral earth pressure behind abutment

Figure 5.15 shows the additional lateral earth pressures behind the abutment at Position II before traffic loading at that position in Test T2 and Test T3 for the second, sixth, and tenth abutment movement cycles. The patterns of additional lateral earth pressures along the abutment in the sixth and tenth abutment top movement cycles were different from those during the second cycle in Test T2 and Test T3. Disturbance of the consolidated-stress state within the upper portion of the backfill by the abutment top movement cycles and traffic loading changed the patterns of additional lateral earth pressures along the abutment in Test T2 and Test T3. However, the additional lateral earth pressures at Position II in Test T3 were higher than those in Test T2 in the second, six, and tenth abutment top movement cycles, especially at elevations of 26 and 33 in.; although the two tests had similar patterns of additional lateral earth pressures along the abutment. The three geogrid layers under the sleeper slab were at elevations of 30, 33, and 37 in., and the left end of the geogrid layers was 19 in. away from the back face of the abutment. Since these geogrids increased the stiffness of the soil under the sleeper slab, it provided more resistance to the abutment movement toward the backfill, thus resulting in higher additional lateral earth pressures at the
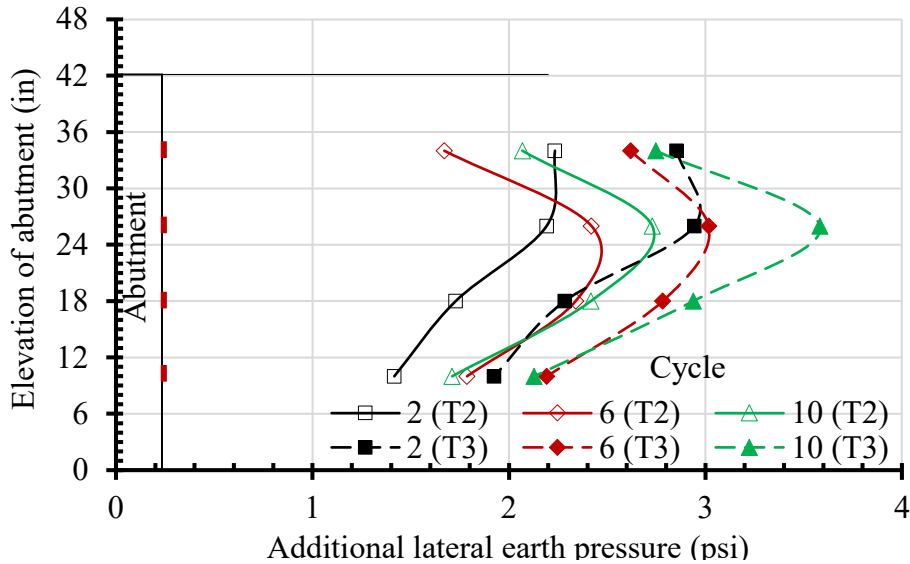
68

elevations of 26 and 33 in. at Position II in Test T3. The overall higher additional lateral earth pressures behind the abutment in Test T3 than in Test T2 will be further discussed in later sections of this report.

Figure 5.15: Additional Lateral Earth Pressures behind the Abutment at Position II in Test T2 and Test T3

5.3.4 Backfill surface settlement

Figure 5.16 shows the backfill surface settlements at the four positions (Position I to Position IV) of the abutment top before traffic loading at each position at distances of 2 and 6 in. (near the abutment) in Test T2 and Test T3. Test T3 had smaller backfill surface settlements at these distances than those in Test T2. As discussed earlier, the geogrid layers under the sleeper slab in Test T3 provided more support to the approach slab; therefore, lower contact stresses developed between the approach slab and the backfill near the abutment due to traffic loading in Test T3 than in Test T2. As a result, smaller settlements occurred in Test T3 than in Test T2.
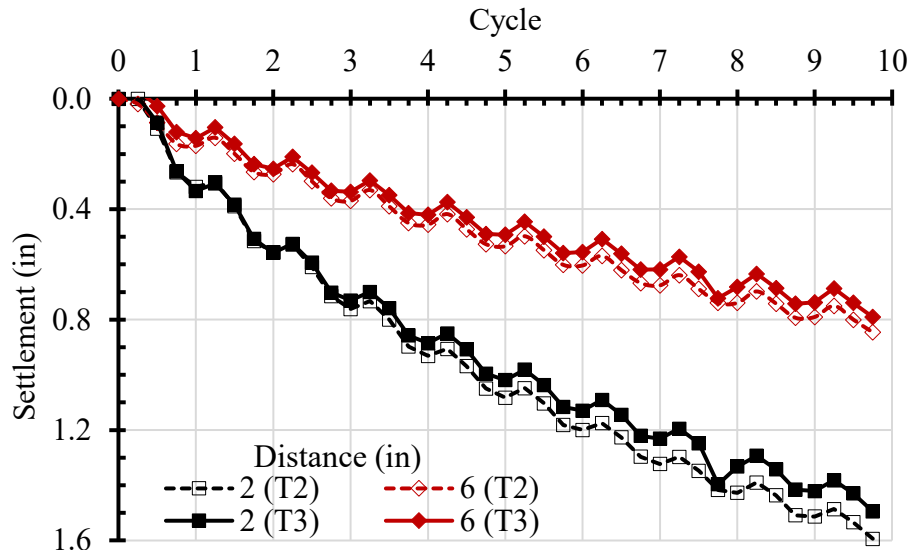
Figure 5.16: Backfill Surface Settlement near the Abutment in Test T2 and Test T3

Figure 5.17 shows the backfill surface settlements behind the abutment at Position II before traffic loading at that position for Test T2 and Test T3 during the second, sixth, and tenth abutment top movement cycles. This figure shows that the geogrid reinforcements in Test T3 significantly reduced the backfill surface settlements at distances of 20 and 28 in. as compared with those in Test T2. In both tests, the left end and the right end of the sleeper slab were 31 and 43 in. away from the back face of the abutment, respectively. In Test T3, the left end and the right end of the geogrid reinforcements were 19 and 54 in. away from the back face of the abutment, respectively. In other words, both the left end and the right end of the geogrid reinforcements were 12 in. beyond the end of the sleeper slab on both sides. Figure 5.5 showed that the abutment top movement cycles had a limited effect on the backfill surface settlements at distances of more than 20 in. away from the back face of the abutment. The above result indicates that traffic loading was the main factor affecting the settlements of the backfill surface at distances of 20 and 28 in. and the settlements of the sleeper slab.

The backfill surface settlements at distances of 33 and 41 in. were the settlements of the sleeper slab at the distance of 2 in. away from the left and the right end of the sleeper slab, respectively. The differential settlement between the left and the right sides of the sleeper slab in Test T3 was smaller than that in Test T2, indicating that the geogrid reinforcements reduced distortion of the sleeper slab due to traffic loading.
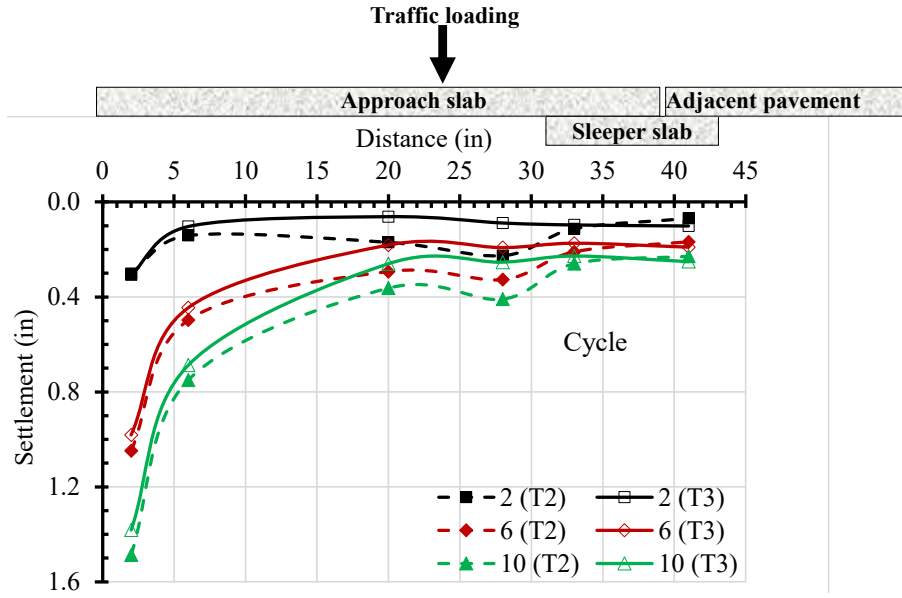
Figure 5.17: Backfill Surface Settlements behind the Abutment at Position II before Traffic Loading in Test T2 and Test T3

5.4 Effect of Reinforced Backfill

5.4.1 Abutment movement

Figure 5.18 shows the measured abutment top movements and the calculated abutment toe movements for Test T2, Test T4, Test T5, and Test T6. As presented earlier, Test T2 did not have any geogrid reinforcement behind the abutment, Test T4 had horizontal geogrid reinforcements without wrap-around facing, and Test T5 and Test T6 had horizontal geogrid reinforcements with wrap-around facing. Top two geogrid layers in Test T6 extended their length passing the sleeper slab. Figure 5.18 shows that the abutment toe in Test T4 moved farthest away from the backfill among all the four tests, while the abutment toe in Test T2 moved farther away from the backfill than that in Test T5 and Test T6. This observation indicates that the resistance to the abutment bottom from the lower portion of the backfill was larger in Test T4, but smaller in Test T5 and Test T6, than that in Test T2. For Test T4, the combined effect of backfill slumping and horizontal geogrids increased the resistance to the abutment bottom, thus increasing the abutment toe movement away from the backfill. On other hand, the amount of the backfill material moving toward and slumping downward the abutment from the upper portion of the backfill was less in Test T5 and Test T6 than that in Test T2, resulting in smaller increases of the resistance to the

71

abutment bottom from the backfill in Test T5 and Test T6 than that in Test T2. However, the geogrid reinforcements in Test T5 and Test T6 increased the resistance to the abutment bottom. As a result, the combined resistance to the abutment bottom was less in Test T5 and Test T6 than that in Test T2. Therefore, the abutment toe movement away from the backfill was less in Test T5 and Test T6 than that in Test T2.
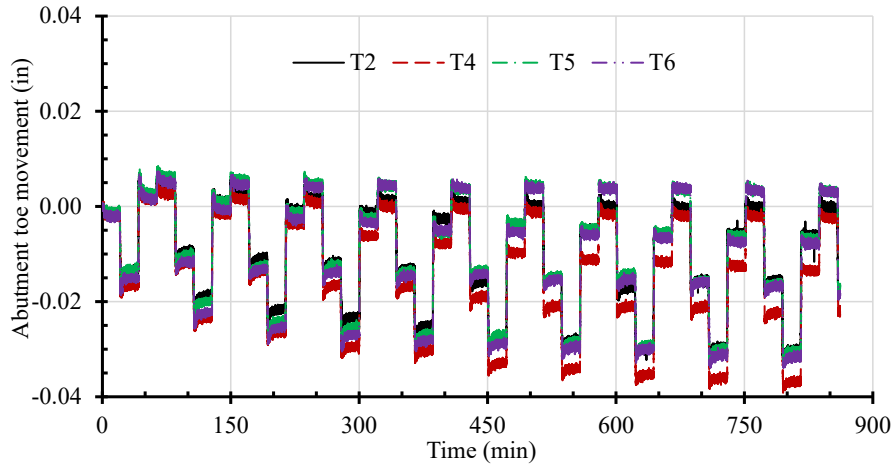
a. Abutment toe movement
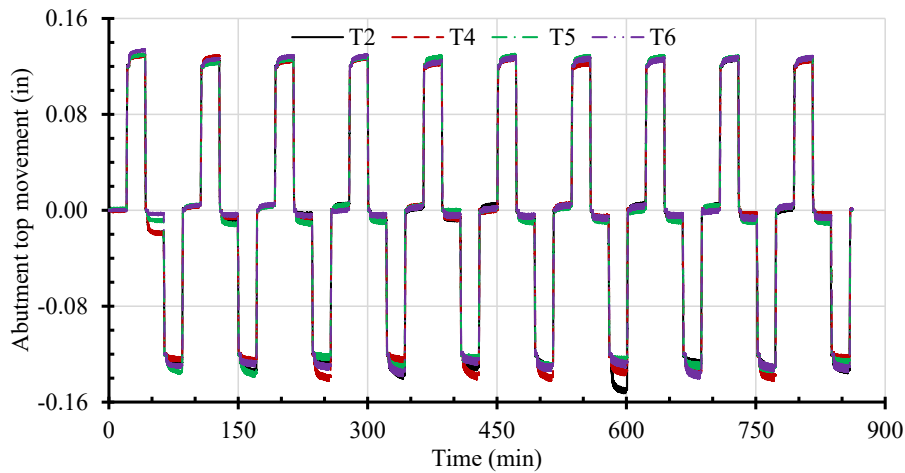
b. Abutment top movement

Figure 5.18: Abutment Movements in Test T2, Test T4, Test T5, and Test T6

5.4.2 Contact stresses under sleeper slab and approach slab

The traffic load on the approach slab was supported by the abutment, the backfill under the approach slab, and the sleeper slab. Figure 5.19 shows that the contact stresses near the abutment decreased to zero or nearly zero during traffic loading after the abutment top movement. The zero or nearly zero contact stress indicates that the approach slab lost support from the backfill due to the excessive settlement of the backfill under the approach slab. Test T5 and Test T6 had smaller ranges of the backfill behind the abutment that did not provide support than Test T2 and Test T4, indicating the wrap-around facing maintained the stability of the backfill behind the abutment better than no reinforcement or horizontal reinforcement only. Figure 5.19 shows that the contact stresses under the approach slab and the sleeper slab decreased with the number of the abutment top movement cycles. This phenomenon indicates that more backfill settlement developed during the abutment cyclic movement and more traffic load was transferred to the abutment.
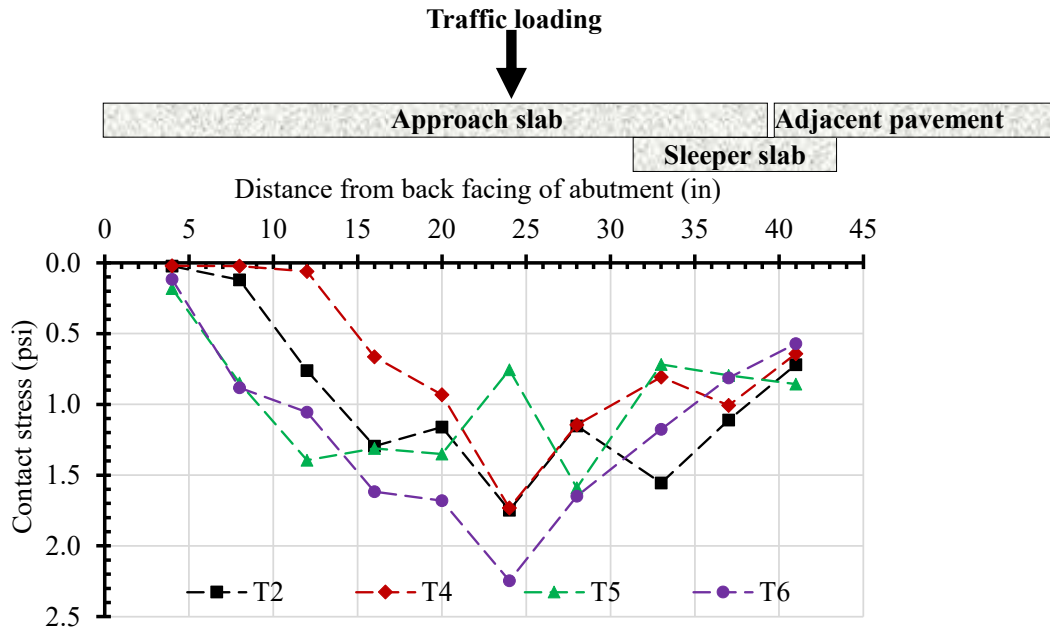
a. Second abutment top movement cycle
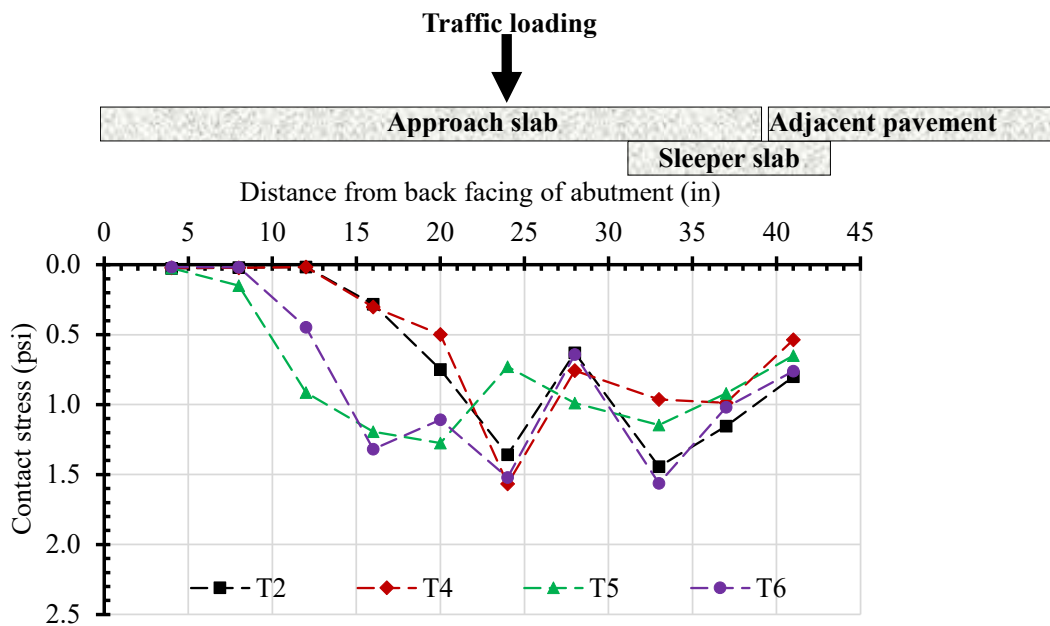
b. Sixth abutment top movement cycle

Figure 5.19: Contact Stresses due to Traffic Loading at Position II in Test T2, Test T4, Test T5, and Test T6

(Continued to next page)

c. Tenth abutment top movement cycle

Figure 5.19: Contact Stresses due to Traffic Loading at Position II in Test T2, Test T4, Test T5, and Test T6 (Continued)

5.4.3 Lateral Earth Pressures behind Abutment

Figure 5.20 shows the additional lateral earth pressures behind the abutment at Position II before traffic loading at that position during the second, sixth, and te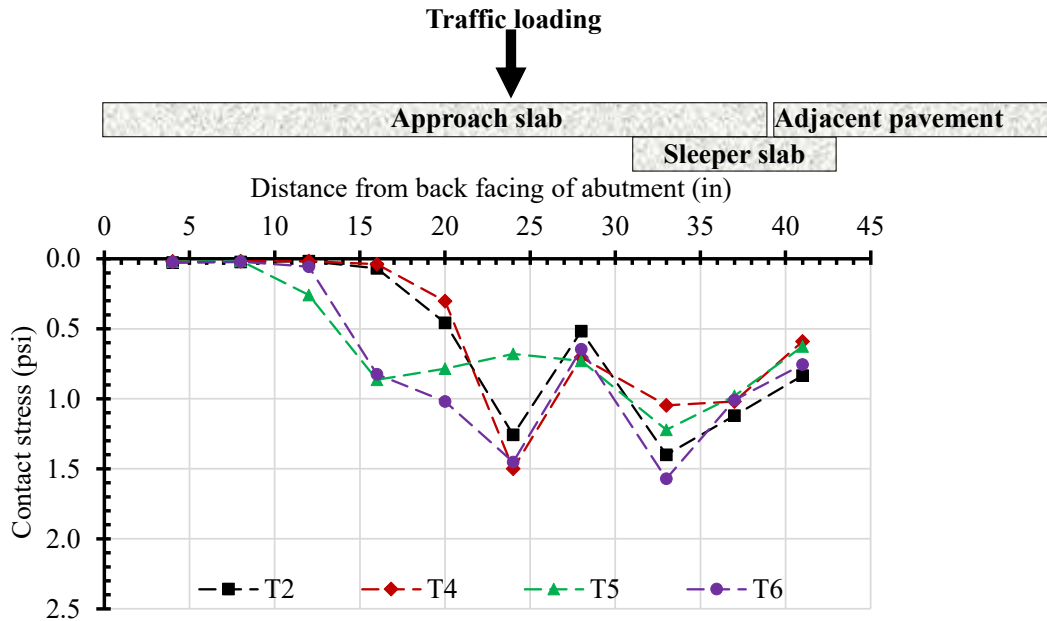nth abutment top movement cycles in Test T2, Test T4, Test T5, and Test T6. In Test T2 and Test T4, the additional lateral earth pressures decreased with the depth along the abutment in the second abutment top movement cycle, while the additional lateral earth pressures increased first and then decreased as the depth increased during the sixth and tenth abutment top movement cycles. As the abutment top moved toward the backfill to Position II, the displacement of the abutment toward the backfill increased as the elevation increased. The increase of the displacement at a higher elevation increased the additional lateral earth pressure with the elevation; however, at the higher elevation (e.g., 33 in.), there was a lower overburden stress, limiting the additional lateral earth pressure due to a passive failure in Test T2 and Test T4. In Test T5 and Test T6, however, horizontal reinforcements with wrap-around facing prevented a passive failure so that higher additional lateral earth pressures developed at higher elevations. In addition, movements of the abutment due to the simulated temperature changes and traffic loading disturbed the over-consolidated stress state of the upper

75

portion of the backfill in Test T2, thus reducing the additional lateral earth pressure at the elevation of 33 in. in the sixth and tenth abutment top movement cycles as shown in Figure 5.20(b) and Figure 5.20(c).

In general, the additional lateral earth pressures behind the abutment at Position II before traffic loading at that position were higher in Test T4 than those in Test T2. Since the horizontal geogrid reinforcements increased the strength and modulus of the backfill, the same displacement of the abutment toward the backfill induced higher additional lateral earth pressures in Test T4 than in Test T2. In addition, the difference in the additional lateral earth pressures at the elevation of 10 in. between Test T2 and Test T4 became smaller as the number of abutment top movement cycles increased. At the lower elevation (e.g., 10 in.), the overburden stress was higher and the backfill had a higher modulus; therefore, its deformation was smaller, and the geogrid reinforcement was less mobilized and beneficial.

a. Second abutment top movement cycle

b. Sixth abutment top movement cycle

Figure 5.20: Lateral Earth Pressures behind the Abutment at Position II before Traffic Loading in Test T2, Test T4, Test T5, and Test T6

(Continued to next page)
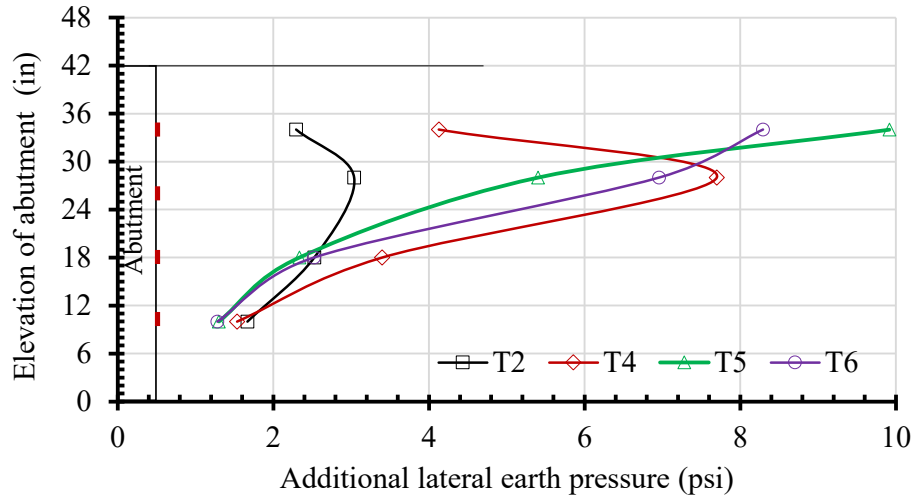
c. Tenth abutment top movement cycle

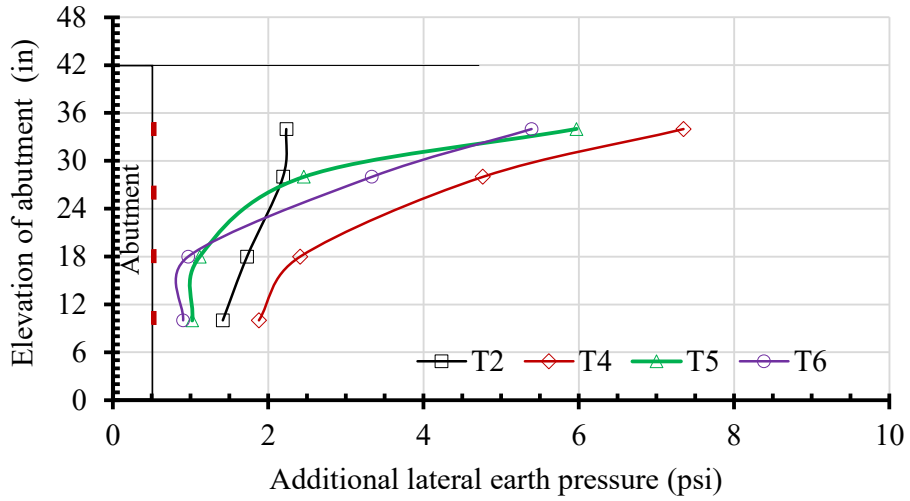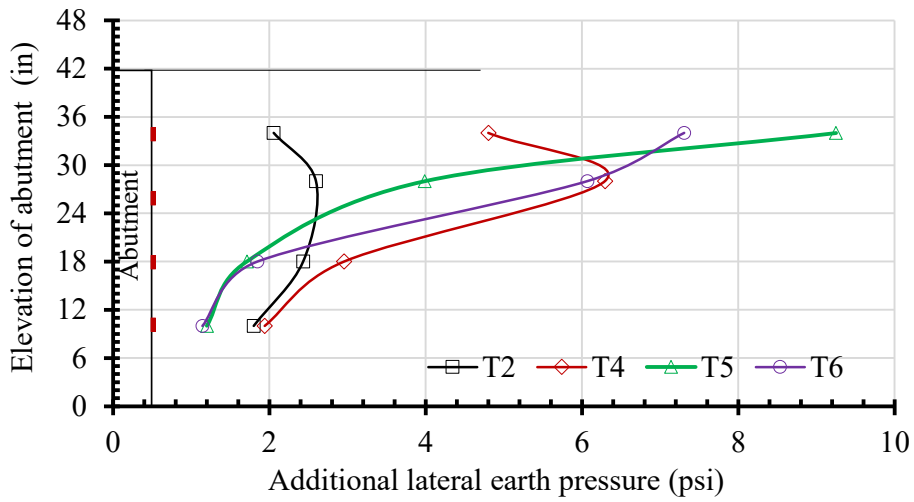**Figure 5.20: Lateral Earth Pressures behind the Abutment at Position II before Traffic Loading in Test T2, Test T4, Test T5, and Test T6 (Continued)**

In Test T5 and Test T6, the backfill was held in place by the wrap-around facing of geogrid reinforcements, and a less amount of sand slumped downward and toward the abutment as a result. The lower portion of the backfill in Test T5 and T6 had less accumulated backfill and provided less resistance as that in Test T2 and Test T4; therefore, the additional lateral earth pressures at the elevations of 10 and 18 in. in Test T5 and Test T6 were lower than those in Test T2 and Test T4. In addition, the backfill material held by the wrap-around facing of the geogrids was densified during the abutment cyclic movements and traffic loading. Consequently, the additional lateral earth pressures at elevations of 26 and 33 in. in Test T5 and Test T6 increased as the number of abutment top movements increased, as shown in Figure 5.16.

The top two layers of geogrids at elevations of 33 and 37 in. in Test T6 were 24 in. longer than those in Test T5. Figure 5.16 shows that the additional lateral earth pressure at the elevation of 33 in. was higher in Test T5 than in Test T6, indicating that the longer geogrid reinforcements reduced the additional lateral earth pressures behind the abutment when the abutment moved toward the backfill because they minimized lateral movement of the backfill when the abutment moved away from the backfill.

5.4.4 Backfill Surface Settlement

Figure 5.21 shows the backfill surface settlements at Position II of the abutment before traffic loading at that position under the approach slab and the sleeper slab in the second, sixth, and tenth cycles of the abutment movement. The backfill surface at a distance of 2 in. from the back face of the abutment in Test T4 settled more, while the backfill at distances of 20 and 28 in. settled less, than that in Test T2. As the abutment moved away from the backfill, the backfill yielded progressively. Since the horizontal geogrids improved the stability of the backfill in Test T4, the yield zone in Test T4 was smaller than that in Test T2 when the abutment top had the same movement away from the backfill. Because the gap created between the backfill and the abutment was almost same for Test T2 and Test T4, the backfill material in the smaller yield zone in Test T4 would settle more than that in the larger yield zone in Test T2. In addition, since the geogrids increased the stability of the backfill in Test T4, the backfill at distances of 20 and 28 in. had smaller settlement in Test T4 than that in Test T2. Geogrids with wrap-around facing in Test T5 and Test T6 reduced the backfill surface settlement significantly because the wrap-around facing could effectively hold the backfill in place when the abutment top moved away from the backfill. In addition, the top two geogrid layers with a longer length in Test T6 further reduced the backfill surface settlements.

a. Second abutment top movement cycle
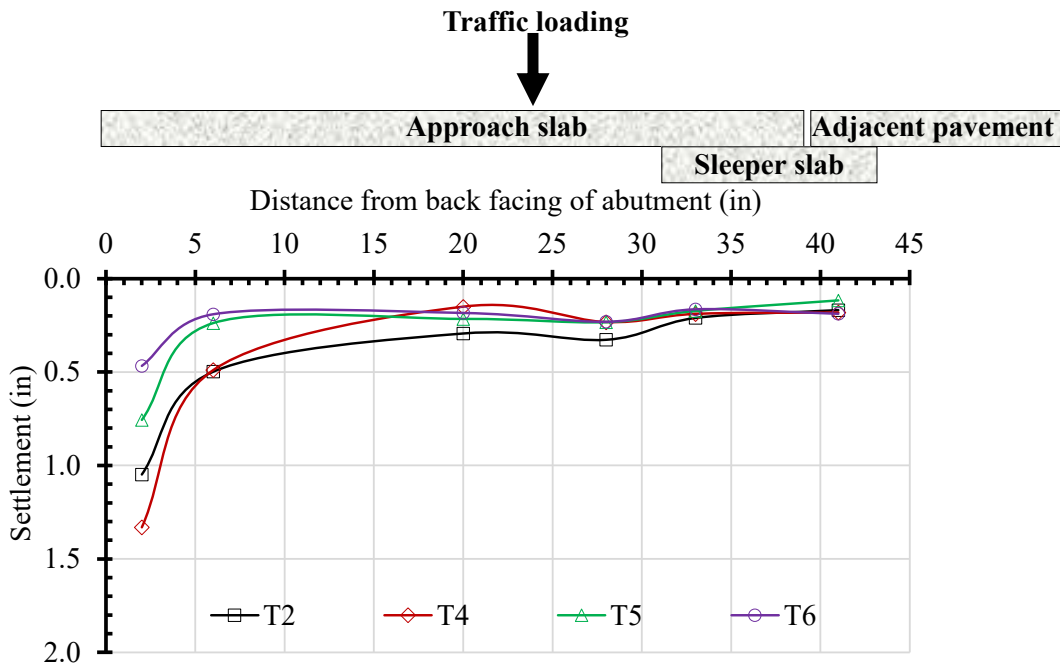
b. Sixth abutment top movement cycle

Figure 5.21: Backfill Surface Settlements before Traffic Loading at Position II in Test T2, Test T4, Test T5, and Test T6

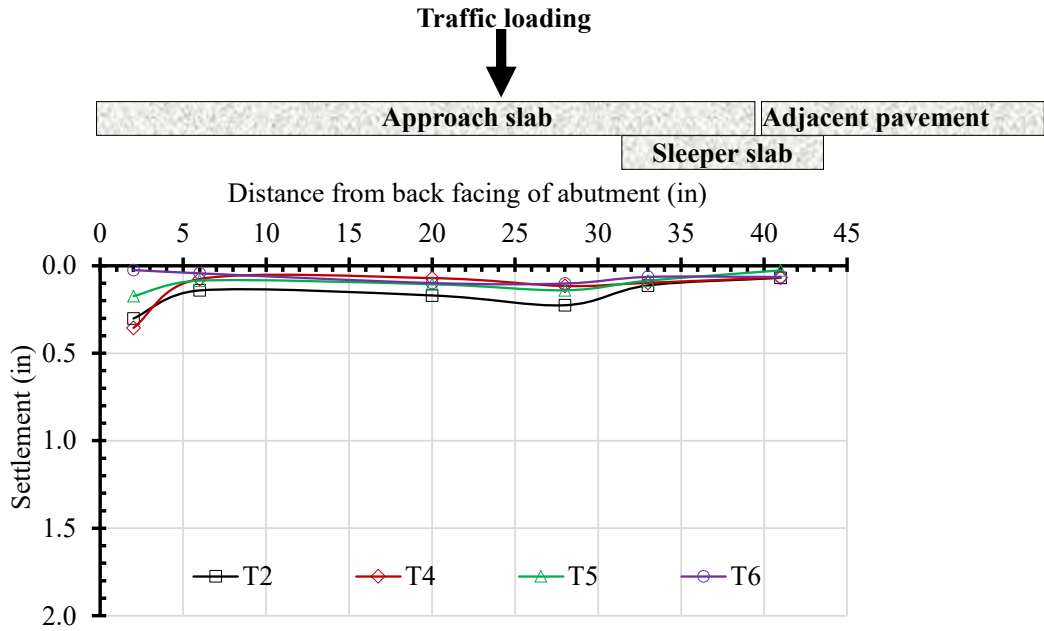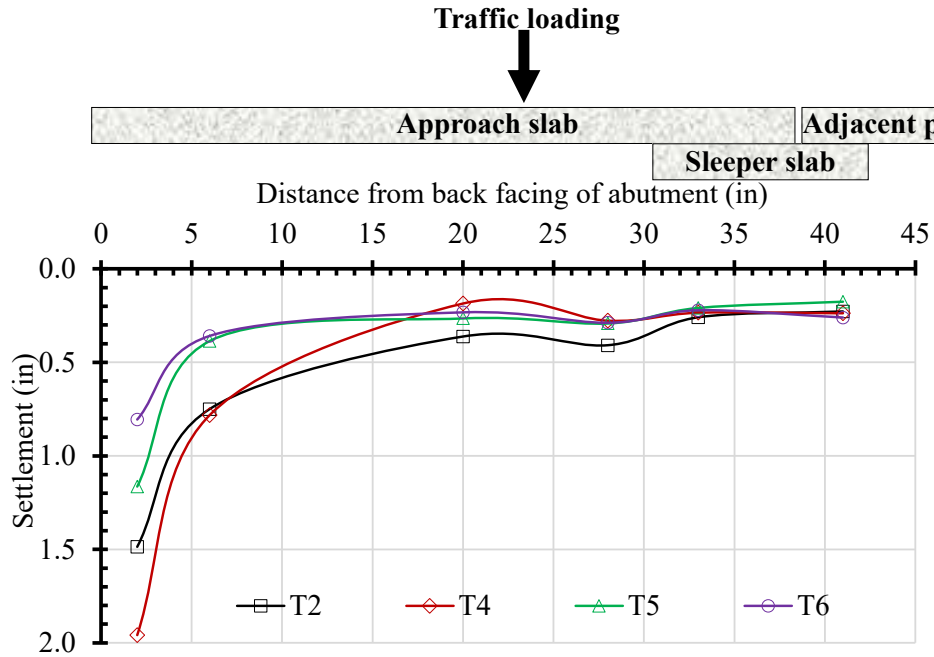(Continued to next page)

c. Tenth abutment top movement cycle

Figure 5.21: Backfill Surface Settlements before Traffic Loading at Position II in Test T2, Test T4, Test T5, and Test T6 (Continued)

Chapter 6: Conclusions and Recommendations

Expansion and contraction of bridge girders due to seasonal temperature changes push and pull an integral bridge abutment, resulting in high lateral earth pressures and backfill surface settlements behind the abutment. An approach slab is commonly utilized to provide a smooth transition between the integral bridge abutment and its adjacent pavement. When the backfill behind the abutment settles, it may provide less or no support to the approach slab. As a result, more traffic load is transferred to the end of the approach slab near the adjacent pavement. Furthermore, one end of the approach slab usually seated on a sleeper slab settles more than the other end of the approach slab supported by the integral abutment. This differential settlement may create an abrupt change of the gradient for the approach slab.

Seasonal temperature change and settlement of the approach slab due to traffic loading are the two main reasons for the distresses of the approach slab in integral abutment bridges. In this study, two physical model tests were conducted to investigate the effects of seasonal temperature changes and traffic loading on the distresses of the approach slab. An additional four physical model tests were conducted to determine the effect of geogrid reinforcements in the backfill and in the soil under the sleeper slab to mitigate the distresses of the approach slab.

6.1 Conclusions

Based on the test results of these six physical model tests, the following conclusions can be made:

1. The abutment toe moved away from the backfill when the abutment top moved toward the backfill due to the simulated temperature increase, and the abutment toe moved toward the backfill when the abutment top moved away from the backfill due to the simulated temperature decrease. Without geogrid wrap-around facing, the backfill material from the upper portion slumped downward and toward the abutment and accumulated within the lower portion when the abutment top moved away from the backfill. The accumulated backfill within the lower portion was densified during

the abutment cyclic movements, thus increasing resistance to the abutment bottom from the backfill and resulting in increasing outward movements of the abutment toe with the number of the abutment top movement cycles.

2. The accumulated backfill followed with densification within the lower portion increased the lateral earth pressures within the lower portion of the backfill with the number of the abutment top movement cycles toward the backfill. However, disturbance of the backfill in the over-consolidated stress state within the upper portion caused by the abutment top movement cycles reduced the lateral earth pressures within the upper portion of the backfill.

3. The backfill surface moved upward when the abutment top moved toward the backfill, while the backfill surface moved downward when the abutment top moved away from the backfill. The effect of abutment top movement cycles on the backfill surface settlement decreased as the distance from the back face of the abutment increased.

4. Traffic loading-induced abutment movement increased the backfill surface settlement behind the abutment and the outward movement of the abutment toe from the backfill. The contact stress under the approach slab and the sleeper slab induced by traffic loading significantly increased the settlements of the backfill away from the abutment and the sleeper slab.

5. Geogrid reinforcements increased the stiffness of the foundation soil that provided support to the sleeper slab. As a result, more traffic load was transferred to the sleeper slab and the abutment. In addition, geogrid reinforcements under the sleeper slab reduced the contact stress and the backfill surface settlement under the approach slab due to traffic loading.

6. Horizontal geogrid reinforcements in the backfill behind the abutment increased the backfill surface settlements near the abutment but reduced the settlements of the backfill surface away from the abutment. In addition, the horizontal geogrid reinforcements increased the lateral earth pressures behind the abutment.

7. Geogrids with wrap-around facing significantly reduced the backfill surface settlement induced by simulated seasonal temperature changes and traffic loading and increased the support from the backfill to the approach slab under traffic loading as a result. Geogrids with wrap-around facing reduced the range of the backfill under the approach slab to develop voids. An increase of the reinforcement length of the top geogrid layers with wrap-around facing was beneficial in reducing the backfill surface settlements.

6.2 Recommendations

Based on this research, it is recommended that geogrids with wrap-around facing, and longer top reinforcements should be used behind the abutment and horizontal geogrid layers should be used under the sleeper slab to provide stiffer support and minimize the distresses of the approach slab.

This research also has some limitations, and the researchers recommend the following studies in the future:

1. The findings from this laboratory study should be verified through field studies with instrumentation.

2. Compressible layers may be used between the abutment and the wrap-around facing of the geogrid-reinforced backfill to minimize higher lateral earth pressures behind the abutment.

3. Different types of geosynthetics should be evaluated for this application.

References

Abendroth, R. E., Greimann, L. F., & LaViolette, M. D. (2007). *An integral abutment bridge with precast concrete piles* (Report No. IHRB Project TR-438). Ames, IA: Iowa Highway Research Board and Iowa Department of Transportation.

Abu-Hejleh, N., Hanneman, D., White, D., Wang, T., & Ksouri, I. (2006). *Flowfill and MSE bridge approaches: Performance, cost, and recommendations for improvements* (Report No. CDOT-DTD-R-2006-2). Denver, CO: Colorado Department of Transportation.

Abu-Hejleh, N., Wang, T., & Zornberg, J.G. (2000). Performance of geosynthetic-reinforced walls supporting bridge and approaching roadway structures. In *Geo-Denver 2000*, 218–243. Denver, CO: American Society of Civil Engineers.

Abu-Hejleh, N., Zornberg, J. G., & Wang, T., McMullen, M., & Outcalt, W. (2001). *Performance of geosynthetic-reinforced walls supporting the founders/meadows bridge and approaching roadway structures. Report 2: Assessment of the performance and design of the front GRS walls and recommendations for future GRS abutments* (Report No. CDOT-DTD-R-2001-12). Denver, CO: Colorado Department of Transportation.

ACI Committee 318. (2008). *Building code requirements for structural concrete*. Farmington Hills, MI: American Concrete Institute.

Al-Naddaf, M. A. M. (2019). *Investigation of soil arching under different modes of soil movement and surface loading* (Doctoral dissertation). The University of Kansas.

American Association of State Highway and Transportation Officials (AASHTO). (2012). *AASHTO LRFD bridge design specifications* (6th ed.). Washington, DC: Author.

Barker, K. J., & Carder, D. R. (2001). *Performance of an integral bridge over The M1-A1 Link Road at Bramham Crossroads* (TRL Report 521). Berkshire, UK: Transport Research Laboratory.

Breña, S. F., Bonczar, C. H., Civjan, S. A., DeJong, J. T., & Crovo, D. S. (2007) Evaluation of seasonal and yearly behavior of an integral abutment bridge. *Journal of Bridge Engineering, 12*(3), 296–305.

Briaud, J. L., James, R. W., & Hoffman, S. B. (1997). *Settlement of bridge approaches (The bump at the end of the bridge)* (NCHRP Synthesis 234). Washington, DC: Transportation Research Board.

Carder, D. R., & Hayes, J. P. (2000). *Performance under cyclic loading of the foundations of integral bridges* (TRL Report 433). Crowthorne, UK: Transport Research Laboratory.

Caristo, A., Barnes, J., & Mitoulis, S. A. (2018). Numerical modelling of integral abutment bridges under seasonal thermal cycles. *Proceedings of the Institution of Civil Engineers-Bridge Engineering*, *171*(3), 179–190.

Chen, Q., & Abu-Farsakh, M. (2016). Mitigating the bridge end bump problem: A case study of a new approach slab system with geosynthetic reinforced soil foundation. *Geotextiles and Geomembranes, 44*(1), 39–50.

Chen, T. J., & Fang, Y. S. (2008). Earth pressure due to vibratory compaction. *Journal of Geotechnical and Geoenvironmental Engineering, 134*(4), 437–444.

Cheng, Y. P. (1999). *Soil-structure interaction of spread-base integral bridge abutments* (Master's thesis). Hong Kong University of Science and Technology.

Civjan, S. A., Breña, S. F., Butler, D. A. & Crovo, D. S. (2004). Field monitoring of integral abutment bridge in Massachusetts. *Transportation Research Record, 1892*, 160–169.

Civjan, S. A., Kalayci, E., Quinn, B. H., Breña, S. F., & Allen, C. A. (2013). Observed integral abutment bridge substructure response. *Engineering Structures, 56*, 1177–1191.

Darley, P., & Alderman, G. H. (1995). *Measurement of thermal cyclic movements on two portal frame bridges on the M1* (TRL Report 165). Berkshire, UK: Transport Research Laboratory.

Darley, P., Carder, D. R., & Barker, K. J. (1998). *Seasonal thermal effects over three years on the shallow abutment of an integral bridge in Glasgow* (TRL Report 344). Berkshire, UK: Transport Research Laboratory.

DeJong, J. T., Howey, D. S., Civjan, S. A., Brena, S. F., Butler, D. S., Crovo, D. S., Hourani, N., & Connors, P. (2004). Influence of daily and annual thermal variations on integral abutment bridge performance. In *Geotechnical Engineering for Transportation Projects* (pp. 496–505). Reston, VA: American Society of Civil Engineers.

Deng, Y., Phares, B. M., Greimann, L., Shryack, G. L., & Hoffman, J. J. (2015). Behavior of curved and skewed bridges with integral abutments. *Journal of Constructional Steel Research, 109*, 115–136.

Duncan, J. M., Williams, G. W., Sehn, A. L., & Seed, R. B. (1991). Estimation earth pressures due to compaction. *Journal of Geotechnical and Geoenvironmental Engineering, 117*(12), 1833–1847.

Elgaaly, M., Sandford, T. C., & Colby, C. (1992). Testing an integral steel frame bridge. *Transportation Research Record, 1371*, 75–82.

England, G. L., Tsang, N. C. M., & Bush, D. I. (2000). *Integral bridge: A fundamental approach to the time-temperature loading problem.* London, UK: Thomas Telford Ltd.

Ertugrul, O. L., & Trandafir, A. C. (2013). Lateral earth pressures on flexible cantilever retaining walls with deformable geofoam inclusions. *Engineering Geology*, *158*, 23–33.

Ertugrul, O. L., & Trandafir, A. C. (2014). Seismic earth pressures on flexible cantilever retaining walls with deformable inclusions. *Journal of Rock Mechanics and Geotechnical Engineering*, *6*(5), 417–427.

Frosch, R. J., Chovichien, V., Durbin, K., & Fedroff, D. (2006). *Jointless and smoother bridges: Behavior and design of piles* (Report No. FHWA/IN/JTRP-2004/24). West Lafayette, IN: Purdue University.

Girton, D. D., Hawkinson, T. R., & Greimann, L. F. (1991). Validation of design recommendations for integral-abutment piles. *Journal of Structural Engineering, 117*(7), 2117–2134.

Guler, E., Hamderi, M. & Demirkan, M. M. (2007). Numerical analysis of reinforced soil-retaining wall structures with cohesive and granular backfills. *Geosynthetics International*, *14*(6), 330–345.

Han, J., Wang, F., Al-Naddaf, M., & Xu, C. (2017). Progressive development of two-dimensional soil arching with displacement. *International Journal of Geomechanics, 17*(12).

Hatami, K. & Bathurst, R. J. (2006). Numerical model for reinforced soil segmental walls under surcharge loading. *Journal of Geotechnical and Geoenvironmental Engineering*, *132*(6), 673–684.

Havinga, M., Tschuchnigg, F., Marte, R., & Schweiger, H. (2017). Small scale experiments and numerical analysis of integral bridge abutments. In *Proceedings-ICSMGE 2017*, 753–756. Seoul, South Korea: International Society for Soil Mechanics and Geotechnical Engineering.

Hopkins, T. C. (1985). *Long-term movements of highway bridge approach embankments and pavements* (Report No. UKTRP-85-12). Lexington, KY: Kentucky Transportation Research Program.

Hopkins, T. C., & Deen, R. C. (1970). The bump at the end of the bridge. *Highway Research Record, 302*, 72–75.

Hoppe, E. J. (1999). *Guidelines for the use, design and construction of bridge approach slabs* (Report No. VTRC 00-R4). Charlottesville, VA: Virginia Transportation Research Council.

Horvath, J. S. (2000). *Integral-abutment bridges: Problems and innovative solutions using EPS geofoam and other geosynthetics* (Report No. CE/GE-00-2). Bronx, NY: Manhattan College.

Horvath, J. S. (2004). Integral-abutment bridges: a complex soil-structure interaction challenge. In *GeoTrans 2004* (pp. 460-469). Reston, VA: American Society of Civil Engineers.

Horvath, J. S. (2005). Integral abutment bridges: Geotechnical problems and solutions using geosynthetics and ground improvement. In *Integral Abutment and Jointless Bridges (IAJB 2005), March 16-18, 2005, Baltimore, Maryland* (pp. 281–291). Washington, DC: Federal Highway Administration.

Huang, J., Han, J., Parsons, R. L., & Pierson, M. (2013). Refined numerical modeling of a laterally-loaded drilled shaft in an MSE wall. *Geotextiles and Geomembranes*, *37*, 61–73.

Huffaker, C. D. (2013). *Behavior and analysis of an integral abutment bridge* (Master's thesis). Utah State University.

Huntley, S. A. (2009). *Field performance and evaluation of an integral abutment bridge* (Doctoral dissertation). University of New Brunswick.

Huntley, S. A., & Valsangkar, A. J. (2013). Field monitoring of earth pressures on integral bridge abutments. *Canadian Geotechnical Journal, 50*(8), 841–857.

Huntley, S. A., & Valsangkar, A. J. (2014). Behavior of H-piles supporting an integral abutment bridge. *Canadian Geotechnical Journal, 51*(7), 713–734.

Jawad, S., Han, J., Al-Naddaf, M., & Abdulrasool, G. (2020). Responses of laterally loaded single piles within mechanically stabilized earth walls. *Journal of Geotechnical and Geoenvironmental Engineering, 46*(12).

Jiang, Y., Han, J., Parsons, R. L., & Brennan, J. J. (2016). Field instrumentation and evaluation of modular-block MSE walls with secondary geogrid layers. *Journal of Geotechnical and Geoenvironmental Engineering*, 142(12).

Jorgenson, J. L. (1983). Behavior of abutment piles in an integral abutment in response to bridge movements. *Transportation Research Record, 903*, 72–79.

Kakrasul, J. I., Han, J., & Rahmaninezhad, S. M. (2020). Load-deformation behavior of geosynthetic-reinforced retaining walls with limited fill space under static footing loading. *Transportation Infrastructure Geotechnology, 7*(3), 309–331.

Kalayci, E., Civjan, S. A., Breña, S. F. (2012). Parametric study on the thermal response of curved integral abutment bridges. *Engineering Structures, 43*, 129–138.

Khodair, Y. A., & Hassiotis, S. (2005). Analysis of soil–pile interaction in integral abutment. *Computers and Geotechnics, 32*(3), 201–209.

Kim, W., & Laman, J. A. (2012). Seven-year field monitoring of four integral abutment bridges. *Journal of Performance of Constructed Facilities, 26*(1), 54–64.

Kirupakaran, K. (2013). *Soil-structure interaction studies for understanding the behavior of integral abutment bridges* (Doctoral dissertation). University of Oklahoma Graduate College.

Kong, B., Cai, C. S., & Kong, X. (2015). Field monitoring study of an integral abutment bridge supported by prestressed precast concrete piles on soft soils. *Engineering Structures, 104*, 18–31.

Kramer, S. L., & Sajer, P. (1991). *Bridge approach slab effectiveness* (Report No. WA-RD 227.1). Olympia, WA: Washington State Department of Transportation.

Kunin, J., & Alampalli, S. (2000). Integral abutment bridges: Current practice in United States and Canada. *Journal of Performance of Constructed Facilities, 14*(3), 104–111.

Laguros, J. G., Zaman, M. M., & Mahmood, I. U. (1990). *Evaluation of causes of excessive settlements of pavements behind bridge abutments and their remedies—Phase II, Executive summary* (Report No. FHWA-OK-89-07). Oklahoma City, OK: Oklahoma Department of Transportation.

Lawver, A., French, C., & Shield, C. K. (2000). Field performance of integral abutment bridge. *Transportation Research Record, 1740*, 108–117.

Lehane, B. M. (2011). Lateral soil stiffness adjacent to deep integral bridge abutments. *Géotechnique*, *61*(7), 593–603.

Liu, H., Han, J., Jawad, S., & Parsons, R. L. (2020). Literature review of causes and mitigation techniques for bumps at ends of bridges. In *Geo-Congress 2020: Geotechnical earthquake engineering and special topics* (pp. 862–871). Reston, VA: American Society of Civil Engineers.

Liu, H., Han, J., Jawad, S., & Parsons, R. L. (2021). Experimental study on settlement of backfill in integral bridge abutments induced by seasonal temperature changes. In *IFCEE 2021: Earth retention, ground improvement, and seepage control* (pp. 12–22). Reston, VA: American Society of Civil Engineers.

Liu, H., Han, J., & Parsons, R. L. (2021a). Mitigation of seasonal temperature change-induced problems with integral bridge abutments using EPS foam and geogrid. *Geotextiles and Geomembranes, 49*(5), 1380–1392.

Liu, H., Han, J., & Parsons, R. L. (2021b). *State of the practice review of integral abutment bridge in response to seasonal temperature change* (Presentation No. TRBAM-21-02675). Transportation Research Board 100th Annual Meeting, Washington, DC.

Mayne, P. W., & Kulhawy, F. H. (1982). K_0 - OCR relationships in soil. *Journal of Geotechnical Engineering Division, 108*(6), 851–872.

Muraleetharan, K. K., Miller, G. A., Kirupakaran, K., Krier, D., & Hanlon, B. R. (2012). *Soil-structure interaction studies for understanding the behavior of integral abutment bridges* (Report No. OTCREOS7.1-37-F). Midwest City, OK: Oklahoma Transportation Center.

Ooi, P. S. K., Lin, X., & Hamada, H. S. (2010). Field behavior of an integral abutment bridge supported on drilled shafts. *Journal of Bridge Engineering, 15*(1), 4–18.

Pierson, M. C., Parsons, R. L., Han, J., & Brennan, J. J. (2011). Laterally loaded shaft group capacities and deflections behind an MSE wall. *Journal of Geotechnical and Geoenvironmental Engineering, 137*(10), 882–889.

Puppala, A. J., Saride, S., Archeewa, E., Hoyos, L. R., & Nazarian, S. (2009). *Recommendations for design, construction, and maintenance of bridge approach slabs* (Report No. FHWA/TX-09/0-6022-1). Austin, TX: Texas Department of Transportation.

Schaefer, V. R., & Koch, J. C. (1992). *Void development under bridge approaches* (Report No. SD90-03). Pierre, SD: South Dakota Department of Transportation.

Seo, J. B. (2003). *The bump at the end of the bridge: An investigation* (Doctoral dissertation). Texas A&M University.

Shoukry, S. N., William, G. S., & Riad, M. Y. (2006). Structural behaviour of an integral abutment bridge under environmental conditions. In *Structures Congress 2006: Structural engineering and public safety* (pp. 1-5). Reston, VA: American Society of Civil Engineers.

Springman, S. M., Norrish, A. R. M., & Ng, C. W. W. (1996). *Cyclic loading of sand behind integral bridge abutments* (TRL Report 146). Berkshire, UK: Transport Research Laboratory.

Tan, S. J. (2007). *Modelling the foundations of idealised integral bridges in granular material* (Doctoral dissertation). University of London, University College London.

Tatsuoka, F., Hirakawa, D., Nojiri, M., Aizawa, H., Nishikiori, H., Soma, R., & Watanabe, K. A. (2009). New type of integral bridge comprising geosynthetic-reinforced soil walls. *Geosynthetics International, 16*(4), 301–326.

Thiagarajan, G., Gopalaratnam, V., Halmen, C., Ajgaonkar, S., Ma, S., Gudimetla, B., & Chamarthi, R. (2010). *Bridge approach slabs for Missouri DOT: Looking at alternative and cost-efficient approaches* (Report No. OR11.009). Jefferson City, MO: Missouri Department of Transportation.

Wahls, H. E. (1990). *Design and construction of bridge approaches* (NCHRP Synthesis 159). Washington, DC: Transportation Research Board.

White, D., Sritharan, S., Suleiman, M., Mekkawy, M., & Chetlur, S. (2005). *Identification of the best practices for design, construction, and repair of bridge approaches* (Report No. CTRE Project 02-118). Ames, IA: Iowa Department of Transportation.

Wong, H. K. W., & Small, J. C. (1994). Effect of orientation of approach slabs on pavement deformation. *Journal of Transportation Engineering, 120*(4), 590–602.

Wood, D., & Nash, D. (2000). Earth pressures on an integral bridge abutment: A numerical case study. *Soils and Foundations*, *40*(6), 23–38.

Xiao, C., Han, J., & Zhang, Z. (2016). Experimental study on performance of geosynthetic-reinforced soil model walls on rigid foundations subjected to static footing loading. *Geotextiles and Geomembranes, 44*(1), 81–94.

Younan, A. H., & Veletsos, A. S. (2000). Dynamic response of flexible retaining walls. *Earthquake Engineering & Structural Dynamics*, *29*(12), 1815–1844.

K-TRAN

KANSAS TRANSPORTATION RESEARCH
AND
NEW-DEVELOPMENT PROGRAM

AD ASTRA PER ASPERA

Kansas
Department of Transportation